THE UNIVERSITY OF CHICAGO

INTRAPERITONEAL ADMINISTRATION OF PLGA LIPID NANOPARTICLE FOR TREATMENT OF COLORECTAL CANCER PERITONEAL METASTASIS

A DISSERTATION SUBMITTED TO

THE FACULTY OF THE PRITZKER SCHOOL OF MOLECULAR ENGINEERING

IN CANDIDACY FOR THE DEGREE OF

DOCTOR OF PHILOSOPHY

BY

LIFENG CHEN

CHICAGO, ILLINOIS

JUNE 2024

COPYRIGHT © 2024 by LIFENG CHEN

ALL RIGHTS RESERVED

Table of Contents

List of Figures

List of Tables

Acknowledgement

While I know that people will be lifted or supported by various individuals at different stages of one's life, I am profoundly overwhelmed and deeply grateful for anyone who generously dedicated their time and extended their assistance and guidance to me during my Ph.D. journey. On the verge of completing graduate school training, I would like to express an outpouring of my deepest gratitude to everyone who has supported me along the way.

First and foremost, I would like to express my deepest gratitude to my Ph.D. advisor, Prof. Xiaoyang Wu, for his guidance, patience, and encouragement throughout these years in graduate school, on both my academic and personal growth. He is an open-minded mentor, never impose limitations on our research projects and always welcome and affirm discussions on any topic of interest, which give us enough space to explore our projects. Not only does he cultivate our multitasking abilities and foster creative independent thinking, but he also encourages us to think on a grand scale, broadening our vision to encompass a larger landscape. My colleagues and I are always impressed by his passion and curiosity for science, which lead to numerous innovative and intriguing projects. Furthermore, his dedication to translate the cutting-edge research to practical application through his daily diligent work in lab is a truly paradigm for us. He is a role model to me, which reflect the same passion that initially drew me to pursue a career in STEM major.

I would like to thank Prof. Jeffrey Hubbell for being my primary academic advisor, offering invaluable support and guidance throughout my academic journey. Additionally, I would like to express appreciation to Prof. Jeffrey Hubbell and Prof. Jun Huang for agreeing to be part of my thesis committee. Their expertise in biomaterials and immunology has significantly enriched my

research and broadened my perspective. I am honored to have had their insightful advice and perspective during the review of my thesis.

I would also like to thank Prof. Stuart Rowan, my training at Professor Stuart Rowan's lab has been an extremely valuable experience for me, as it has sharpened my technical skills in polymeric materials under his supervision.

I would like to thank Rovana Popoff for all the support and consideration throughout my Ph.D. journey over the years.

I would like to thank Dr. Xiaomin Jiang for his generous sharing of his informative research experience and invaluable advice on my work. I would like to thank Dr. Suman Suman for helping me with collecting tissue sample, Dr. Jimmy Lee for setting up mouse model with me, Dr. Han Liu for mRNA synthesis, also for all their guidance and patience during numerous discussion that cover cell biology, anatomy, immunology, protein, and pathology when I started in this new field as a novice. I would like to thank Parisa Tajalli Tehrani Valverde and Alex Hoover for helping me with proofreading my thesis draft and providing advice during practice talk rehearsal. I would like to thank Jing Zhao, Dr. Sarah Ann King, Dr. Jian Zhang for being great colleagues to work with.

I would like to thank Dr. Longhe Zhang, Dr. Philip Griffin, Dr. Debbie Schneiderman, Dr. Forrest Etheridge, Dr. Yefei Zhang and Dr. Qiong Wu for their generous guidance and mentorship in experiments design, data analysis with their solid background. They have exemplified the qualities of a professional researcher, setting a strong example for me to follow.

I would like to thank Dr. Nansheng Li, Dr. Ruyi Wang and Dr. Lingbowei Hu for their invaluable discussion about my organic chemistry research work.

I would like to thank Ani Solanki for helping me collecting blood sample for the project. I would like to thank Dr. C. Jin Qin for teaching me how to use and trouble shoot with Liquid Chromatography–Mass Spectrometry. You clear explanation greatly help me understand the principles and rationale behind this technique. I would like to thank Yimei Chen for helping me with Transmission Electron Microscopy experiment setup.

I would like to thank Dr. Yin Fang for his generous and invaluable advice regarding my career path and for providing professional guidance in my research endeavors. The words that you said "Just help other people the way I helped you, when they need your help" will always echo in my mind and I will extend the kindness and support to others in the future.

I would like to thank Dr. Yongshan Ding (also my gym buddy) for his companionship and encouragement when I feel frustrated. It means a lot to me.

I would like to thank Dr. Xinlei Sheng and Ce Mo for the wonderful memories we shared together. And I am so happy to be part of and witness your wedding ceremony. Thank you for the professional photography service that you provided for Rui's graduation photo as well.

Finally, and most importantly, I would like to thank my family. I am always grateful to my parents, Guitong Chen and Xiuxia Yang, for their endless encouragement, understanding and unconditional love. Even they knew little about my research field, they always try to engage in discussions with me, approaching the work from a broader perspective. To my wife, Rui He, your ceaseless support has been my greatest pillars. Thank you for taking good care of my fragile gastrointestinal system with each meal you prepared. It is my serendipity to meet you and marry you in Chicago, my second hometown where I have been for 8 years. Also, I would like to thank my kitten, Qimiao He (even you are already 7 years old and considered a grownup, you are

forever a baby for me), for the countless moments of joy that effortlessly and unconsciously lift my spirits.

Abstract

Colorectal cancer peritoneal metastasis (CRC-PM) has the poorest prognosis compared to other metastasis sites. It is often considered an end-stage as malignant tumors are difficult to completely eradicate and have a high recurrence rate of carcinomatosis. Recently, the combination of cytoreductive surgery (CRS) with intraperitoneal (IP) therapy (CRS-IP) has emerged as a promising modality and has shown improvements over traditional intravenous (IV) therapies.

Both the fast absorption of chemotherapeutic drugs during IP therapy, which results in impaired accumulation at the tumor site, and the use of toxic solubilizer Cremophor EL impedes the widespread application of IP therapy. Although current drug delivery systems have shown promising results, due to the hydrophobicity, moderate biocompatibility, and instability in peritoneal cavity and plasma environment, they fail to fully address the limitation during IP treatment.

Chapter 1 comprehensively introduced the anatomical background of the colon, rectum, peritoneum, and its microenvironments, followed by the mechanisms of CRC and CRC-PM. Furthermore, Chapter 1 covered the current treatments and their associated limitations, along with an investigation of current nanotechnology-based advancements in IP treatment field.

In Chapter 2, we introduced a novel PLGA lipid nanoparticle (PLGA lipid NP) to address the limitations of current drug delivery system since it combines the advantages from each component: structural integrity from PLGA polymer, high biocompatibility from lipids, and low immunogenicity from PEGylated lipids (lipids modified by polyethylene glycol). Our goal is to optimize retention time, penetration capability, stability, and efficacy to maximize the overall outcome of IP therapy. We employed PTX as a model chemotherapeutic drug to evaluate the

effectiveness of our drug delivery system. We described the synthesis and mechanism of three PTX delivery vehicles: PTX encapsulated in PLGA lipid NP (PTX-PLGA lipid NP), PTX encapsulated in Cremophor EL/ethanol micelle (PTX-Cre Micelle, current formulation in clinical use), and free PTX dissolved in DMSO or ethanol solvent (Free PTX).

In Chapter 3, we verified the successful coating of the lipid layer by dynamic light scattering (DLS), zeta potential analysis, and transmission electron microscopy (TEM). In addition, we performed *in vitro* experiments to assess the physicochemical properties of each vehicle, including *in vitro* release profiles and stability tests in different biological environments. We showed improved stability and enhanced sustained release of the PLGA lipid NP. Furthermore, cell-based assays indicated that the PTX-PLGA lipid NP exhibited an enhanced cellular uptake profile with an IC_{50} value comparable to canonical formulations.

In Chapter 4, we used plasma pharmacokinetics (PK) and biodistribution (BD) in major organs and tumor tissue to study the outcome of IP therapy from different PTX formulations. Both PK and BD studies revealed that the PLGA lipid NP formulation resulted in a substantial accumulation of the drug in both the tumor and the circulatory system, demonstrating that the PLGA lipid NP can facilitate the drug accumulation through both direct disposition within the peritoneal cavity and indirect pathway via the circulatory pathway. Furthermore, survival curve analysis showed an improved antitumor effect from PLGA lipid NP, without inducing significant toxicity in mice.

Chapter 1. Introduction

1.1 Introduction of Colorectal Cancer

1.1.1 General Introduction of Colorectal Cancer

Colorectal cancer (CRC) ranks as the third most commonly occurring form of neoplasm, with an annual incidence of more than 1.9 million cases,[1, 2] and ranks third among the causes of death in developed countries. It is also the second most fatal cancer in the United States.[3, 4] CRC refers to cancer originating in the tissues of either the colon or rectum,[5, 6] which are parts of the digestive system. The colon, being the initial and longest muscular tube of the large intestine, constitutes

Figure 1. Anatomic subsites of the colon and rectum

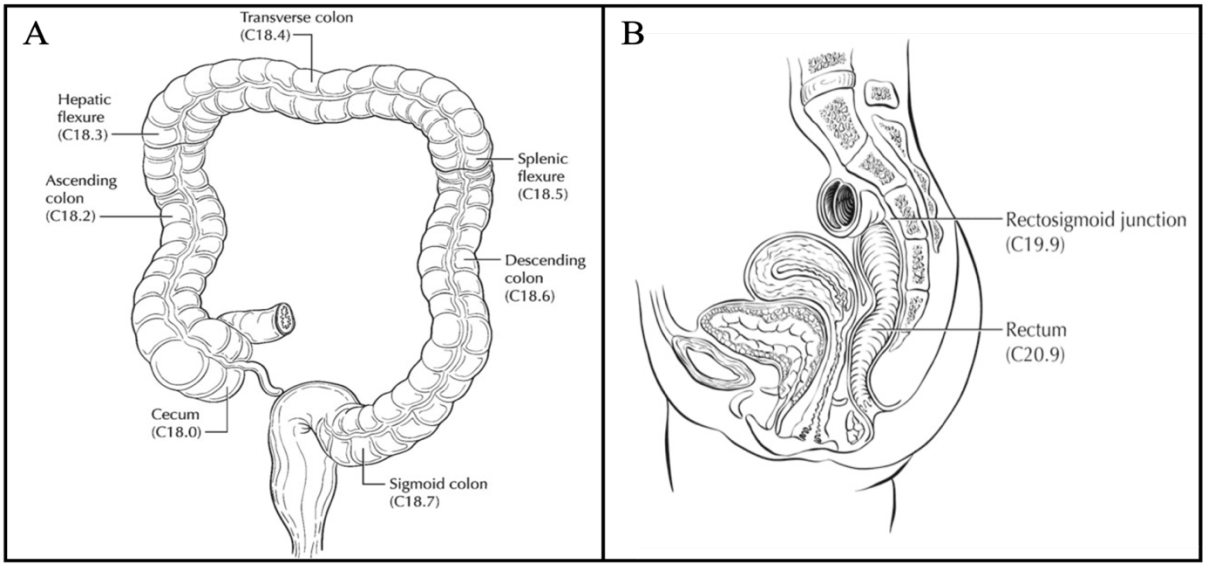

(A) Colon and (B) rectum. Used with the permission of the American Joint Committee on Cancer (AJCC), Chicago, Ill. The original source for this material is the *AJCC Cancer Staging Atlas* **(2006) edited by Greene et al[7] and published by Springer Science and Business Media LLC, www.springerlink.com**

most of this organ. It starts at the cecum, extends along the right side of the abdomen, traverses the abdomen, and descends the left side. It is an organ that absorbs water and electrolytes from

undigested food and transforms it into solid waste (feces). The solid waste will move through colon and store in the rectum, which is near the anus, located at the final segment of the large intestine (Figure 1).[7] Colon cancer refers to malignancies originating in the colon, whereas rectal cancer indicates cancers originating in the rectum. Despite their distinct locations, these two cancers are often grouped together due to their shared characteristics in terms of cancer development and treatment modalities.[8]

Most CRC typically initiate as growths of cell clusters known as polyps on the inner lining of the colon or rectum. Most colorectal polyps are benign, asymptomatic, and inconspicuous without health concerns. However, they can potentially evolve into cancer over time. The likelihood of a polyp progressing to cancer depends on the polyp type.[9-11] Various types of polyps include:

1. Adenomatous Polyps (adenomas): These polyps are benign but have the possibility to transform into cancer over time.
2. Hyperplastic Polyps: Though common, these rarely progress to cancer. However, these can vary in size, shape, and number and larger hyperplastic polyps may carry a risk for malignancy.
3. Sessile Serrated Polyps (SSP): SSP usually have serrated appearance and only occasionally be precancerous.
4. Inflammatory Polyps: These polyps are not true polyps and are usually the result of chronic inflammation in the colon. Generally, they don’t carry the risk of developing into cancer.

1.2 Introduction of Colorectal Cancer Peritoneal Metastasis

1.2.1 Colorectal Cancer Peritoneal Metastasis

As cancer develops from polyps, it gradually infiltrates the wall of the colon or rectum, leading to metastasis and start spreading. The dissemination of the disease contributes to CRC being the second leading cause of cancer-related deaths globally.[12] Despite hepatic and pulmonary metastases being common, peritoneal seeding emerges as one of the most prevalent forms of metastasis in CRC, affecting up to 10% of all CRC patients. Because of the small size and wide distribution of tumors that metastasize to the peritoneal cavity, as well as the limited contrast resolution in the peritoneum, peritoneal metastasis are challenging to diagnose with routine imaging method.[4, 13] Patients often present at advanced stages, characterized by impaired bowel function and intra-abdominal fluid accumulation (ascites), when seeking clinical treatment. These factors significantly complicate prognosis and treatment, with patients facing lower survival rates compared to those with metastasis into other organs affected by CRC.[14] Typically, patients face a median survival of 6-9 months after diagnosis.[15]

Beginning with the penetration of CRC to the bowel wall, the cancer cells have the potential to directly spread into the peritoneum through subsequent steps (Figure 2A and B).[16] Initially, this penetration process increases the likelihood of individual cancer cells or clusters detaching from the primary tumor and disseminating into the peritoneal cavity. For example, the rapid proliferation rate of cancer cells, coupled with the unique characteristics of cancerous tissue such as high interstitial fluid pressure and increased permeability of blood vessels, create a conducive environment for the detachment of cancer cells.[17] In addition, during this detachment process, there is a reduction in the expression and functionality of cell-cell adhesion molecules like E-

cadherin, facilitating the detachment of cancer cells. Another frequent cause contributing to the introduction of the cancer cells into peritoneal cavity involves improper iatrogenic factors, such as intraoperative implantation of viable shed cancer cells, incomplete resection of cancer, or leakage from blood or lymph vessels where the cancer cells are transported within the vessel and spread via this route to other organs such as the liver.

Secondly, once the primary tumor sites release the cancer cells, they traverse through the peritoneal cavity to the peritoneum due to gravity. During this process, some molecular changes that occur in the cancer cells are beneficial for them to survive before reaching the peritoneum. For instance, cancer cells can acquire anoikis resistance to evade cell death and ultimately survive by modifying the surface molecules of the cancer cells.

Figure 2. Mechanism of peritoneal metastasis

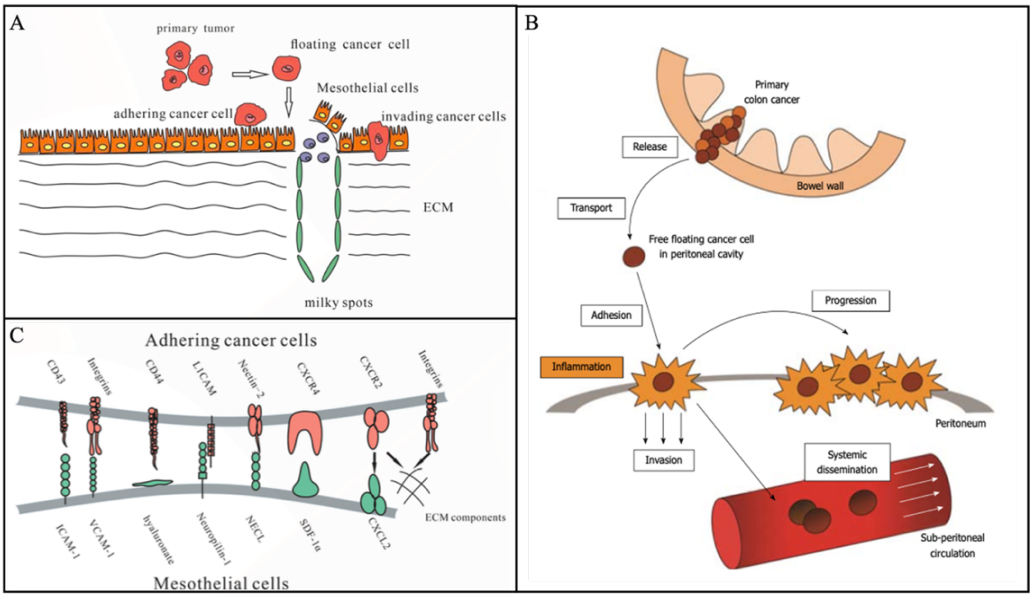

(A) Steps of peritoneal metastasis process.[16] Copyright 2022, Journal of Clinical Medicine. (B) Colon cancer peritoneal metastasis develops through a complex series of steps.[18] Copyright 2014, World Journal of Gastroenterology (C) The molecular mechanisms underlying adhesive interactions that mediate peritoneal metastasis.[16] Copyright 2022, Journal of Clinical Medicine.

Thirdly, only the floating cancer cells adhere to the peritoneum, they initiate their propagation, colonization, and establishment of peritoneal carcinomatosis on the peritoneum. Throughout this progression, inflammation plays a pivotal role, as the inflammatory milieu can prompt peritoneal cells to enhance the expression of adhesion molecules and cytokines, thereby expediting the process (Figure 2C). For instance, vascular cell adhesion molecule 1 (VCAM-1 or CD106), intercellular adhesion molecule 1 (ICAM-1 or CD54), and platelet endothelial cell adhesion molecule (PECAM-1 or CD31) all facilitate the adhesion between mobile cancer cells and the mesothelial layer, which forms the surface of the peritoneum. Additionally, the involvement of pro-inflammatory mediators such as IL-1β, IL-6, and epidermal growth factors has been suggested to assist external cancer cells in attaching before invading the peritoneum as well.[18] Fourthly, before the clustering of settled cancer cells, those that remain free begin to penetrate the sub-mesothelial tissue by invading the mesothelial layer. Studies have indicated that cancer cells possess the ability to induce apoptosis in mesothelial cells, rendering some of them vulnerable through a FAS-dependent mechanism, thus facilitating access. Finally, following the invasion of the sub-mesothelial stroma, cancer cells can access the bloodstream and lymphatic microcirculation system, initiating angiogenesis to procure nutrients.

1.2.2 Anatomy and Physiology of Peritoneal Cavity and Peritoneum

Originating from the embryonic coelomic cavity, the peritoneal cavity is a closed compartment within the abdomen which houses the abdominal organs. In males, it is entirely enclosed, while in females, it remains partially open due to the presence of the uterus, fallopian tubes, and ovaries, which create a connection between the female reproductive system and the peritoneal

cavity.[19] Consequently, infections in the female reproductive tract can migrate to the peritoneal cavity, resulting in pelvic inflammatory disease and peritonitis.[20] The peritoneal cavity is anatomically partitioned into two sections: the greater sac, which encompasses the abdominal cavity, pelvis, and subdiaphragmatic region, and the lesser sac, a space located between the stomach and colon (Figure 3A and B). Within the peritoneal cavity, there is a delicate layer of fluid known as peritoneal fluid. This fluid contains water, electrolytes, proteins, leukocytes, and antibodies etc.[21] Notably, the peritoneal fluid contains plasma proteins, with a concentration of approximately 50% of that found in plasma itself. In healthy humans, the typical volume of peritoneal fluid ranges from 50 to 75 milliliters, while in mice, its volume is typically between 0.02 milliliters and 0.1 milliliters.[22, 23]

The membrane that covers the fluid-filled peritoneal cavity and encompass, provides support to the abdominal organs, is called the peritoneum.[24, 25] This serous membrane lines the inner surfaces of the abdominal and pelvic walls and envelops the organs within these cavities. As the largest serous membrane in terms of surface area and distribution, the peritoneum is characterized by its thin, smooth structure, comprising mesothelium and a small amount of connective tissue. It consists of two continuous parts: the visceral peritoneum, which covers the abdominal viscera and internal organs, and the parietal peritoneum, which lines the inner surface of the abdomen and pelvic wall (Figure 3A). The peritoneal cavity and peritoneal fluid provide enough space and lubricate the abdominal viscera with minimal friction, facilitating essential biological processes.

Figure 3. Sagittal view of the abdominal cavity

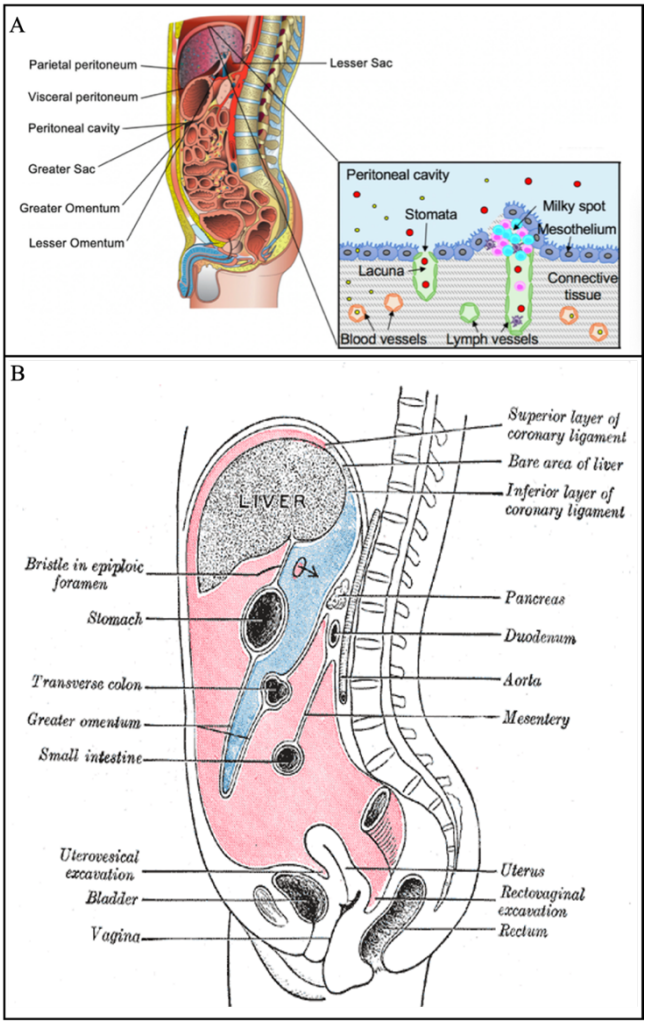

(A) Peritoneal Cavity, lining with continuous parietal and visceral peritoneum. The picture that was zoomed in, exhibit the ultrastructural view of peritoneum, which is composed of a mesothelial cell layer studded with lymphatic stomata and lymphoid tissue (milky spots) that drain into lymphatic vessels. The mesothelial cell layer is supported by connective tissue layer with embedded blood and lymphatic vessels.[24] (B) Detailed anatomy structure of peritoneum and peritoneal cavity (Anatomy zone from youtube)

On top of the peritoneum there is a single layer of mesothelial cells that are connected via tight junctions, adherens junctions, gap junctions, and desmosomes. Critically, these mesothelial cells contain microvilli which increase the surface area thus enhance functionality of the peritoneum (Figure 3A).

1.2.3 Peritoneal Blood Vessel

Under the peritoneum, the complex blood and lymphatic system play crucial roles in homeostasis within the peritoneal cavity. The connective tissue is below the mesothelial cells, made up of collagen, lymphocytes, blood vessels and lymphatics. Most of the blood vessels beneath the mesothelial cells are blood capillaries, few arterioles are present within sub mesothelium as well. These blood capillaries are widely distributed throughout the entire peritoneum, forming the basis to facilitate frequent small molecule exchange between the peritoneal cavity and plasma.[26]

1.2.4 Peritoneal Lymphatic System

Within the connective tissue, a well-organized lymphatic network helps prevent the accumulation of fluid (lymphedema) by regulating fluid balance in the body, absorbing excess fluid, proteins, or other substances released from tissues.[27-29] Within this lymphatic network, two unique types of lymphoid tissue exist: milky spots and fat-associated lymphoid clusters (FALC). Both milky spots and FALC are atypical lymphoid tissues characterized by an abundance of macrophages with active phagocytic capabilities. As depicted in Figure 3A, milky spots are typically situated near the stomata in the peritoneum. As the primary immune defense system within the peritoneal cavity, the aggregation of macrophages and lymphocytes can engulf particles, bacteria, and other substances in the peritoneal cavity. On the other hand, FALCs are more widely distributed throughout the peritoneal cavity and can be found in many places including the omentum, mesentery, mediastinum. Both B and T lymphocytes can be found within FALC as well. Within milky spots and FALC, the macrophages can respond to inflammation triggered by external

substances, including macromolecular therapeutics or particle delivery systems administered via IP administration.

1.2.5 Background of Absorption Route for Small Molecule, Macromolecule, and Nanoparticle Formulations from Peritoneal Cavity

Because of its extensive surface area (approximately 125 cm^2 in rats), numerous microvilli on mesothelial cells, and intricate network of blood vessels and lymphatic vessels beneath the peritoneum, the peritoneal cavity serves as an efficient gateway for accessing the systemic circulation following intraperitoneal administration.

Figure 4. Absorption pathways from peritoneal cavity

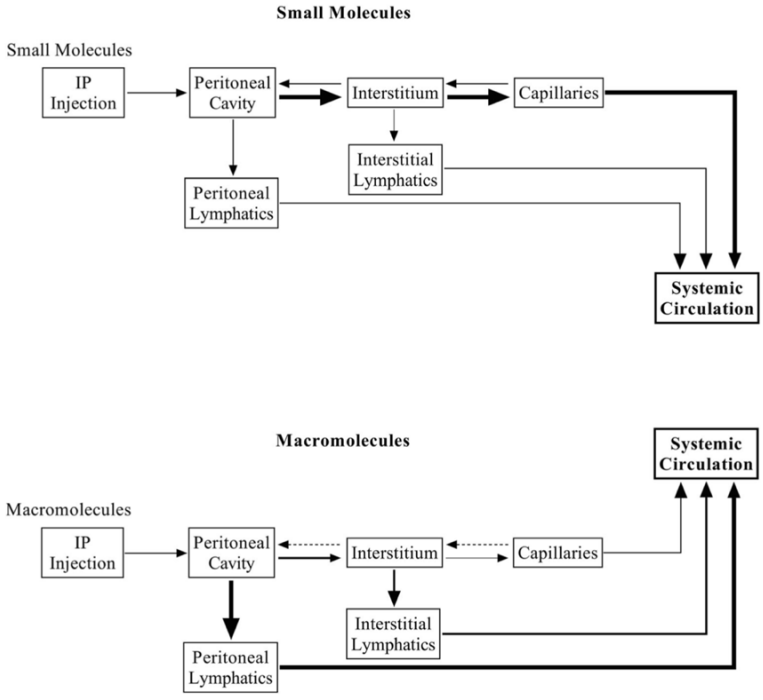

Flow chart of absorption pathways for small and macromolecules from the peritoneal cavity to systemic circulation[25]

Due to the highly permeable peritoneum, the compound will finally enter the bloodstream or lymphatic vessels after IP injection via crossing through peritoneal fluid, penetrating the mesothelial cells and vessel wall. The compound typically traverses via the transcellular or intercellular spaces in the visceral and parietal mesothelium. As illustrated in Figure 5, the visceral mesothelium is more permeable than parietal mesothelium, attributed to the numerous pinocytic vesicles that facilitate the absorption process of molecules.

Many studies have demonstrated that the size of the administered substance determines the pathway by which it is absorbed. Small or medium sized substances (MW<5000) are primarily absorbed through capillaries and directed towards the portal vein. In the peritoneum, thin and highly permeable capillaries facilitate the rapid exchange of water or small molecules between the peritoneal cavity and the vascular system. On the other hand, larger molecules (MW>5000),

Figure 5. Microstructure of mesothelial cells

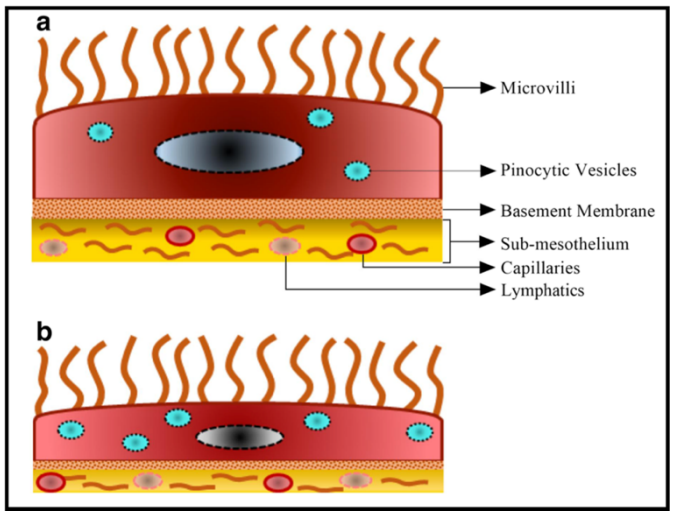

(a) Depicts parietal mesothelial cells characterized by a modest quantity of pinocytic vesicles and a basement membrane with more maturity. In contrast, (b) illustrates visceral mesothelial cells featuring a greater abundance of pinocytic vesicles and a less developed basement membrane.[25]

including macromolecules or nanoparticles, are absorbed via the lymphatic system (Figure 4).

Small particles and cells enter lymphatic circulation through open stomata located in the peritoneum. Compared to other routes such as oral or subcutaneous administration, numerous studies have demonstrated that IP administration exhibit faster and more complete absorption of small molecules (Figure 4).[25]

1.3 Treatment for Colorectal Cancer Peritoneal Metastasis

1.3.1 Current Treatment for Colorectal Cancer Peritoneal Metastasis

Peritoneal metastasis often occurs at the advanced stages of colorectal cancer when the aggressive tumor has infiltrated the wall of the colon or rectum, initiating the dissemination process from primary site to distant organs like liver, lung, and peritoneal cavity. Due to the small metastatic nodules in peritoneum, the diagnosis of colorectal cancer peritoneal metastasis is complex. In its early stage, peritoneal metastasis can often be asymptomatic due to the small metastatic nodules. The common symptoms include abdominal distension, weight loss, anorexia, dyspnea, and fatigue. Intestinal obstruction is one of the most common serious complications of peritoneal metastasis.[30] Current diagnosis of peritoneal metastasis relies on the imaging examination, laparoscopy, or intraoperative findings. As traditional imaging tool, computed tomography (CT) lack sensitivity to the small tumor nodules in the peritoneum. Even magnetic resonance imaging (MRI) or positron emission technology (PET) may increase sensitivity, due to its own limitation like high cost, lack of meaningful clinical correlation, they are not widely used in the diagnosis stage. These difficulties weaken the impact of diagnosis during early state where intervention could have been involved earlier.[31, 32]

The prognosis for patients diagnosed with colorectal cancer peritoneal metastasis is poor with low survival rate. Historically, it has long been considered as an incurable phase of peritoneal metastasis of colorectal cancer, the median survival of patients who were treated with systemic chemotherapy and supportive care as the primary palliative care can be extended to 7.8~15.2 months, compared to patients without active therapy, who survive less than 5 months. [33-37] Given the low efficiency of traditional systemic chemotherapy and its associated systemic toxicity, there is a pressing need for alternative treatments, particularly for local cancer diseases. Recently, the combination therapy of cytoreductive surgery (CRS) and IP therapy has emerged as one of the most promising approaches, offering significant clinical benefits. Studies have shown that this combination treatment can extend median survival ranging from 22 to 47 months.[37] As postulated by Dedrick et al., IP therapy holds the potential to achieve higher concentrations localized within peritoneal tumors compared to systemic treatment.[38] Instead of being administered through systemic circulation, regional IP therapy can not only achieve high drug exposure in tumors within peritoneal cavity specifically, but also mitigate the systemic toxic side effects.[39]

The CRS-IP procedure is an aggressive combination of surgery and chemotherapy to eradicate as many tumors as possible. During the CRS step, the surgeon needs to remove all visible macroscopic tumors within the peritoneal cavity. However, this surgical procedure is challenging and time-consuming and takes approximately 8 to 10 hours to complete. The second step includes the repeated IP perfusion of chemotherapeutic agents into the patient's abdomen through catheters right after CRS. These catheters are removed upon completion of the final cycle of IP treatment. Especially, the liquid chemotherapeutic agents are heated above normal body temperature but below 42^{o}C before entering the patient’s peritoneal cavity. This procedure,

which last 90 minutes usually, is called Hyperthermic (or Heated) Intraperitoneal Chemotherapy (HIPEC) (Figure 6).[40]

Figure 6. Illustration of Hyperthermic Intraperitoneal Chemotherapy (HIPEC) setup

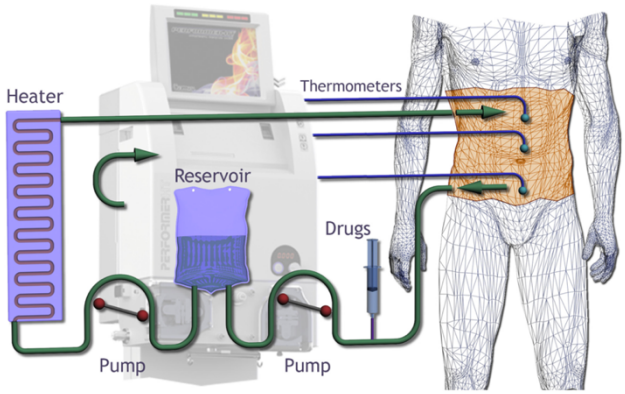

Closed-loop perfusion system is utilized to heat and circulate chemotherapy directly into the abdominal cavity.[40]

There are two main types of HIPEC procedures: open HIPEC and closed HIPEC. During the open HIPEC procedure, the open abdomen allows for better visualization of abdomen, which ensures the optimal distribution of chemotherapeutic solution, though it becomes more difficult to maintain heated temperature of abdomen as well as increase potential for leakage of the therapeutic agents. In contrast, closed HIPEC procedure allows for a better temperature control without chemotherapeutic agent loss, compromising the homogeneous distribution of the perfusion fluid in the meantime. In 1988, Dr. Sugarbaker first proposed the concept by leveraging both surgical procedure and post-operative intraperitoneal chemotherapy recurrent intraabdominal cancer, demonstrated the benefit to enhance patients' quality of life and survival duration.[41] By concentrating the chemotherapeutic drugs within the peritoneal cavity, HIPEC procedure is considered as targeted but aggressive surgical approach for peritoneal cancer.

Another novel therapeutic method for administering chemotherapy localized within the peritoneal cavity is Pressurized IntraPeritoneal Aerosol Chemotherapy (PIPAC). This approach allows for improved distribution of chemotherapeutic agents, minimal invasion, enhanced tissue penetration, and more effective treatment with lower required dosages of chemotherapy. PIPAC

Figure 7. Principle of Pressurized Intraperitoneal Aerosol Chemotherapy (PIPAC)

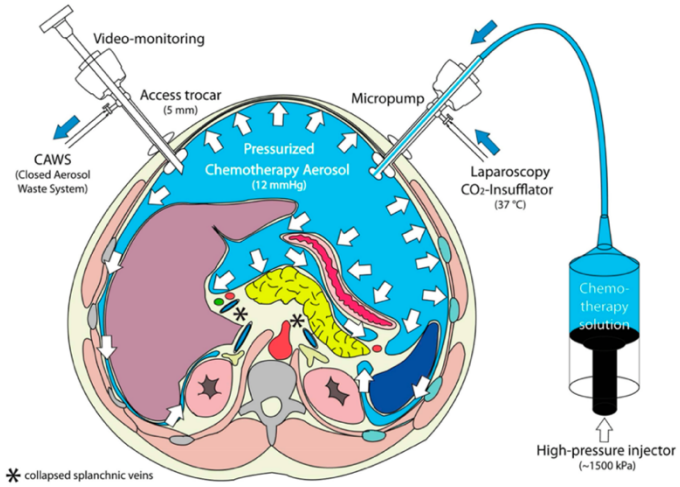

In a staging laparoscopy, an aerosol cytostatic agent is dispersed within the abdominal cavity via a nebulizer, facilitating its uniform distribution throughout the area.[44]

was first introduced to the clinic by Reymond on November 5th, 2011.[42, 43] Unlike traditional methods, PIPAC is performed during laparoscopy. During the PIPAC procedure, a CO_2 pneumoperitoneum is created with working pressure ranging from 12 to 15 mmHg. Then the chemotherapeutic solution is nebulized through nebulizer or micropump before injecting into the peritoneal cavity, creating an aerosol in the abdomen. The aerosol is a suspension of liquid droplets in the gas. The smaller the droplets, the closer the behavior of aerosol is to a gas, which can facilitate the penetration of chemotherapeutic solution droplets into tissues more homogeneously by the high CO_2 pressure, compared to traditional HIPEC procedure. Moreover, the whole PIPAC procedure takes less than 1 hour. Upon completion of the procedure, a suction

system is utilized to extract the aerosol and deflate the CO_2 pneumoperitoneum (Figure 7).[44] Solass and colleagues have demonstrated that nebulization is feasible to allow enhanced drug concentration in peritoneal tumor tissues with low doses of doxorubicin. It highlights the potential efficacy and advantages of PIPAC in delivering chemotherapy directly to peritoneal tumors while minimizing local toxicity within the peritoneal cavity since the use of excessive concentration of chemo drug during HIPEC procedure has elevated risk of causing local toxicity.[45]

PTX has gained recognition as an effective anticancer medication used in the treatment of advanced tumors, such as colorectal cancer.[46, 47] PTX stabilizes microtubules by promoting the assembly of tubulin dimers and preventing their depolymerization, thereby inhibiting the normal dynamic reorganization of microtubules that is critical for cell function during interphase and mitosis. Subsequently, it can arrest the cell cycle and trigger the apoptosis process, inducing interruption of G2/M phase, causing mitosis to be abnormal or stopped, hindering the replication of tumor cells, and making the cancer cells unable to continue to divide and die at the end.[48] Especially for IP treatment, PTX stands out from many other chemotherapeutic agents including mitomycin-C, cisplatin/oxaliplatin, adriamicin[46, 49-53] as it is highly lipophilic resulting in a slow absorption as compared to other hydrophilic drugs. Its potential in treating colorectal cancer has been examined in a phase II trial study.[54]

Given the hydrophobic nature of PTX (Figure 8A), PTX is formulated in 50% Cremophor EL /absolute ethanol for clinical use, such as Taxol®. It is likely that the amphiphilic Cremophor EL can form micellar structure to trap PTX, increasing its solubility in aqueous environment.[55]

Figure 8. Paclitaxel structure and Cremophor EL structure

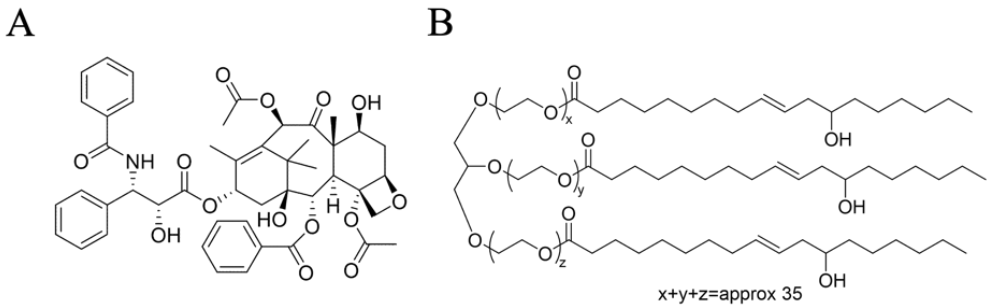

(A) Chemical structure of paclitaxel, (B) Chemical structure of Cremophor EL, x, y, z represent the number of oxyethylene units in each chain

However, the Cremophor EL in FDA-approved Taxol® formulations has been reported with severe anaphylactoid hypersensitivity reactions, hyperlipidaemia etc., further impedes the usage of PTX chemotherapy.[56, 57]

1.3.2 Drawbacks of Current IP Treatment

Although IP treatment has exhibited its potential benefits, it has not been widely adopted. To date, there are no IP chemotherapeutic formulations approved by the FDA. Instead, current practice is off-label use of drugs designed for intravenous administration, including doxorubicin,[58] fluorouracil,[59] paclitaxel,[60] and platinum-based therapeutics.[61]

Various challenges hinder the utilization of IP treatment. The setup and high costs associated with machines are not accessible to people in rural areas with limited healthcare resources. All the clinical limitations are attributed to the intrinsic drawback of IP therapy. During IP therapy,

substantial chemotherapeutics will be absorbed into the systemic circulation and undergo metabolism through permeable peritoneal membranes, which cause significant loss of drugs within the peritoneal cavity to exert effectiveness. Therefore, the HIPEC procedure needs to be prolonged with excessive drug concentration to compensate for the drug loss, resulting in low patient compliance due to the indwelling peritoneal catheters throughout the treatment for several months. Moreover, the Cremophor EL used in the PTX formulation can induce other severe side effects. Given these concerns and the importance of effective drug delivery to the peritoneal cavity, there is an urgent need to explore alternative methods.

1.3.3 Rationale for Using Micro/ Nanomedicines for IP Treatment as Potential Alternatives

After IP administration, the size of the injected substances significantly influences their absorption rate and retention time in the peritoneal cavity. In general, bigger substances can retain in the peritoneal cavity longer than smaller substances. In the drug delivery sector, both microparticles and nanoparticles can potentially address the limitation of IP therapy by slowing down the absorption rate and increasing retention time. The biodegradable polymeric micro/nanoparticles and lipid-based nanoparticles are two prevalent carriers among them. Biodegradable polymers can degrade through hydrolysis or enzymatic mechanisms, regardless of whether they originate from natural or synthetic sources. During the degradation process, the by-products are biocompatible without toxicity and eliminated through metabolism in body subsequently.[62] Synthetic biodegradable polymers have traditionally formed the foundation of polymer-based micro/nanoparticle formulations, allowing for modification or adjustment in terms of structures, molecular weight, functional groups etc for specific therapeutic context.[63, 64]

For instance, polyamides,[65, 66] poly(amino acids),[67, 68] polyesters,[69-71] and polyurethanes[72-74] have been utilized in drug delivery platform applications.

1.3.3.1 PLGA Biodegradable Polymer Based Strategy

Thermoplastic aliphatic polyester poly (lactic-co-glycolic acid) (PLGA) is one of the most successfully developed biodegradable polymers. PLGA nanotechnology has been approved by FDA and is now widely used in pharmaceuticals and medical engineering sectors since 1989.[75-78] PLGA has been implemented in numerous medical application, including excipient for injectable micro/nano capsules and spheres,[79-81] sustained-release formulation for implantation,[82-84] and porous scaffold for cell cultures,[85-87] etc.

PLGA is a linear copolymer that can be prepared at different ratios between lactic acid (LA) and glycolic acid (GA) monomers by different synthesis routes. In general, the PLGA with low molecular weight (Mw<10 kDa) can be synthesized by poly-condensation of LA and GA under water-removal condition, whereas the ring-opening copolymerization of cyclic dimers of LA and GA is the typical method for synthesizing PLGA with high molecular weight. Common catalysts involved in this process include tin (II) 2-ethylhexanoate, tin (II) alkoxides, or aluminum isopropoxide.[62, 88]

Following the synthesis route, the monomer units of LA and GA are linked through ester bonds. The ester linkages within PLGA can be degraded by hydrolysis, yielding the original monomers, LA and GA, respectively. These monomers are byproducts from metabolic pathways in the body under normal physiological conditions and will be eliminated from the body through metabolism as carbon dioxide and water via the Krebs cycle.[88-90]

PLGA copolymers typically exhibit a glass transition temperature (Tg) around 40ºC, which is above the body temperature (37°C). Once administered into the body, PLGA will remain in a glassy state with rigid chain structure.[91] This rigidity provides substantial mechanical strength, making PLGA conducive to delivering drugs with robust integrity.[92, 93] Additionally, the monomers of PLGA have different crystallinity. The polymer PLA can exist either in a highly crystalline form as PLLA or completely amorphous as PDLA. In contrast, PGA has a highly crystalline structure without methyl side groups.[94] The rate of hydrolysis of PLGA can also be tailored by controlling the crystallinity of monomers and the ratio of monomers.

Considering the properties of PLGA, the high Tg (above body temperature), crystalline structure, high molecular weight with mechanical strength renders PLGA-based particle system a promising drug delivery platform for peritoneal metastasis-related diseases. As an example, Arianna et al. demonstrated the combination between positively charged PLGA nanoparticles and electrostatic precipitation can enhance tumor uptake of curcumin-encapsulated nanoparticles during PIPAC treatment in a urinary bladder model.[95] In addition, Ana et al. illustrated that PLGA nanoparticles can facilitate the delivery of cannabidiol for ovarian cancer during IP treatment.[96]

Besides its conventional functions, Yolonda synthesized pH responsive PLGA nanoparticles for enhancing local control with slower drug release kinetics, which results in a prolonged intracellular accumulation of PTX in the peritoneal cavity.[97] However, researchers did not address the issue of rapid loss of the entire drug delivery platform. Moreover, they did not address the challenge from the macrophages in the peritoneal cavity, which can potentially remove nanoparticles before they can exert their intended function.

Considering the size dominant effect within the peritoneal cavity, microparticles (>1 μm) represent another potential drug delivery system with prolonged release profile. Their large size renders them less susceptible to absorption by the peritoneum. Max et al. have illustrated that PTX-loaded PLGA microparticles with diameters of 5-6 μm can extend survival rates twice as long as those observed with Cremophor micelle solutions by repeated dosing, owing to its sustained release behavior and long retention time within peritoneal cavity over one month.[98] While microparticles significantly prolong drug retention within the peritoneal cavity, they also fail to distribute evenly and tend to induce inflammatory reactions and peritoneal adhesions.[99]

1.3.3.2 Liposome Based Strategy

Another prominent nanoparticle that is widely used in drug delivery for colorectal cancer peritoneal metastasis is liposome. It is an artificial spherical lipid vesicle composed of one or more lipid bilayers through a self-assembly process in aqueous solution (Figure 9).[100-102] Artificial liposomes are primarily synthesized from amphiphilic phospholipids. The hydrophobic tails of these molecules tend to aggregate together, avoiding contact with the aqueous phase,

Figure 9. Schematic structure of liposome

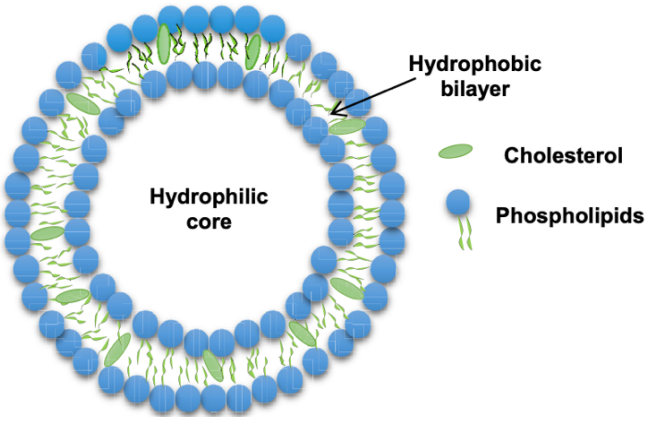

A spherical lipid bilayer enclosing an aqueous core. The lipid bilayer is typically made up of phospholipids, which have a hydrophilic head and hydrophobic tails.[124]

while the hydrophilic heads are exposed to the aqueous phase. This results in the formation of closed vesicles with a bilayer structure.

Due to its amphiphilic nature, liposomes can encapsulate both hydrophilic and hydrophobic drugs. When prepared from phospholipids, the lipid bilayer enhances biocompatibility, making biomimetic liposomes akin to biological membranes.[103] Griffin et al. demonstrated that the peritoneal retention time of resiquimod was prolonged by using 1,2-stearoyl-3-trimethylammonium-propane chloride (DSTAP) cationic liposomes for delivery, while the systemic absorption could be suppressed, compared to free resiquimod.[104] Mirahmadi et al. demonstrated that positively charged liposomes exhibit longer retention times within the peritoneal cavity compared to negatively charged liposomes, possibly due to the reduced macrophage uptake process.[105] However, they did not investigate whether this extended retention was caused by the aggregation of cationic liposomes, which could potentially render them more unstable. Furthermore, the issue of liposome instability, one of the most significant challenges, was not addressed in these studies. Liposome platforms used in the peritoneal cavity remain

susceptible to oxidation and hydrolysis of unsaturated bonds in unsaturated phospholipid, even the phospholipid is the most vital component for liposome delivery in the meantime.[106] Therefore, optimization of the current delivery system for IP treatment is needed.

Chapter 2. Preparation and Mechanism of PLGA Lipid Nanoparticle

2.1 Introduction

One of the biggest hurdles that impact the effectiveness of IP treatment is fast metabolization of administered chemotherapeutic agents. Drugs can be absorbed through the peritoneum and eliminated by the immune system within the peritoneal cavity prior to entering systemic circulation.[107-109] This significantly reduces the efficacy of the treatment and prevents a complete removal of unresectable malignant cells and increased risk of metastasis.[110-112] To address this limitation, it is necessary to develop therapeutic strategies that maintain a critical drug level within the tumor site.

To maximize the effectiveness of cytotoxic drugs across various drug delivery platforms, it is essential to understand the fate of nanomedicine post-administration, as it directly influences treatment outcomes. In IP treatment, drug delivery to peritoneal cavity tumors primarily occurs

Figure 10. Fate of nanomedicine following IP administration into the peritoneal cavity

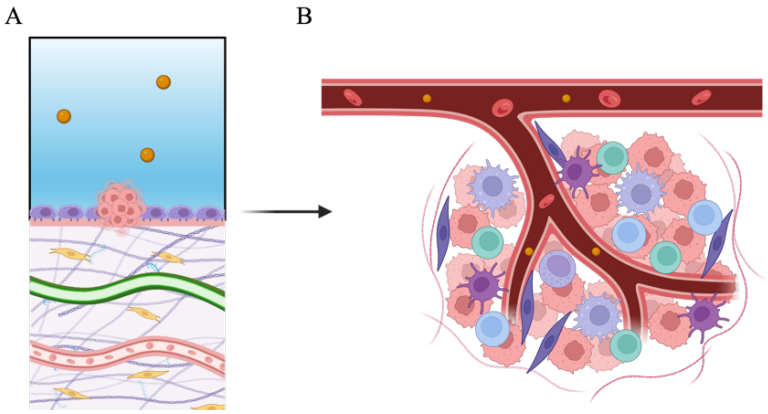

(A) Direct disposition route for nanomedicine to accumulate at the tumor site; (B) Indirect route for accumulation at the tumor site via systemic circulation after absorption by peritoneum. Adapted from "Extracellular Matrix" and "Tumor Microenvironment 2", by Biorender.com (2024). Retrieved from https://app.biorender.com/biorender-templates

through two pathways.[113, 114] The first involves direct disposition, wherein drugs diffuse or convect through the interstitial space within solid tumors due to spatial proximity (shown in Figure 10A and Figure 11). The second pathway is indirect, relying on the re-circulation of drugs absorbed from the peritoneal cavity via systemic circulation and deposit back into the tumor (shown in Figure 10B).

The size and physicochemical properties of the drug delivery platform are crucial to improve penetration into the tumor tissue, and therefore the effectiveness of IP treatment. Typically, nanosized delivery systems exhibit more efficient penetration within tumors compared to larger systems such as microparticles.[115, 116] However, this size advantage in penetration poses a dilemma because it can be fastly absorbed by the peritoneum and subsequently enter systemic circulation, where they are prone to metabolism and loss of function. In contrast, micro sized platforms tend to prolong drug retention in the peritoneal cavity. Whereas micro sized

Figure 11. Overview of perfusate after IP delivery

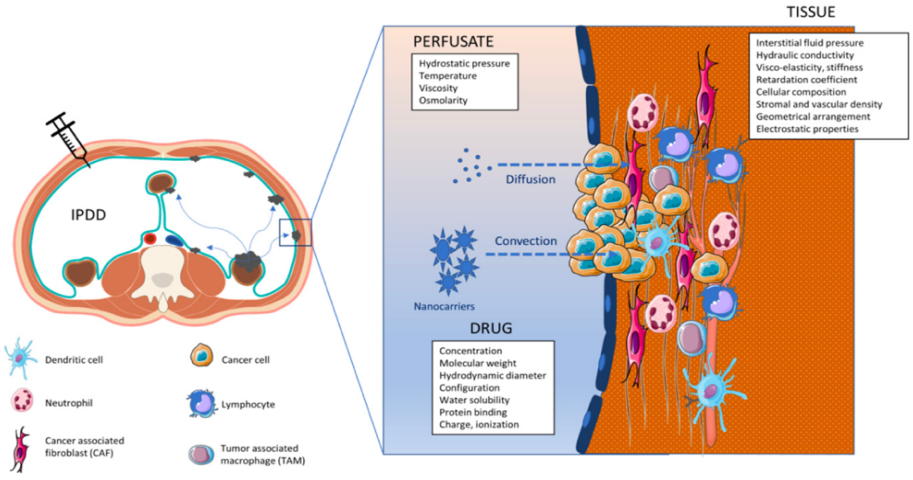

The movement of mass within the interstitial space is primarily governed by two mechanisms: convection, propelled by bulk fluid flow due to pressure differentials, and diffusion, stemming from concentration gradients.[114]

formulations have been shown to accumulate in lower part of peritoneal cavity due to gravity and may introduce higher cytotoxicity effect, the accompanying induced peritoneal adhesion and inflammation poses an additional fatal issue during the treatment.[107, 117, 118]

This variation in retention time among different platform sizes is primarily attributed to peritoneal absorption. In summary, striking the right balance between retention time, adhesion concerns, and efficacy as well as safety of drug delivery platforms in intraperitoneal treatment poses a significant challenge in clinical practice.

In the realm of drug delivery systems for IP therapy, both PLGA nanoparticles and liposomes have been utilized as a drug delivery platform. However, each of these methods presents limitations in clinical application.[119] The hydrophobicity of PLGA nanoparticles leading to rapid clearance by immune cells via opsonization process presents a hurdle to optimal duration of

Figure 12. Dynamics of Nanoparticle Clearance Through Opsonization, and Long Chain Polymer Evasion

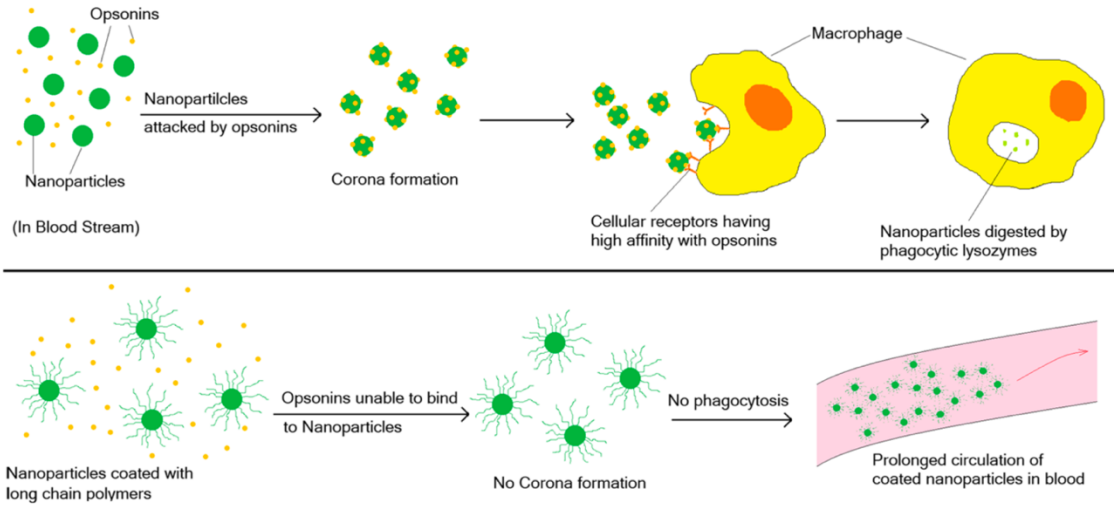

Opsonization process facilitate the recognition of external nanoparticles by immune system and get cleared at the end. However, the presence of a long-chain polymer coating can inhibit corona formation, thus extending the circulation time of the coated nanoparticles.[119]

particles in circulation. Opsonin proteins recognize and adhere to the surface of foreign particles upon their introduction into the body thus mediating their removal via phagocytosis by the immune system's reticuloendothelial system (RES).[119] Notably, serum complement C3 stands out as an important opsonin as it has a high binding affinity to the exposed surfaces of nanoparticle carriers (Figure 12).

Another drawback of PLGA nanoparticles is their tendency towards burst release behavior related to their hydrophobic characteristics. This burst release behavior refers to the phenomenon of PLGA nanoparticle-encapsulated drugs being abruptly released within a brief timeframe upon administration into an aqueous environment inside of the body cavity.[83, 120] This rapid release may be a result of drug leakage near the particle's surface during preparation, or from easy diffusion of poorly encapsulated drugs.[121] Burst release is an unwanted phenomenon when it comes to the cancer treatment that request concentrated release as it not only shortens the overall effective treatment duration of the drug but also results in the release of an excessive amount of the drug at an undesired location, leading to unnecessary toxicity.

Originally developed as models for biomembranes, liposomes have also expanded its application into clinically valuable drug carriers.[122] While their phospholipid bilayers mimic biological membranes, and are able to provide superior biocompatibility, they are also susceptible to disruption and degradation, rendering liposomes chemically and physically unstable. This fast degradation can lead to similar problems as PLGA-based materials when designated as an oncology treatment platform.[123, 124] Chemical instability arises from different chemical reactions such as ester bond hydrolysis or oxidation of unsaturated acyl chains, causing the breakdown of the lipid bilayer and compromising its structural integrity. Additionally, the exchange of bilayer-stabilizing lipids can contribute to the progressive membrane destabilization, where lipids with

larger headgroups, shorter chain lengths, and higher degrees of unsaturation promote lipid exchange process.[125, 126] Physical instability can manifest in variations in size and shape. Smaller liposomes are especially prone to reduced stability due to heightened curvature strain and surface energy. Furthermore, the aggregation as well as fusion of small vesicles can lead to their increased recognition by the RES,[124] speeding up the clearance from the bloodstream. Besides chemical instability, the degradation may also be accelerated by its physical instability, the mechanical release of drugs from the vesicles. Moreover, inconsistency in batch-to-batch reproducibility presents a significant challenge in real-world application to the widespread adoption of liposomes, and an easy-to-maintain formula that allows consistent manufacturing is in need.

Given the clinical imperative of finding an optimal balance between retention time, adhesion concerns, and drug delivery efficacy in IP therapy, and to address the limitations of both current PLGA nanoparticles and liposomes, PLGA lipid nanoparticles (PLGA lipid NP) emerge as a promising platform. This design (Figure 13) brings together, into one entity, the advantages of PLGA nanoparticles with characteristic of liposomes. The PLGA core facilitates the encapsulation of highly lipophilic paclitaxel with controlled release behavior. Meanwhile, the phospholipid layer on the PLGA surface prevents leakage of encapsulated substances and slows down polymer degradation by regulating water diffusion rates. Additionally, the outermost polyethylene glycol (PEG) circumvents the opsonization process extending the platform's *in vivo* circulation time.

Figure 13. Illustration of structure of PLGA lipid nanoparticle

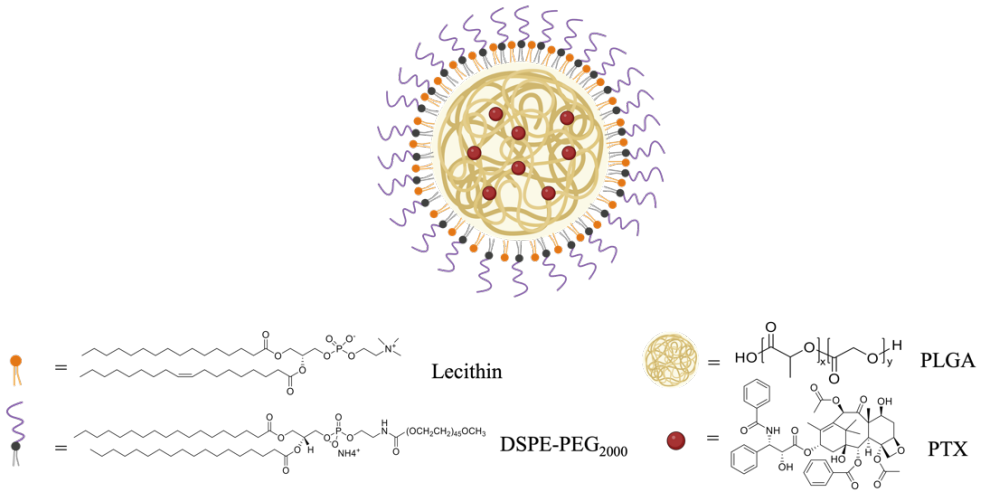

PLGA lipid NP structure, created with BioRender.com

The reason why the absorption of opsonins to traditional PLGA NP or liposome seems inevitable is that the opsonization process between PLGA nanoparticles and opsonins is spontaneous, facilitated via hydrophobic interactions.[127-130] Once hydrophobic substances are introduced into the aqueous medium, hydrogen bonds among water molecules are initially disrupted, forming an ice-like cage structure around the hydrophobic molecule. This structure exhibits a more organized arrangement compared to the free-water environment without the hydrophobic molecules. According to the Gibbs Free Energy equation:

$$\Delta G = \Delta H - T\Delta S$$

the relatively small ΔH stems from the enthalpic difference between newly formed and broken hydrogen bonds, while the considerably negative ΔS arises from the structured order resulting from water-hydrophobe interactions. Mathematic calculation gives $\Delta G > 0$, indicating a non-spontaneous process. However, when hydrophobic molecules aggregate rather than dispersing evenly in the water, the water molecules can reduce contact with the hydrophobic molecules,

leading to the disruption of hydrogen bonds within the ice-like cage structure and increasing overall disorder in the system. In this scenario, $\Delta H > 0$ and $\Delta S \gg 0$ gives $\Delta G < 0$, resulting in spontaneous aggregation of hydrophobic molecules in the aqueous environment, representing the essence of hydrophobic interactions between hydrophobic molecules.

The introduction of hydrophilic PEG chain can prevent the spontaneous absorption between hydrophobic part of opsonin proteins with the hydrophobic surface of PLGA NP, because of its high hydrophilicity, which can strongly bind with water molecules to form a hydration layer, thereby preventing the attachment of opsonin proteins.[131]

Upon administration of PLGA lipid NP into the peritoneal cavity, the PEG layer can prevent nanoparticles from absorption by plasma protein in peritoneal fluid, also the phospholipid layer facilitates penetration into tumors via a direct disposition pathway. Following absorption into the systemic circulation, the PEG layer prevents the platform from dysfunction by immune system and ensures the re-accumulation to tumor through the enhanced permeability and retention (EPR) effect, thereby optimizing the efficiency of the indirect pathway for tumor treatment.

Furthermore, owing to improved controlled release properties, the platform can replace the use of long-term catheter-mediated perfusion with a several discrete intraperitoneal injections, extending the treatment duration while minimizing therapeutic concentration during systemic circulation and peritoneal cavity.

To our knowledge, there are currently no organization/research groups employing the PLGA lipid NP platform for the treatment of peritoneal metastasis in colorectal cancer. This chapter demonstrates a revised method for preparing PLGA lipid NP to prevent particle aggregation during the concentration process. Additionally, the preparation method for the control group is introduced for later comparison of both *in vitro* and *in vivo* properties during IP treatment,

including paclitaxel (PTX) solubilized in a mixture of Cremophor EL and anhydrous ethanol as micelles (PTX-Cre-Micelle), or PTX solubilized in DMSO or anhydrous ethanol as free PTX. Detailed synthesis steps for preparing PLGA lipid NP, including nanoprecipitation mechanisms, synthetic temperatures for dispersing phospholipids, and concentration processes post-synthesis, are emphasized.

2.2 Experimental Details

2.2.1 Materials

All chemicals were used as received unless otherwise specified: PLGA (poly(D,L-lactide-co-glycolic acid), Resomer RG 505) with a 50:50 monomer ratio, ester-terminated, Mw 54,000-69,000 was purchased from Sigma-Aldrich. Soybean lecithin consisting of 90% phosphatidylcholine was obtained from Thermo Scientific Chemicals. DSPE-PEG_{2000}(1,2-diastearoyl-sn-glycero-3-phosphoethanolamine-N-[amino(polyethylene glycol)2000]) was purchased from Avanti Polar Lipids. Paclitaxel with 99.96% purity was obtained from MedChemExpress. Acetone (ACS Grade) was obtained from Fisher Scientific. Absolute Ethanol (200 Proof, Molecular Biology Grade) was obtained from Fisher BioReagents. Cremophor EL (Assay:99.52%) was purchased from MedChemExpress. Milli Q water was obtained by Milli-Q EQ 7000 Ultrapure Water Purification System connected with 0.22µm Millipak Filter. PVDF 0.45µm filter was purchased from Celltreat Scientific Products. Amicon Ultra-15 centrifugal filter with a molecular weight cutoff of 10,000 Da was purchased from Millipore.

2.2.2 Preparation of PLGA lipid NP

The development of the PLGA lipid NP platform involved adapting the nanoprecipitation technique developed by previous research groups.[132-134] This method utilized PLGA, soybean lecithin, and DSPE-PEG_{2000} to encapsulate paclitaxel. Initially, 0.84mg of soybean lecithin and 1.5mg of DSPE-PEG_{2000} were dispersed in a 9ml 4% ethanol aqueous solution within a 20ml glass vial, heated to 68°C for 3 minutes to form a homogenous lipid dispersion under 650rpm (C-MAG HS 7; IKA Works, Inc.). Subsequently, a solution containing 9mg of PLGA and 0.45mg of paclitaxel in 3ml acetone (with a 5 wt% drug loading: paclitaxel/PLGA mass) was added dropwise into lipid dispersion within 1 minute. The mixed solution was vortexed vigorously (mini vortexer, VWR Scientific Products) for 3 minutes followed by gentle stirring with 650 rpm for 2 hours at room temperature under a nitrogen flow to facilitate the complete evaporation of the organic solvent. The hybrid nanoparticle suspension was filtered by 0.45μm PVDF filter to remove the free paclitaxel. Finally, the filtered hybrid nanoparticles were washed and concentrated by an Amicon Ultra-15 centrifugal filter with a molecular weight cutoff of 10,000 Da. The final concentration was adjusted by LCMS analysis for the following experiments.
For scale-up, PLGA lipid NPs were synthesized in a 100ml round bottom flask with elliptical stir bar, maintaining a constant concentration with threefold volume. After multiple tentative trials testing, this approach is determined to maintain the optimal diameters for the hybrid nanoparticles and encapsulation efficiency. Specifically, 2.52 mg of soybean lecithin and 4.5 mg of DSPE-PEG_{2000} were dispersed in a 27 ml 4% ethanol aqueous solution within 100ml round bottom flask, heated to 68°C for 3 minutes to form a homogenous lipid dispersion under 500rpm.

Subsequently, a solution containing 27mg of PLGA and 1.35mg of paclitaxel in 9ml acetone (with a 5 wt% drug loading: paclitaxel/PLGA mass) was added dropwise into lipid dispersion within 3 minutes. The mixed solution was vortexed vigorously under 1000 rpm for 3 minutes followed by gentle stirring at 500 rpm for 2 hours at room temperature under a nitrogen flow to facilitate the complete evaporation of the acetonitrile organic solvent.

To prepare pure PLGA lipid NP without paclitaxel, only the PLGA was dissolved in acetone before the nanoprecipitation process.

To prepare pure PLGA NP, the acetone solvent with PLGA was added dropwise to pure aqueous solution without lipid mixture at 68°C.

2.2.3 Preparation of Cremophor EL/ethanol Micelle (Cre-Micelle) Formulation

The paclitaxel was dissolved in a mixed solvent comprising 50% Cremophor EL and 50% absolute ethanol, then further diluted with PBS to achieve the desired concentration before use.

2.2.4 Preparation of Free Paclitaxel Formulation

The paclitaxel was dissolved in DMSO or absolute ethanol, and then further diluted with water to achieve the desired concentration before use.

2.3 Result and Discussion

In order to design a better drug delivery platform to treat colorectal cancer peritoneal metastasis, it is essential to understand the chemical and physical properties of PLGA. The primary factors

affecting the biocompatibility and degradation rate of the PLGA include: 1) the ratio of lactic acid/ glycolic acid (LA/GA); 2) the functionalization of end groups; and 3) molecular weight. In this study, ester-terminated PLGA with a 50:50 monomer ratio, Mw 54,000-69,000, was utilized as the primary hydrophobic polymer model for forming the polymeric core of the nanoparticle, which encapsulated the model drug, paclitaxel.

The polymer poly (lactic acid) (PLA) has two distinct optical isomer forms: an optically active stereoregular isomer known as L-PLA and an optically inactive racemic form referred to as D,L-PLA. Due to the stereo-regularity of L-PLA, it exhibits semicrystalline characteristics, whereas D,L-PLA is amorphous because of the structural irregularities. Thus, the D,L-PLA is prioritized over L-PLA due to its capacity to promote a more homogeneous dispersion of drugs throughout the polymer matrix. On the other hand, poly (glycolic acid) (PGA) exhibits a high degree of crystallinity due to the absence of methyl side groups. Overall, even though crystalline PGA is present, PLGA synthesized from D,L-PLA and PGA remains amorphous. Gilding and Reed have claimed that PLGA formulations containing less than 70% glycolic acid exhibit an amorphous structure, facilitating the well-dispersion of drug within polymer core.[135, 136] Absence of methyl side group in GA makes it more hydrophilic than LA segment. Each segment in PLGA has its own limitation. The hydrophobic PLA constrains its biomedical utility due to low water sorption and long degradation time,[137] whereas, the hydrophilic PGA accelerates the water hydrolysis process. In this thesis, PLGA with a 50:50 monomer ratio is utilized as a polymer model to balance the effect from each segment[138] along with its widespread application and favorable properties in nanotechnology.[88, 139]

In polymer chemistry, end groups refer to the functional groups situated at the end of a macromolecule or oligomer. End group functionalization can influence various polymer

properties including degradation, self-assembly. In the meantime, it can further modify the polymer backbone with additional properties, such as ligand/antibody-receptor interaction[140-143] or fluorescence labeling.[144-147] Commercially available PLGA can be obtained with two distinct end-group functionalization options: end-capped or acid-terminated. End capping of PLGA entails the introduction of an alkyl ester as the terminal group, achieved by reacting PLGA with an alcohol group, thereby replacing the last acid group of PLGA with an ester group.[148] Acid-terminated PLGA denotes PLGA that lacks capping, leaving a free carboxylic group at the end of the polymer chain. The presence of ester end groups renders PLGA more hydrophobic compared to acid-terminated PLGA, potentially leading to a delay in its degradation, where acid-terminated PLGA will accelerate the autocatalysis process of PLGA degradation.[149-151] Additionally, the end-capped PLGA enhances the hydrophobic interaction with lipids during subsequent self-assembly processes. Moreover, it is well-documented that PLGA with higher molecular weights degrades at a slower rate than those with lower molecular weights. Overall, for this investigation, ester-terminated PLGA with a 1/1 lactide/glycolic acid monomer ratio and a moderately high molecular weight ranging from 54,000 to 69,000 was selected.

Soybean lecithin is the predominant phospholipid in mammalian cell membranes. It was utilized to form a lipid monolayer around the PLGA core to improve its biocompatibility. Additionally, PEG chain is covalently linked to 1,2-distearoyl-sn-glycero-3-phosphoethanolamine (DSPE), functioned as the representative hydrophilic polymer to create the "stealth" shell of the nanoparticle for extending its *in vivo* circulation time. DSPE also contributed as a lipid monolayer component in the nanoparticle system.

There are two common methods for nanoparticle fabrication. One is top-down method, the other is bottom-up method. In top-down approaches, bulk materials are divided into nanostructures

Figure 14. Preparation of PLGA lipid NP

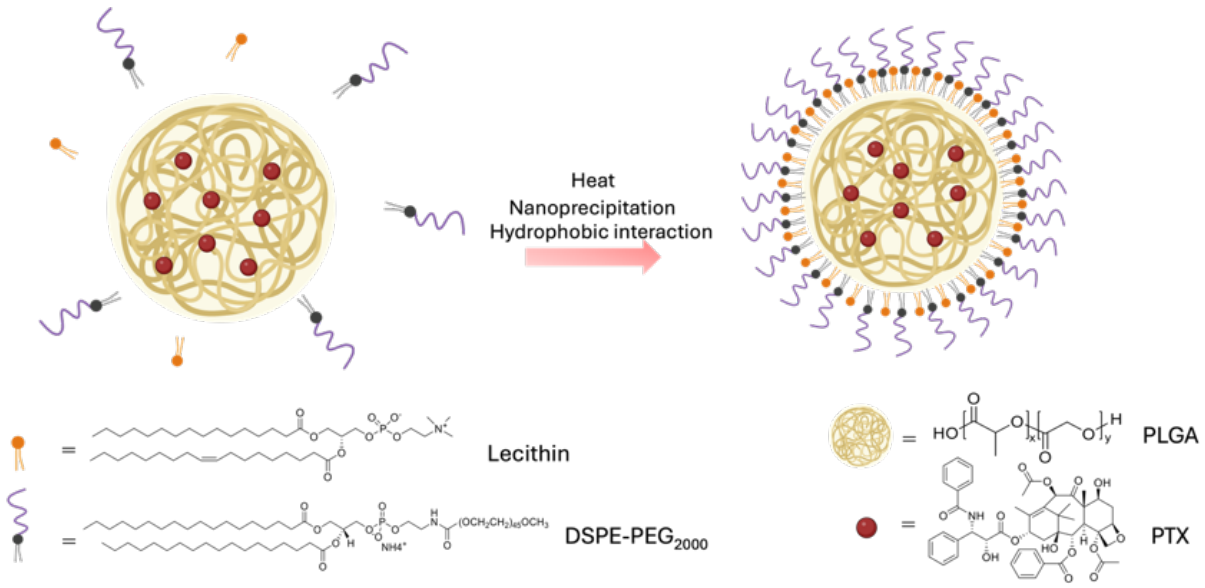

Synthesis route for PLGA lipid NP, created with BioRender.com

with predetermined shape and size without control at the atomic level over the individual atoms. In bottom-up strategy, desired nanostructures are constructed from fundamental components through different processes such as molecular recognition, nucleation, precipitation, chemical reactions, or self-assembly. These processes rely on the interactions between basic units to generate organized structures.[152] Illustrated in Figure 14, a modified nanoprecipitation method, employing a bottom-up approach along with self-assembly, was employed to fabricate hybrid nanoparticles composed of PLGA and lipids. Instead of using the conventional two-step method where preformed polymeric nanoparticles through nanoprecipitation are mixed with preformed lipid vesicles during thin-layer hydration method,[153-156] one-step method with higher efficiency and lower energy expenses are utilized.

In the single-step method, the formation of PLGA lipid NP relies on nanoprecipitation and self-assembly processes. Nanoprecipitation involves preparing water-miscible solvent (typically

Figure 15. Schematic diagram of the nanoparticle formation during the nanoprecipitation process

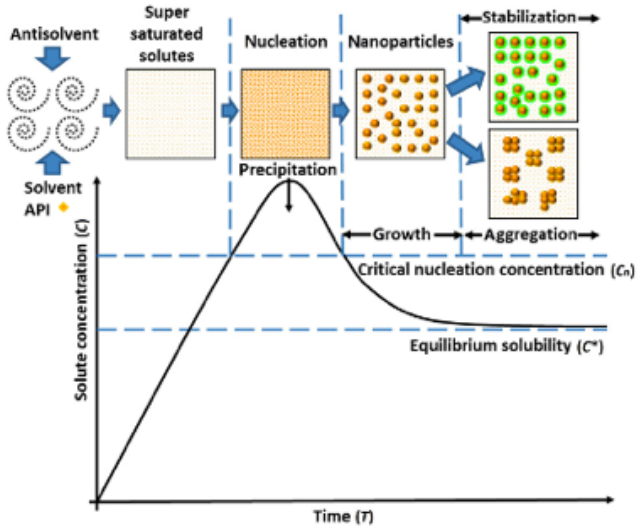

Nanoprecipitation initiates with the creation of supersaturation by rapidly blending a polymer solution with a non-solvent, prompting nucleation, followed by particle growth. Ultimately, aggregation may occur, resulting in the formation of nanoparticles suitable for drug encapsulation and other biomedical purposes.[159]

organic solvents capable of dissolving hydrophobic polymers and drugs like acetone or acetonitrile) and nonsolvent phases (typically water), followed by gradually adding one phase to another while moderately stirring. In this thesis, two phases were prepared: one is organic phase, that contains water-miscible acetone to dissolve PLGA and paclitaxel, the other is aqueous phase, that contains dispersed lipid mixture. The organic phase, containing PLGA and paclitaxel dissolved in acetone, was added dropwise to the heated aqueous solution containing the lipid mixture under stirring. By mixing the two phases, high supersaturation condition for PLGA and paclitaxel was created, it is unstable and will initiate their nucleation process. The nuclei are the initial building blocks for the future formation of PLGA NP. As acetone evaporate, more PLGA

solute will continue to deposit onto the growing nuclei, causing them to increase in size, with paclitaxel becoming entrapped within the polymer matrix through partitioning into the PLGA phase during nanoparticle formation via hydrophobic interactions between PLGA and paclitaxel. As the nanoparticles continue to grow, they may encounter each other and lead to aggregation.[157] Without using surfactant in the organic phase, the emulsification process will not happen, leading to a specific nanosphere structure for the nanoparticles, rather than a nanocapsule with polymer shell and void core (Figure 15).[158]

After the formation of a hydrophobic core to entrap the poorly water-soluble paclitaxel within the PLGA polymeric matrix, lecithin and DSPE-PEG_{2000} self-assemble around the PLGA core, surrounded by the outer layer of the PEG shell via hydrophobic interaction. This process is facilitated by hydrophobic interactions, wherein hydrophobic substances in an aqueous environment tend to aggregate while avoiding water molecules.[159-161] From a thermodynamic perspective, these hydrophobic interactions are favorable ($\Delta G<0$), indicating this aggregation between hydrophobes is spontaneous based on the equation $\Delta G=\Delta H-T\Delta S$.[162] Hydrophobic interactions play a crucial role as nonspecific interactions within biological systems. For instance, they contribute to the formation of lipid bilayers, where hydrophobic tails aggregate inwardly while hydrophilic heads face the outer aqueous environment,[163] and facilitate protein folding by burying hydrophobic groups within the protein structure.[164, 165] Both lecithin (a major component of phosphatidylcholine) and DSPE are phospholipids, possessing amphiphilic properties with hydrophobic fatty acid chains and hydrophilic moieties. Particularly, the hydrophobic acyl chains of phosphatidylcholine and DSPE interact with the PLGA core, anchoring the lipid mixture onto its surface and forming a lipid monolayer fence around the

polymeric core. This is followed by the extension of PEG segments from DSPE to create the outermost shell.

To form a homogeneous lipid mixture dispersion to facilitate the self-assembly process between PLGA core and phospholipid, the lipid mixture in 4% ethanol aqueous solution needs to be heated to ~65-70^{o}C, which is above the lipid transition temperature. Lipids have different properties that can switch in between. They can be in a liquid (also called liquid crystalline phase) or a solid (also called gel) phase depending on the conformation alternation of their two acyl chains. Although not all lipids have two acyl chains, the phospholipids and DSPE-PEG$_{2000}$ that I used in this dissertation both comprise two acyl chains. Therefore, we will focus on this specific feature.

At the phase transition temperature or melting temperature (T_c or T_m), lipids can transform between the liquid and gel phases. Above the T_m, lipids exist in a liquid phase with disordered

Figure 16. Energetics of rotation in ethane and butane

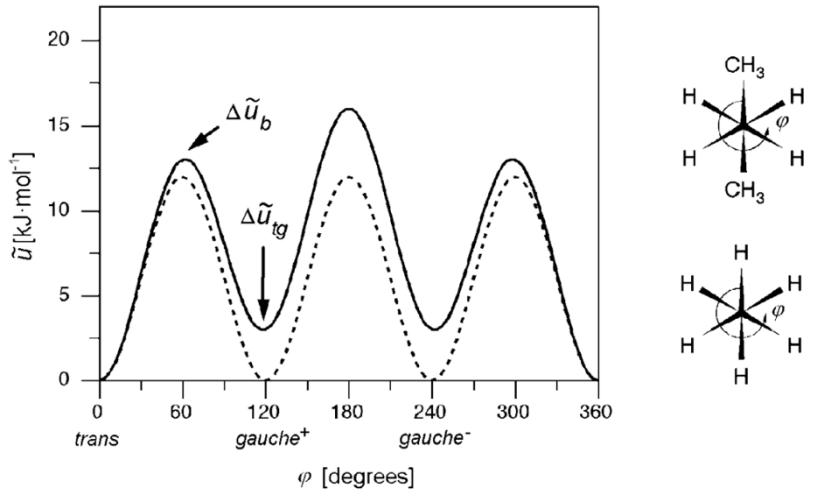

Potential energies associated with the rotation of the central C-C bond for ethane (broken line) and butane (continuous line). The sketches show the two molecules in views along the C-C bond.[168]

and increased thermal motion. In this state, the high kinetic energy of individual lipid molecule has greater flexibility and internal rotation of the acyl chains. There is a propensity for gauche conformation to prevail, leading to increased kinks and curvature in the acyl chains and make the acyl chains more flexible and less packed (In this context, ethane and butane were used as analogies for long acyl chains Figure 16 depicts the potential energy alongside the corresponding Newman projection[166]. When the temperature is below Tm, lipids exist in its gel phase, where individual lipid lose kinetic energy, causing their acyl chain tails to become fully extended, rigid, and straight. During transition from the liquid phase to the gel phase without energy input, most of the acyl chain tails undergo an isomerization from gauche conformation to trans conformation because the trans conformation has the lowest potential energy and is the most stable, prompting the acyl chains to remain in this configuration spontaneously without requiring external energy. During this process, acyl chains of lipid become stiffer and fully extended without kinks. The lipid head groups become more tightly packed. Consequently, applying heat to the lecithin and DSPE lipid mixtures in aqueous solution can make them more flexible with more kinks characteristic, facilitating the attaching process onto surface of PLGA core.

In addition to the lipid phase transition behavior, lipid/PLGA weight ratio (L/P ratio) also need to be considered since it significantly influences the optimization of nanoparticle pharmacokinetic properties *in vivo*. Zhang and his team showed that nanoparticles with a lipid/polymer ratio of 10-20% possess favorable characteristics for drug delivery applications with 70-80 nm size and -30 to -35 mV ζ potential.[134, 167] This choice is based on the interplay between the L/P ratio and nanoparticle size,[168] as well as the lipid-PEG fraction to ensure the colloidal stability through steric stabilization provided by the PEG chain.[169] For instance, PLGA NP without lipid coating form aggregation in PBS, even lipid coated PLGA NPs with 9:1 ratio between lecithin and

DSPE-PEG_{2000} were unstable and easily form 2 μm aggregation as well.[132] In this dissertation, we used 25% lipid-to-polymer (L/P) ratio, consisting of 0.25mg/ml lecithin and approximately 67% DSPE-PEG_{2000} in the lipid formulation to synthesize PLGA lipid NP. The 25% L/P ratio aligns with the optimal range identified in previous research for achieving nanoparticle sizes with approximately 100nm, which is associated with prolonged blood circulation and a relatively low rate of clearance by the mononuclear phagocyte system.[168] Under this ratio, sufficient lipid and PEG chains can cover the hydrophobic core of PLGA, stabilize the hybrid nanoparticle respectively. Otherwise, when the L/P ratio is too high, lecithin concentration will above the critical micellar concentration (CMC) of lecithin (0.4mg/ml, data from manufacturer) and lecithin liposomes may form. On the other hand, when the L/P ratio is low, inadequate lipid will fail to fully cover the PLGA core and compromise the system stability within biological environment.

After finishing the preparation of PLGA lipid NPs, we reconsidered the commonly employed concentration technique. In this method, the NP solution is centrifuged with some residual organic solvent to eliminate solubilized free PTX, followed by washing the NP solution with water. [132, 170] We observed that even small amount of organic solvent could potentially promote the fusion of PLGA lipid NPs, which make aggregation eventually. Instead, we opted for nitrogen purging to thoroughly eliminate the organic solvent before the concentration process. Subsequently, by filtering out the free PTX using a 0.45μm filter, we successfully removed the free PTX without causing clog in the concentrator during the concentration step.

Given the hydrophobic nature of PTX, Cremophor EL and ethanol (in a 50:50 ratio, v/v) were used to create micellar structures (CMC~0.02%) for encapsulating PTX to improve its solubility.

This thesis employs the same preparation method, with subsequent dilution in PBS before *in vitro* or *in vivo* experiments.

2.4 Conclusion

In this chapter, we emphasized the need for strategies to enhance the drug accumulation within tumor in colorectal cancer peritoneal metastasis during chemotherapy IP treatment. To increase the efficacy of IP therapy, it is important to understand the fate of nanomedicine post-intraperitoneal administration, where drugs primarily deliver through the direct disposition facilitated by spatial proximity and indirect pathway by systemic circulation after absorbing from peritoneum.

However, the challenges associated with each pathway are significant and become obstacles in maximizing the treatment efficacy. In the direct disposition pathway, only the drug delivery platform can remain intact when interacting with the peritoneal fluid in peritoneal cavity, which contains plenty of plasma proteins and abundant macrophages, they can penetrate tumor tissue after administration. Failing to avoid the recognition and clearance by the immune system in the opsonization process will potentially compromise their therapeutic effect dramatically. On the other hand, during indirect pathway, nanosized drug delivery platforms have risk with metabolism during systemic circulation and the inability to recirculate back to tumor sites via the enhanced permeability and retention (EPR) effect. It turns out challenging to identify an optimal window to balance the retention time, adhesion concerns, and drug delivery efficacy since each drug delivery platform candidate may not meet all requirements simultaneously.

While micro sized particles have longer retention times compared to nanosized systems, the peritoneal adhesion induced by microparticles can deteriorate the treatment process. Herein, we

focused on nanotechnology in this dissertation. As one of the most popular nanomedicines in colorectal cancer peritoneal metastasis, both PLGA nanoparticles and liposomes have shown the barriers for further adoption. PLGA nanoparticles encounter issues with opsonization recognition due to hydrophobicity and burst release behavior. Whereas, liposomes face challenges related to chemical and physical instability, resulting in rapid drug release and reduced stability.

By synergistically integrating the complementary characteristics of both PLGA nanoparticles and liposomes, PLGA lipid NP emerge as a promising platform to enhance clinical performance during IP treatment.[169] PLGA lipid NP can firstly maintain fundamental integrity based on the PLGA core, while providing a controlled drug release profile that mitigates burst release behavior from lipid layer. Additionally, they may exhibit higher biocompatibility and prolonged circulation time since lipid layers can not only facilitate tumor penetration, but also prevents opsonization, enhancing retention both within the peritoneal cavity and in systemic circulation.

After selecting the drug delivery candidate, we thoroughly investigated the complex physicochemical properties of each component within the nanoparticle. The detailed examination allowed us to understand the corresponding roles in the formation of nanoparticles for efficiency drug delivery during IP treatment with high encapsulation efficiency, increased stability, improved drug release profile etc. These examinations include the rationale about LA/GA ratio, end group functionalization, molecular weight, phospholipid function, PEG chain property and L/P ratio, applying insight on optimizing the biocompatibility, degradation rate, hydrophobicity, and drug encapsulation efficiency of PLGA-based nanoparticles for IP treatment.

During the fabrication process of the nanoparticles, we utilized modified nanoprecipitation method and improved concentration process to facilitate nanoparticle formation by self-assembly for controlled nanoparticle formation while prevent further aggregation after synthesis. Soybean

lecithin and DSPE-PEG_{2000} facilitate the formation of a lipid monolayer around the PLGA core with optimal L/P weight ratio, enhancing biocompatibility and extending circulation time *in vivo*. We aimed to develop a nanoparticle system as an initial model for effective drug delivery used for IP treatment. To our knowledge, this is the first study to leverage PLGA lipid hybrid NP for treating the colorectal cancer peritoneal metastasis. This system will be evaluated with the current Taxol formulation, prepared following traditional methods, and free paclitaxel without carriers in following comprehensive *in vitro* and *in vivo* studies.

Chapter 3. Physicochemical Characterization and *In Vitro* Profile Study Across Various Formulations

3.1 Introduction

Before subsequent *in vitro* and *in vivo* experiments, the first experiment that needs to be conducted is to confirm the effective coating of the lipid layer on the PLGA NP, as part of the development of new nanosized drug delivery platforms. Dynamic light scattering (DLS), zeta potential analysis, and transmission electron microscopy (TEM) were utilized to validate both the narrow size distribution and the lipid layer coating on the nanoparticles.

The complex interaction between formulations and biological environment in peritoneal cavity may cause interferences and influence the real impact of administered formulation. It is crucial to conduct thorough screenings about their potential biological impacts under simulated biological conditions before any *in vivo* experiments. Because of the cheap and easy setup, these preliminary assessments such as the colloidal stability study, release profile and cell-based assays, can efficiently provide essential guidelines or references for setting up the subsequent *in vivo* experiments.[171]

In vitro release experiment is an important measurement to verify our assumption on the improved drug release profile and possibility to avoid using catheters in the future application. By comparing the *in vitro* release profiles between PLGA lipid NP and PLGA NP, we can evaluate the effectiveness of the lipid layer on drug release kinetics. This impact potentially dominates two aspects, in terms of delivering and sustained releasing of PTX to tumors. Firstly, with the protection of PLGA lipid NP, higher drug concentrations can be used without causing extreme local toxicity. This may also extend the effective lifetime of formulation and circumvent

the traditional long-term perfusion. Secondly, the enhanced protection of the PLGA lipid platform can minimize the drug leakage during systemic circulation, which maximizes the accumulation of active drugs at the tumor site after systemic circulation. To better predict the *in vivo* behavior of PLGA lipid NP, we elucidated the polymer degradation mechanisms behind the drug release *in vitro*. Understanding *in vitro* release profile not only demonstrate the impact of the lipid layer on drug release, but also facilitate the design of optimal drug delivery systems for enhanced therapeutic outcomes.

In addition to the physicochemical property characterization that only focuses on material perspective, the *in vitro* cell-based experiment is the initial assessment to compare the cytotoxicity potency between PTX-PLGA lipid NP and current clinical formulations against colorectal cancer cells before the final *in vivo* study in a living organism. The experiment results represent the corresponding toxicity of treatment with each formulation through cell viability monitoring, providing a solid evaluation of suitability and dosage requirement for each formulation during *in vivo* experiment development.

To further study the interaction between various carriers and cells during cytotoxicity experiments, the cellular uptake experiment can reflect the role that each carrier played during cytotoxicity experiments. By quantifying the amount of dye internalized by cells through the carrier over time, we may have clue about the uptake mechanism of each carrier.

The previous size testing is not reliable enough to well demonstrate the real situation, where the drugs will interact with complex aqueous mixture including serum, protein, macrophages etc., in both the peritoneal cavity and systemic circulation during IP treatment. This interaction may affect the physiochemical properties such as size, aggregation, and final efficacy. In stability testing, by subjecting designed drug formulations under simulated physiological conditions

outside of a living organism, researchers can quickly gain valuable information on optimization of formulation parameters, prediction of *in vivo* behavior and assurance of product quality.
The defining feature of PLGA lipid NP lies in their lipid/PEG layer coating. This dual-layered structure plays a fundamental role in stability among biological environment by shielding the platform from protein attachment in plasma and peritoneal fluid. Through *in vitro* stability testing, by monitoring the size alterations in drug formulation, we can gauge the resilience of the formulation under diverse biological environments. Such experiment ultimately propels the translation of nanoparticle-based technologies from laboratory prototypes to clinical applications.

3.2 Experimental Details

3.2.1 Materials

All chemicals were used as received unless otherwise specified: Uranyl acetate dihydrate (Assay: 98.0-102.0%) was purchased from Thomas Scientific. Milli Q water was obtained by Milli-Q EQ 7000 Ultrapure Water Purification System connected with a 0.22µm Millipak Filter. Slide-A-Lyer MINI Dialysis Device with a molecular weight cutoff of 10,000 Da, volume 2ml was purchased from Thermo Scientific. Dulbecco's Phosphate Buffered Saline (PBS, Modified, without calcium chloride and magnesium chloride) powder was purchased from Gibco from Thermo Fisher Scientific. Acetonitrile (HPLC grade) was purchased from Fisher Scientific. MTT (Thiazolyl Blue/ Terazolium Bromide, Purity>98%) was purchased from Dot Scientific. HCT116 cell line was obtained from ATCC (isolated from the colon of an adult male with colon cancer). Firefly Luciferase Lentivirus (G418, Hygromycin and Puromycin) was purchased from BPS Bioscience. Nutrient Mixture F-12 Ham (with L-glutamine, without sodium bicarbonate)

powder was purchased from Gibco from Thermo Fisher Scientific. Dulbecco's Modified Eagle Medium (DMEM)-high glucose (with L-glutamine, pyridoxine hydrochloride, without sodium pyruvate, sodium bicarbonate) powder was purchased from Gibco from Thermo Fisher Scientific. Sodium hydroxide (ACS reagent, ≥97.0%) was purchased from Sigma-Aldrich. Hydrochloric Acid (ACS Plus, 36.5-38%) was purchased from Fisher Scientific. Sodium bicarbonate (powder, Bioreagent) was purchased from Sigma-Aldrich. Penicillin-streptomycin was purchased from Gibco from Thermo Fisher Scientific. Bovine serum albumin (BSA) was purchased from Siama-Aldrich. Heparin sodium salt (170 units/mg; M.W.: 15000-19000) was purchased from J&K. Fetal bovine serum (FBS) was purchased from Gibco from Thermo Fisher Scientific. Dimethyl Sulfoxide (DMSO, cell culture reagent) was purchased from Chem Cruz. Nalgene™ Rapid-Flow™ Sterile Disposable Filter Unit was purchased from Thermo Fisher. PVDF 0.45μm filter was purchased from Celltreat Scientific Products. Alexa Fluor 488 annexin V was purchased from Invitrogen from Thermo Fisher Scientific. Propidium Iodide was purchased from Invitrogen from Thermo Fisher Scientific. Versene solution was purchased from Gibco from Thermo Fisher Scientific. 0.25% Trypsin-EDTA was purchased from Gibco from Thermo Fisher Scientific. Coumarin-6 was purchased from Sigma-Aldrich. All autoclave processes were conducted via steam sterilizer from Primus Sterilizer Company.

3.2.2 Dynamic Light Scattering (DLS) Analysis

The size of hybrid nanoparticles and zeta potential was determined from three repeat measurements by DLS using zetasizer (NanoZS, Malvern, UK). Before concentrating the synthesized hybrid nanoparticles, the dispersant was established as water with a viscosity of

0.8872cP, a refractive index of 1.330, and a dielectric constant of 78.5, 1ml of diluted sample solution was placed into the disposable plastic cuvette for size measurement, and into the disposable folded capillary cells for zeta potential measurement.

3.2.3 Transmission Electron Microscopy (TEM) Analysis

Particle morphology was visualized by TEM (FEI Tecnai G2 F30 300kV Super Twin Electron Microscope). Before concentrating the synthesized hybrid nanoparticles, the diluted particle sample solution was dropped onto a 400-mesh carbon-coated grid, after washing three times with DI water. Samples on the grid were blotted away after 10 min and the grids were negatively stained for 10min at room temperature with freshly prepared 1wt% uranyl acetate solution. The uranyl acetate solution was blotted away, and the grids were air-drying before imaging.

3.2.4 Characterization of Drug Loading and Encapsulation Efficiency

An aliquot of the freshly prepared and concentrated nanoparticle solution was extracted, dissolved, and diluted in acetonitrile to fully dissolve PLGA and the released paclitaxel. The paclitaxel content was quantified by reversed-phase liquid chromatography-mass spectrometry (LC-MS, Agilent 6540 Quadrupole Time-of-Flight (Q-Tof) Accurate MS-MS with 1290 UHPLC).

Drug loading (%) was calculated as:

$$\frac{\text{Weight of drug in nanoparticle}}{\text{Weight of nanoparticle}} \times 100\%$$

Encapsulation efficiency was calculated as:

$$\frac{\text{Weight of drug in nanoparticle}}{\text{Weight of initial drug added}} \times 100\%$$

3.2.5 *In Vitro* Release Study of PTX-PLGA lipid NP and PTX-PLGA NP

A concentrated nanoparticle solution (100µl, 0.2mg/ml concentration) was introduced into the integrated membrane of a Slide-A-Lyer MINI Dialysis tube with a molecular weight cutoff of 10,000 Da. This membrane was dialyzed in 50ml of PBS buffer at 37°C with gentle agitation. The PBS buffer was replaced every 24 hours throughout the dialysis procedure. At specified intervals, nanoparticle solutions were retrieved from the membrane, mixed with acetonitrile to dissolve the nanoparticles, and then diluted tenfold. The resulting content of free paclitaxel from each interval was analyzed using LC-MS equipment.

3.2.6 LC-MS Analysis of Paclitaxel

Quantitative analysis of PTX was conducted by LC-MS, including a 1290 Infinity UHPLC system, an Agilent 1200 Series autosampler, an Agilent G1960-80040 model pump, and a 6540 UHD Accurate-Mass Q-TOF LC/MS system. A ZORBAX RRHD Eclipse Plus C18 analytical column (2.1×100nm, 1.8µm) was used. A mobile phase comprising 0.1% formic acid in water-acetonitrile (40:60, v/v) was pumped at a rate of 0.2ml/min under 40°C, with a runtime of 6 minutes. After each sample run, a 3-minute wash step using 0.1% formic acid in water-acetonitrile (5:95, v/v) was conducted for 2 minutes, before returning to the initial mobile phase condition for the next sample run.

The column eluate was analyzed using a 6540 UHD Accurate-Mass Q-TOF MS-MS spectrometer operating in positive electrospray mode (ESI+) to detect the 854.3384 m/z peak for PTX. By maintaining the nozzle voltage at 1000V and varying the fragmentor voltage from 50V to 250V, the optimal fragmentor voltage for obtaining the maximum integrated area of the EIC peak of PTX can be determined. The fragmentor voltage was set at 190 V with two reference mass corrections (m/z=121.050873, m/z=922.009798).

Data acquisition was performed with the Agilent MassHunter Workstation. Standard curves for PTX were generated by plotting the integrated area of the extracted ion chromatogram (EIC) peak against the known concentration of standard samples containing 0.01, 0.005, 0.002, 0.001, 0.0005, 0.0002, 0.0001, 0.00005, 0.00002 mg/ml PTX.

3.2.7 DMEM/F-12 Medium Preparation

Two packets of F12 powder and two packets of DMEM powder were added into 3.5 liters of Milli-Q water. Then 4.8 grams of sodium bicarbonate and 40 milliliters of 100X Penicillin-streptomycin powder were added. After stirring for 20 minutes, the pH was adjusted to 7.2. The total volume was then adjusted to 4 liters with Milli-Q water. Subsequently, 444 milliliters of FBS were mixed into the solution. Finally, the medium underwent sterilization in the cell culture room's hood using the Nalgene™ Rapid-Flow™ Sterile Disposable Filter Unit.

3.2.8 Transduction of HCT116 Cells

HCT116 cells were seeded in a 12-well plate to achieve ~70% confluency the following day before being combined with Firefly Luciferase Lentivirus stock. To initiate infection, the

medium was aspirated and replaced with fresh complete medium containing a final concentration of 5 μg/ml polybrene reagent. The mixture was gently agitated, and the lentivirus stock was added to achieve the desired MOI of 5. The cells were then incubated at 37°C with 5% CO_2 overnight. The following day, the medium was replaced with fresh complete medium and incubated for an additional 2 days. Prior to antibiotic selection, the effective concentration of puromycin necessary to kill the majority of HCT116 cells (same cell amount during infection) was determined using a serial dilution method to prepare medium with varying concentrations of fresh puromycin. Finally, the resistant colonies could be identified.

3.2.9 Cell Culture

The HCT116-Luc cells were cultured in DMEM-F12 medium under standard conditions, maintained at 37°C in a humidified atmosphere with 5% CO_2, and passaged every two days using trypsin-EDTA solution.

3.2.10 Cellular Viability Assay

To determine the cytotoxicity of PTX-PLGA lipid NP, PTX-Cre Micelle, and Free PTX (in DMSO), MTT (3-[4,5-dimethylthiazol-2-yl]-2,5 diphenyl tetrazolium bromide) assay was used with HCT116-Luc cell. HCT116-Luc cells were seeded onto 96-well plates at a density of 2000 cells per well. After incubation for 24 hours in 100 μl of medium, the medium was replaced with three formulations at various concentrations in fresh medium in triplicate. The cells were further incubated for 48 hours. After incubation, the medium was replaced with 100 μl fresh medium to prevent interference in subsequent assays. Subsequently, 10 μl 5 mg/ml MTT solution was added

to the medium, and the cells were again incubated at 37°C for 4 hours. Finally, 200 µl of DMSO was added to each well to dissolve the formazan crystals, the mixture in each well was thoroughly mixed with pipette to ensure complete solubilization. MTT absorbance was measured at 570 nm, with background noise subtracted at 630 nm, using a Synergy Neo HST Plate Reader (Agilent). The higher MTT absorbance values, after background subtraction, indicate the higher cell viability and lower cell cytotoxicity. The results were plotted using Origin software.

3.2.11 Medium-Containing Formulation Preparation

To produce paclitaxel in three distinct formulations (PTX-PLGA lipid NP, PTX-Cre Micelle, and Free PTX) at varying concentrations, a stepwise serial dilution was conducted. Basically, fresh medium was added to prepared stock solutions from PTX-PLGA lipid NP, PTX-Cre Micelle, and free PTX to prepare desired concentration. Initially, a defined volume of the stock solution was combined with a specific volume of medium to attain the highest desired concentration in an Eppendorf tube. Subsequently, a portion of this mixture was transferred to the next tube for further dilution with medium to achieve the desired concentration, and this process was repeated successively until the most diluted sample.

3.2.12 Qualitative Cellular Uptake Assay

HCT116-luc cells were plated in 12-well culture plates at a density of $1*10^5$ cells per well and incubated overnight. The impact of various drug delivery carriers on cellular uptake efficiency was examined by incubating HCT116-luc cells with coumarin-6 (C6) encapsulated PLGA lipid nanoparticles (C6-PLGA lipid NP), coumarin-6 encapsulated Cre micelles (C6-Cre Micelles),

and free coumarin-6 in DMSO (Free C6) (0.15 μg/ml equivalent to C6) for 1 hour.[172] After incubation, the culture medium, extracellular particles, and free C6 that was outside the cells were removed by triple washing with PBS. Subsequently, the cells were detached by trypsin and suspended in a 0.5 wt% BSA PBS solution for qualitative flow cytometry analysis on fluorescent signal of C6.

The synthesis method for C6-PLGA lipid NP closely followed the protocol outlined in Chapter 2 for PTX-PLGA lipid NP, with the substitution of PTX with C6.

3.2.13 Stability Study

To assess the influence of the lipid layer on colloidal stability, PLGA lipid NPs, PLGA NPs (as a control), and Cre micelle were incubated in various solutions: a 5 wt% BSA solution, a 5 vol% plasma solution (derived from nude mice used in later *in vivo* experiments, with heparin solution at concentrations of 10mg/ml or 1700 units/ml), a 5 vol% FBS solution, and PBS. The incubations were carried out in a capped glass vials at 37°C, with gentle stirring at 180 rpm in an incubator (Benchmark Scientific Incu-Shaker 10L Shaking Incubator). At designated intervals, samples were collected from the solutions for size measurement using disposable plastic cuvettes and DLS and returned to their respective glass vials for incubation after DLS test. Each measurement was conducted in triplicate at room temperature.

To conduct *in vitro* stability assessments of PTX encapsulated formulations in a biological milieu, PTX-PLGA lipid NPs and PTX-Cre micelle were incubated in solutions containing 5 wt% BSA, 5 vol% plasma (obtained from nude mice designated for subsequent *in vivo* experiments, supplemented with heparin solution at concentrations of 10mg/ml or 1700

units/ml), and 5 vol% FBS, respectively. These incubations were carried out at 37°C with gentle stirring at 180 rpm, maintaining a concentration of 0.5mg/ml, within an incubator (Benchmark Scientific Incu-Shaker 10L Shaking Incubator). At designated intervals, samples were collected from the solutions for size measurement using disposable plastic cuvettes and DLS and returned to their respective glass vials for incubation after DLS test. Each measurement was conducted in triplicate at room temperature.

3.3 Result and Discussion

3.3.1 DLS and zeta potential

DLS showed monodisperse pure PLGA NP and the PLGA lipid NP with Z average hydrodynamic diameters (D_h) of 81.3±0.7nm and 101.1±0.6nm, respectively, and the polydispersity indices of 0.09 and 0.1, respectively (Figure 17). In DLS analysis, the initial data is analyzed with the autocorrelation function via the cumulant approach and exponential fitting expression. This process yields the intensity-weighted Z average size and polydispersity index (PDI), where PDI is calculated as the square of the standard deviation divided by the mean.

Figure 17. DLS of PLGA lipid NP and PLGA NP

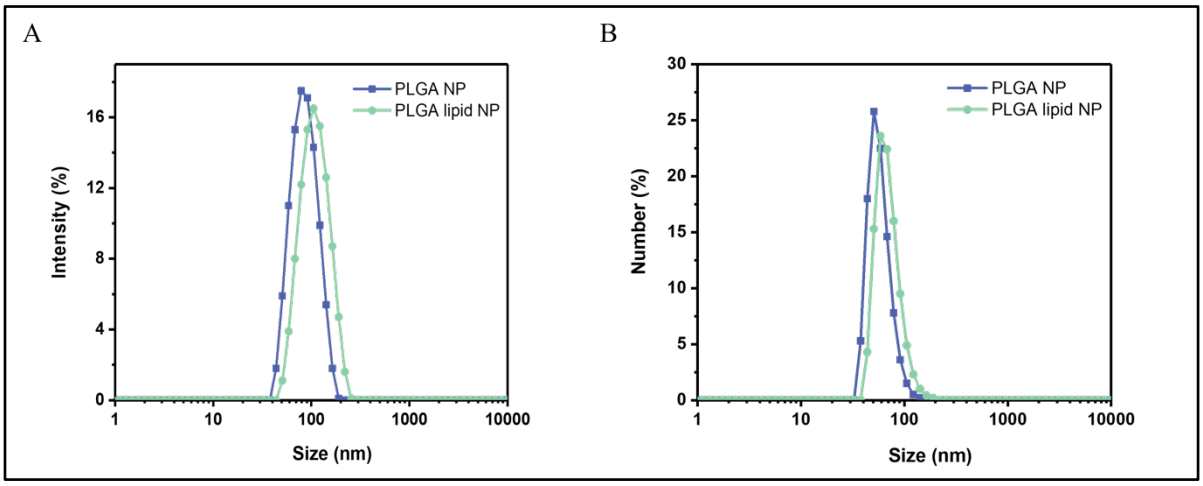

(A) Intensity distribution of PLGA NP and PLGA lipid NP (B) Number distribution of PLGA NP and PLGA lipid NP. Dark blue: PLGA NP, Green: PLGA lipid NP

In polymer and nanoparticle characterization, there are mainly two definitions of polydispersity. In polymer science for Gel Permeation Chromatography (GPC) or Size Exclusion Chromatography (SEC) analyses, the molecular weight distribution is described by mass weighted molecular weight (Mw) and number weighted molecular weight (Mn). When PDI = Mw/Mn equals to 1, both Mw and Mn would be the same, demonstrating the uniformity of the polymer sample. In nanoparticle field, DLS is used to describe the size difference among the sample, where PDI = standard deviation/mean. For a perfectly uniform sample, the standard deviation should be 0, leading PDI = 0. Samples exhibiting a PDI value below 0.1 are considered monodispersed, both PLGA NP and PLGA lipid NP were considered as monodispersed in our study.[173-175]

Based on the data from DLS, PLGA lipid NPs exhibited a slightly larger size compared to pure PLGA NP, attributed to the lipid layers on the surface of the PLGA lipid NP. Moreover, the surface modification of the PLGA polymeric core by lipid layers was confirmed by measuring

the surface ζ potential (refer to Figure 18). Due to the low ionization of ester end group of the PLGA, the zeta potential of the bare PLGA NP was close to neutral.[176, 177] This contrasts with acid-terminated PLGA nanoparticles, which exhibit a more negative ζ potential (~-49mV).[178, 179] Upon the addition of neutral lecithin (major component phosphatidylcholine, possessing additional positively charged groups, thus rendering it neutral) and anionic DSPE-PEG2000 (where the ammonium cation is ionized, leaving an anionic phosphate group at neutral pH environment[180, 181]), the ζ potential became more negatively charged (from -11.8mV to -56.9mV).

Figure 18. Zeta potential of PLGA NP and PLGA lipid NP

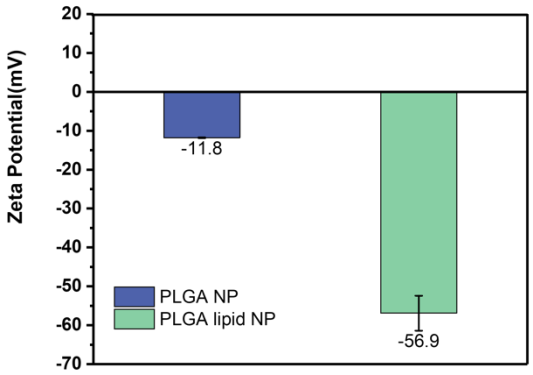

Both DLS and zeta potential characterization of the PLGA lipid NP demonstrated the successful incorporation of the lipid layer, as compared to pure PLGA NP. There are in principle two mechanisms affect nanoparticle stability. One is steric repulsion; the other is electrostatic stabilization. The integration of the lipid layer can potentially enhance the colloidal stability of the hybrid nanoparticle due to the steric repulsion from the PEG chains and electrostatic stabilization from anionic lipid, preventing close contact between particles. Besides the promising stability contribution, the PEG chains can increase the hydrophilicity of nanoparticle

system to reduce opsonin adsorption for longer circulation time *in vivo*. It is worth noting that the PLGA lipid NP system in this study exhibits a narrower size distribution compared to similar hybrid nanoparticle systems.[176]As for the current clinical formulation, micelle formulation (Cre Micelle) also exhibited narrow size distribution with Z average hydrodynamic diameters of 7.88 ± 2.3nm, and the PDI of 0.156 (Figure 19).

Figure 19. DLS of Cre Micelle

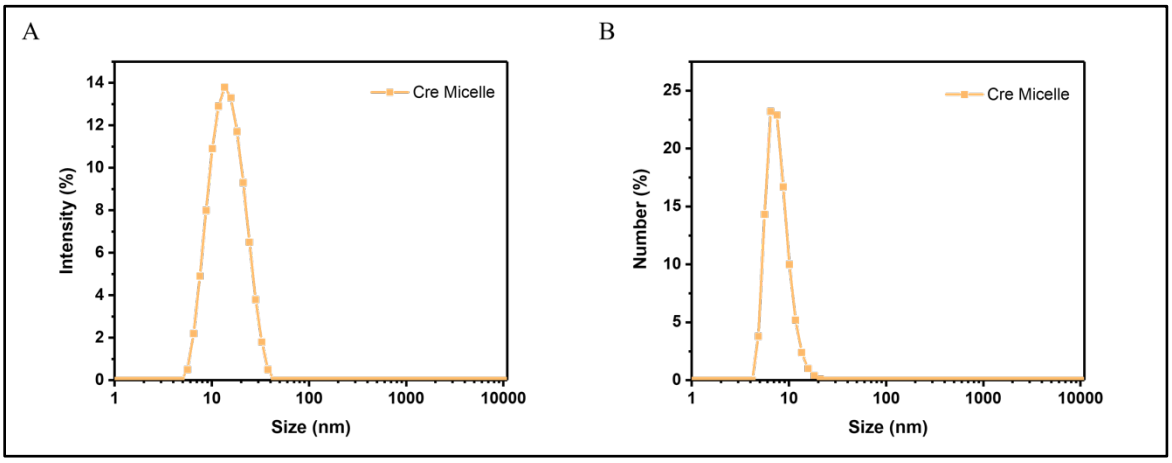

(A) Intensity distribution of Cre Micelle (B) Number distribution of Cre Micelle

3.3.2 TEM Analysis

TEM analysis was conducted to further investigate the core-shell structure of the nanoparticles. However, PLGA lipid NP are composed of elements with low atomic numbers. These elements have fewer interactions with the electron beam during TEM analysis, which lead to weak electron scattering, indistinct contrast between dark and bright areas, and vague structural details. To address this limitation, we utilized a uranyl acetate solution containing heavy elements. The uranyl stain can form a contour around the particle, which scatters electrons strongly and creates the dark contrast, while leaving the particle bright.[182] In particular, the uranyl ions in the solution

can react with the phosphate groups of lipids, resulting in the formation of an irregular coating with increased electron density around the solid nanoparticle. With the uranyl acetate staining, distinguishing biophysical characterization between PLGA NP and PLGA lipid NP could be obtained.

Figure 20. TEM image of PLGA NP and PLGA lipid NP

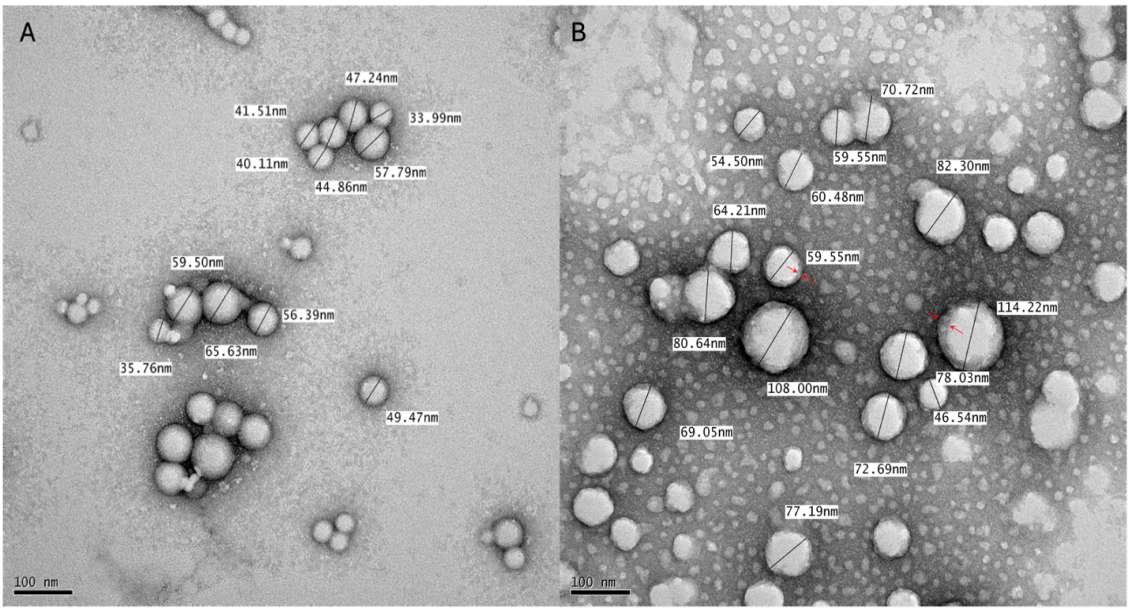

(A) TEM image demonstrated the structure of PLGA NP (B) TEM image demonstrated the core-shell structure of PLGA lipid NP, the lipid shell was highlighted between red arrows.

Remarkably, there is a subtle ring encircling the PLGA core in PLGA lipid NP sample. This ring extends and even invade into the core (highlight between red arrows), whereas the uranyl solution only outlines the contour of the edge in pure PLGA NP sample. This observation confirmed the presence of a lipid layer enveloping the polymeric core in PLGA lipid nanoparticles. (Figure 20).

The lipid layer shown in TEM analysis is a bit vague (Figure 20B). It is probably attributed to the air-drying process during sample preparation,[183] where water evaporates as sample deposits

and fixed on the grid. During this process, lipid may be extracted and disrupt the interactions with the PLGA core and resulting in defects.[184-186] Additionally, this dehydration process may also contribute to the loss of hydrophobic interaction between the lipid layer and the polymeric core.

Based on the DLS and TEM results, the hydrodynamic size detected from DLS is larger than the size from TEM method.[187] This variance can be attributed to two reasons. Firstly, DLS measurement relies on intensity weighting, where larger particles contribute significantly more to the overall size result than smaller particles. Secondly, particles measured via DLS are in a solvated state. The nanoparticle will be surrounded by double layers of oppositely charged ions known as the stern and diffuse layer, which results from the adherence of solvent molecules to the particle's surface through hydrogen bonding and electrostatic interaction. The hydrodynamic diameter measured by DLS theoretically represents the interfacial of these double layers, considered as the diameter of a hard sphere that diffuses at the same rate as the particle being measured. The DLS result includes both the inorganic core and the attached solvent layer as an integrated entity moves within an aqueous environment under Brownian motion. In contrast, TEM measurements are conducted on dehydrated samples, where the projected area under the electron beam corresponds solely to the particle's own sphere.

3.3.3 *In Vitro* Release Profile of PTX-PLGA NP and PTX-PLGA Lipid NP: Insights into Mechanisms

To assess the drug release characteristics *in vitro*, the nanoparticles were dialyzed in 50ml PBS buffer at 37°C. At specified intervals, the nanoparticle solutions inside the membrane were retrieved and combined with acetonitrile to dissolve the nanoparticles and release all encapsulated paclitaxel. At the 3-hour time point, only 5% of the drug was released from the PLGA lipid NP, in contrast to approximately 70% release from pure PLGA NP (Figure 21). Max et al. provided similar release profile with 600 nm pure PLG NP as well.[188, 189] Moreover, at a 10-hour time point, approximately 30% of the drug was released from the PLGA lipid NP, while around 80% was released from pure PLGA NP, which is consistent with observation from Liangfang et al.[134]

Figure 21. *In vitro* drug release profile from PTX-PLGA NP and PTX-PLGA lipid NP

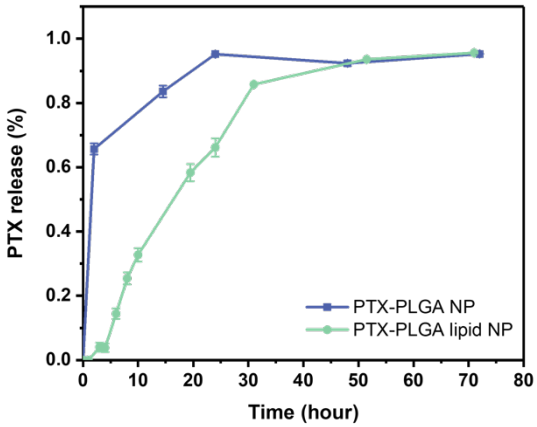

Before further investigating the suppressed release behavior of the PLGA lipid NP, it's essential to study the release mechanism of the PLGA based nanoparticle system first. The primary mechanisms associated with drug release from a PLGA-based platform are degradation/erosion and diffusion.[190] PLGA degrades via ester bond hydrolysis in the polymer backbone and

generates oligomers and monomers as products. During the erosion process, the diffusion of these oligomers and monomers out of the material leads to mass loss.[191] There are two main

Figure 22. Release mechanism of polymer based materials

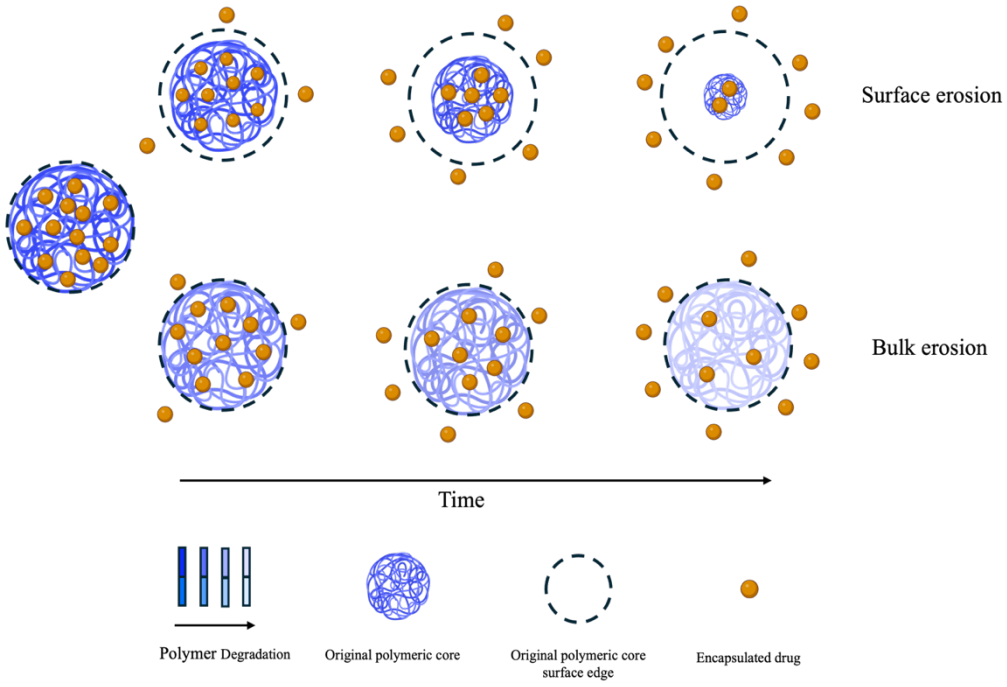

Diagram demonstrating the process of drug release and polymer degradation, including bulk-erosion and surface-erosion mechanisms, from polymeric platform. Created with BioRender.com

types of erosion: surface (heterogeneous) erosion and bulk (homogeneous) erosion (Figure 22). In surface erosion, polymer degradation is faster than water imbibition into the polymer bulk, resulting in major surface erosion. Conversely, polymer degrades at a slower rate in bulk erosion, where water penetration into the system is faster than polymer degradation. As a result, the entire material becomes rapidly hydrated, leading to an entire degradation with polymer chain cleavage throughout the system. PLGA systems have been demonstrated to be bulk erosion based.[192, 193] When PLGA-based nanoparticles are introduced to an aqueous environment, water penetrates the PLGA matrix, hydrolytic PLGA polymer degradation and drug diffusion start. The drug can

diffuse through different pathways including polymer or through water-filled pores. Particularly for hydrophobic drugs like PTX, it can only diffuse through polymer erosion without any transportation. As degradation proceeds, the degraded PLGA fragments accelerate both the erosion process and drug diffusion due to the carboxyl functional groups.[194]

We hypothesized that the incorporation of lipid layer may contribute to the delayed drug release behavior of PLGA lipid NP. This layer not only hinders the free diffusion of small hydrophobic drugs from the core, but also reduces the rate of water penetration into the PLGA core. Overall, the polymer matrix degradation and erosion are slow down due to the reduction of water penetration, which result in a slower drug release from the platform. In general, it requires more time for water penetrates in PLGA microparticles, which always exhibit a prolonged release profile compared to nanoparticles due to their larger size. However, because of the lipid layer, our PLGA lipid NP demonstrated a similar release profile as the PLG microparticles made from Max et al., where 70% of paclitaxel was released within 24 hours (comparable to our nanoparticles).[189] The PLGA lipid NP exhibited superior drug release profile than pure PLGA nanoparticles from the investigation conducted by Max et al., where 100% of paclitaxel was released within 4 hours even though their size of PLG NP is 600nm, much bigger than the size of our PLGA lipid NP.[189] Leveraging nanoparticles with a release profile akin to microparticles can mitigate the persistent peritoneal adhesions caused by microparticle intraperitoneal injection, even 7 months after completion of treatment with microparticles.[189, 195, 196]

3.3.4 Encapsulation Efficiency

Initially PTX standard stock solution sample with 1mg/ml was prepared in acetonitrile (one of the mobile phases in LCMS), a series of standard samples with lower concentration were prepared by serial dilution with acetonitrile. The concentration for these standard samples ranges from 0.01, 0.005, 0.002, 0.001, 0.0005, 0.0002, 0.0001, 0.00005, to 0.00002 mg/ml. The calibration curve, depicted in Figure 23, was generated by plotting the peak area of PTX against its concentration. By dissolving the concentrated PLGA lipid NP in acetonitrile to release the encapsulated PTX, the amount of PTX encapsulated within the PLGA lipid NP can be determined. The encapsulation efficiency was calculated to be 20% of the input weight of PTX.

Figure 23. Calibration curve of PTX standard samples

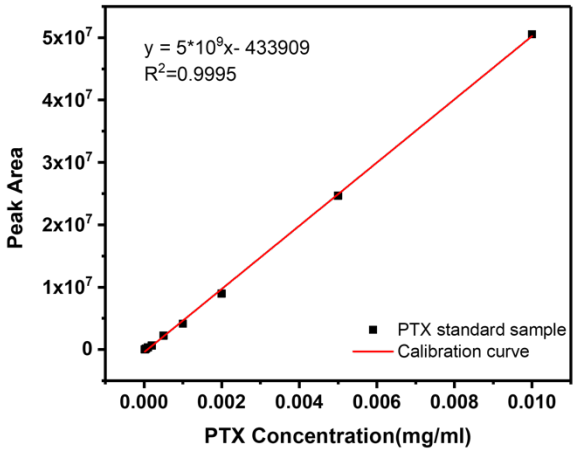

3.3.5 MTT Assay

Figure 24. Cell viability of HCT116 cells after treatment with PTX-PLGA lipid NP, PTX-Cre Micelle and free PTX in DMSO

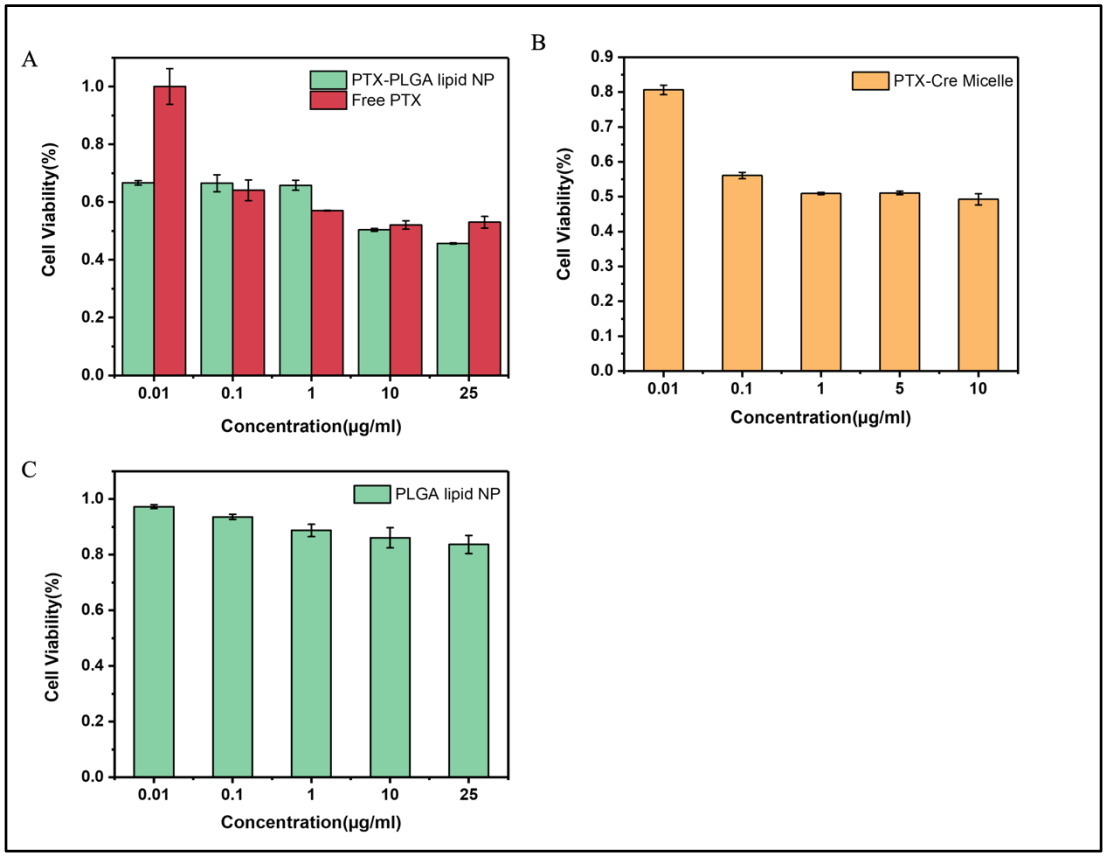

(A) Cell viability of HCT116 cells after treatment of PTX-PLGA lipid NP and free PTX (B) Cell viability of HCT116 cells after treatment of PTX-Cre Micelle (C) Cell viability of HCT116 cells after treatment of PLGA lipid NP

Table 1. IC_{50} of three formulations

Formulation	PTX-PLGA lipid NP	PTX-Cre Micelle	Free PTX
IC_{50}(μg/ml)	10~25	1~10	>25

Cell-based assays are commonly utilized for gaining deeper insights into the impact of those three formulations on the proliferation of colorectal cancer cells and their ability to induce cytotoxic effects.[197, 198] Among different kinds of methods available for multi-well detection of viable cells, the MTT assay stands out as a widely employed approach to assess cellular metabolic activity and toxicity.[199-201] The MTT reagent, 3-(4,5-dimethylthiazol-2-yl)-2,5-diphenyl-2H-tetrazolium bromide, is a compound dye capable of accepting hydrogen ions, carrying a positive charge, and exhibiting cell membrane permeability. Within the live cells, the MTT can be reduced to form a purple-blue water-insoluble formazan by mitochondrial succinate dehydrogenase, while dead cells lack this function. These crystals cannot penetrate the cell membrane and therefore accumulate within proliferating and undamaged cells.[202-204] By dissolving the crystals, the absorbance signal can be read and is directly proportional to the number of live cells.

Before conducting the cytotoxicity assay with PTX encapsulated formulations, it is important to exclude the cytotoxicity impact from carriers and solvents first. Due to the amphiphilic nature, Cremophor EL is able to form a solution with water as a non-ionic surfactant to interact with hydrophobic portion of the cell membrane, which dissolves the lipids in the cell membrane and lyse the cell at the end,[205] akin to other surfactants like Triton-X 100, which has long been used for cell lysis process.[206, 207] In addition, DMSO is also reported to inhibit cell proliferation due to its high permeability.[208] Ethanol can also easily disrupt the structure of cell membrane.[209, 210] To avoid the interference from Cremophor EL, ethanol and DMSO on cell viability with PTX formulations, the volume percentage of the solvent in each well was limited to less than 0.01 vol%, consistent with previous reports.[211, 212] Considering both the impact of solvent on the final assay readout and the exceedingly low solubility of PTX in aqueous solutions during serial

dilution with the stock PTX formulation solution, the concentration of the PTX during the MTT assay was confined to a narrow range, which can't reach to very high concentrations. Shown in the Figure 24C, the nanoparticle alone didn't exhibit significant cytotoxicity against the cells. The cellular cytotoxicity assay was conducted with three different formulations (PTX-PLGA lipid NP, PTX-Cre Micelle, and free PTX in DMSO) against HCT116 cells. Cytotoxic activity was assessed with different concentrations for each formulation by diluting with DMEM-F12 medium during the serial dilution process. After 48-hour incubation with various concentrations of the formulations, cell viability was evaluated by MTT assay. The results are presented in Figure 24A and B. As a quantitative measurement, the half-maximal inhibitory concentration (IC_{50}) is widely used to indicate the potency of a compound in inhibiting biological function process. It represents the concentration of a drug required to inhibit the cell proliferation by half. Due to the limited concentration spectrum, it is difficult to determine precise IC_{50} values for each formulation. Nevertheless, within current concentration range, we can estimate the IC_{50} to a narrow range to compare the efficacy of drugs facilitated by different carriers (outlined in Table 1). Notably, the IC_{50} for free PTX in DMSO exceeded 25 μg/ml, while IC_{50} for PTX-PLGA lipid NP and PTX-Cre was between 10~25 μg/ml,1~10 μg/ml, respectively. Both the PTX-PLGA lipid NP and PTX-Cre Micelle exhibited higher cytotoxicity than the free PTX form at each concentration, as evidenced by their respective IC_{50} value range. The lower IC_{50} of the nanoparticle may be attributed to its lipid layer, which facilitates the cytosolic delivery of paclitaxel[132, 213-215]. For the PTX-Cre Micelle, the Cremophor EL and ethanol could disrupt the cell membrane structure to some extent, further aiding in the transport of PTX.

3.3.6 Cellular Uptake

Figure 25. Cellular uptake of coumarin6 by PLGA lipid NP, Cre Micelle and free form

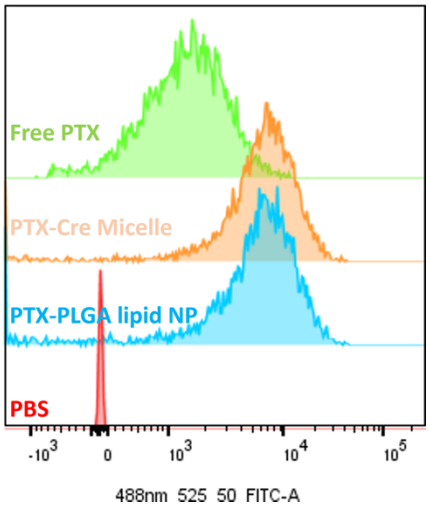

To verify the hypothesis about higher cytotoxicity from PTX-PLGA lipid NP and PTX-Cre Micelle, coumarin 6 dye was used as a model for examining the cellular uptake patterns of PTX encapsulated formulations (via PLGA lipid NP, Cre Micelle, and free form in DMSO), due to the similar hydrophobic nature with PTX. By encapsulating coumarin 6 in different formulations, after 1 hour incubation, the signal from dye within cells can be detected. A rapid cellular uptake was observed particularly with PLGA lipid NP and Cremophor micelle, possibly attributed to the presence of a bioavailable lipid layer and the high lipophilic nature of Cremophor EL/ethanol, respectively.

3.3.7 Stability Experiment

The stability of drug delivery carrier in both peritoneal fluid after administration and during systemic circulation after absorption is critical for their effectiveness for disease treatment *in vivo*. Protein adsorption of proteins in the circulation and peritoneal cavity significantly

influences the fate of the formulation, leading to opsonization and subsequent phagocytosis by macrophages of the RES.[216, 217] In this thesis, we initiate our investigation from a low concentration of biological fluid as a representative demonstration.

As depicted in Figure 26, both PLGA lipid NP and Cre micelle are stable in PBS, whereas the PLGA NP starts aggregation. Due to the high ionic strength environment in PBS, there might be a charge screening effect on nanoparticles. Without the stabilizer during the synthesis of PLGA NPs, the stability of these NPs primarily relies on the surface charge from the ionization of carboxyl groups at the ester end. In low ionic strength environments, such as the aqueous solution after synthesis or BSA, FBS solutions during stability test, these surface charges effectively prevent NP aggregation through electrostatic repulsion. However, PBS has increased ionic strength than normal aqueous solution with approximately 2.7mM potassium chloride, 1.5mM potassium phosphate monobasic, 137mM sodium chloride, and 8mM sodium phosphate dibasic, ions in the solution can screen these initial surface charges.[218] This screening effect allows cations to neutralize the negatively charged NP surfaces, diminishing repulsive forces between NPs and facilitating aggregation.

As illustrated in Figure 27, in 5wt% BSA solution, all three types of drug delivery carriers (PLGA NP, PLGA lipid NP, and Cre micelle) were relatively stable, probably due to the weaker interaction between BSA and PLGA NP, PLGA lipid NP, Cre micelle. It is consistent with findings by Jiao et al., who also observed minimal BSA absorption in their polymeric micelle system.[216] Furthermore, in 5 vol% FBS solution (Figure 28), PLGA lipid NP kept stable with almost no alternation in size change, compared to both PLGA NP (with a slight change of approximately 1.2-fold) and Cre micelle (with a slight change of approximately 2-fold). Over 1000 components, including growth factors, hormones, and transport proteins, in FBS obtained

from bovine fetuses may increase the likelihood of interaction between particle and its protein component.

Conversely, in 5 vol% plasma environment, PLGA lipid NP showed a slight increase in size from 99.5 ± 0.07nm to 130.1 ± 0.42nm at its peak, while PLGA NP underwent a significant increase from 84.76 ± 0.34nm to 4702 ± 379 nm at its peak, and Cre micelle increased from 13.96 ± 0.06 nm to 6248 ± 953 nm at its peak (Figure 29). It may further verify our previous assumption that PEG in PLGA lipid NP is able to prevent adsorption of plasma proteins from nude mice onto the nanoparticle surface, compared to pure PLGA NP and Cre micelle, which are readily absorbed by plasma proteins.

To further study the real formulation that will be used during *in vivo* experiment, we also studied the stability of PTX encapsulated formation, PTX-PLGA lipid NP and PTX-Cre micelle, at concentration which will be used during *in vivo* experiment under different biological environment (Figure 30). Both PTX-PLGA lipid NP and PTX-Cre micelle are stable in 5vol% FBS solution. Whereas the PTX-Cre micelle showed significant size fluctuations when exposed to 5wt% BSA solution and 5 vol% serum solution, in contrast to the consistently stable behavior of PLGA lipid NPs in both environments. Upon exposure to BSA or serum solution, the PTX-Cre-micelle is easier affected by the protein, compared with the stability profile of the Cre micelle. The more significant size change of PTX-Cre micelle at BSA solution, compared to Cre micelle at BSA solution profile, may attribute to the high affinity between PTX and BSA.[219, 220] The rationale behind the improved solubility of PTX in the Cre micelle compared to water is the favorable partitioning results from the micelle. However, this partitioning process is an equilibrium that can be influenced by environmental factors such as size, surface properties, and protein adsorption, which may disrupt the partition equilibrium and cause PTX leakage. Due to

the strong affinity between PTX and protein, the protein may accelerate the release of the drug from the micelle.[221]

The DLS data of the PTX-Cre micelle before and after interacting with plasma (as depicted in Figure 31) have shown that while numerous original PTX-Cre micelles with intact structures can be found in the system, there is a spike of a significant amount of aggregated or damaged particles in the system as well. These aggregations could be the precipitated PTX, the complexes between PTX and albumin, or the Cremophor EL polymer aggregation. Furthermore, some aggregations are also found after encapsulating PTX into Cre micelle, when comparing the DLS data between PTX-Cre micelle and the Cre-micelle (as shown in Figure 19). These may be the PTX aggregations during the partitioning equilibrium. As the PTX-Cre micelle was filtrated with a 0.22 μm filter before the DLS experiment, any PTX aggregation that remains insoluble should not exist in the system, meaning that these PTX aggregations are not the undissolved substances that Cremophor EL fails to partition. So even after filtration, the remaining aggregation may be the PTX that exhibit outside the micelle during the PTX dynamic equilibrium. However, PTX-PLGA lipid NPs exhibit a consistent and similar stability profile before and after interaction with plasma, due to the protection of PEGylated lipid layer (Figure 32).

Figure 26. Stability study of PLGA NP, PLGA lipid NP and Cre Micelle in PBS

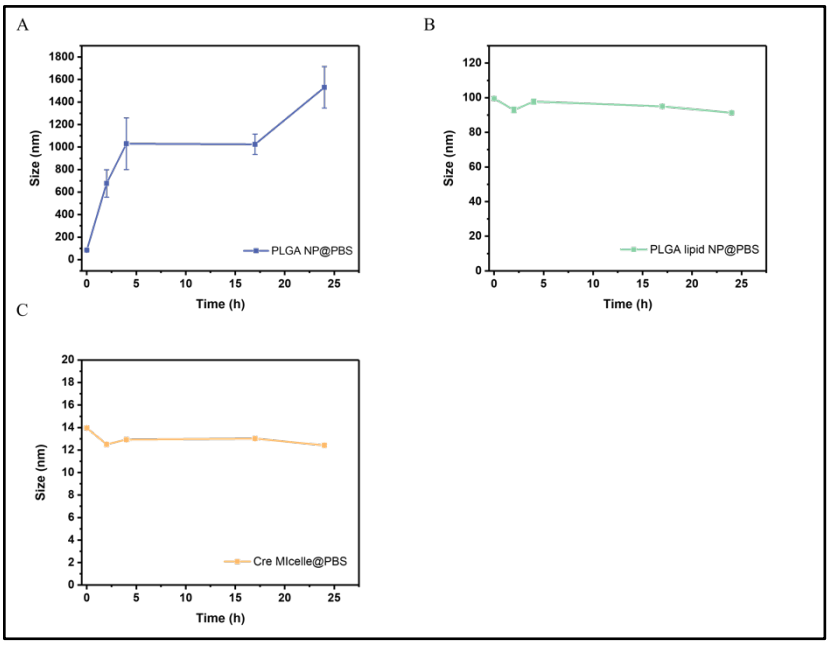

Figure 27. Stability study of PLGA NP, PLGA lipid NP and Cre Micelle in BSA

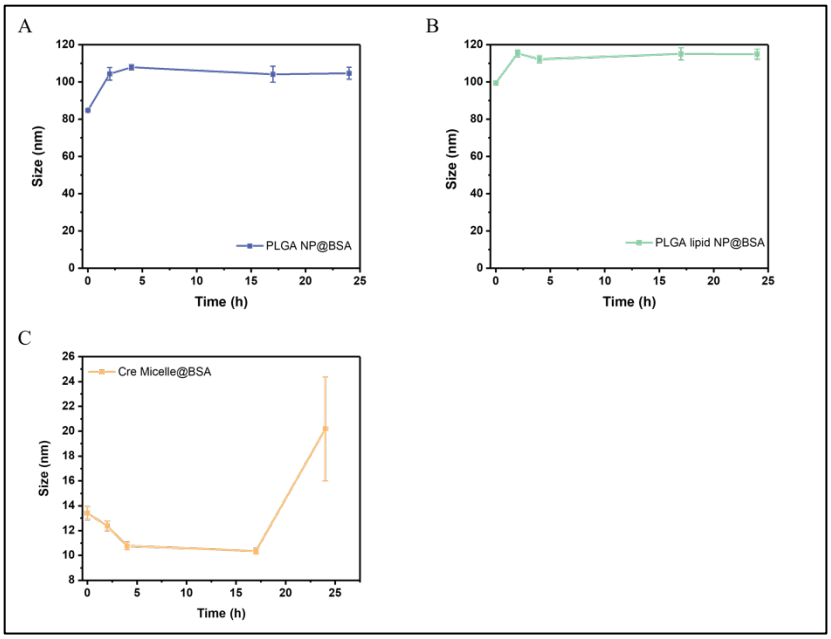

Figure 28. Stability study of PLGA NP, PLGA lipid NP and Cre Micelle in FBS

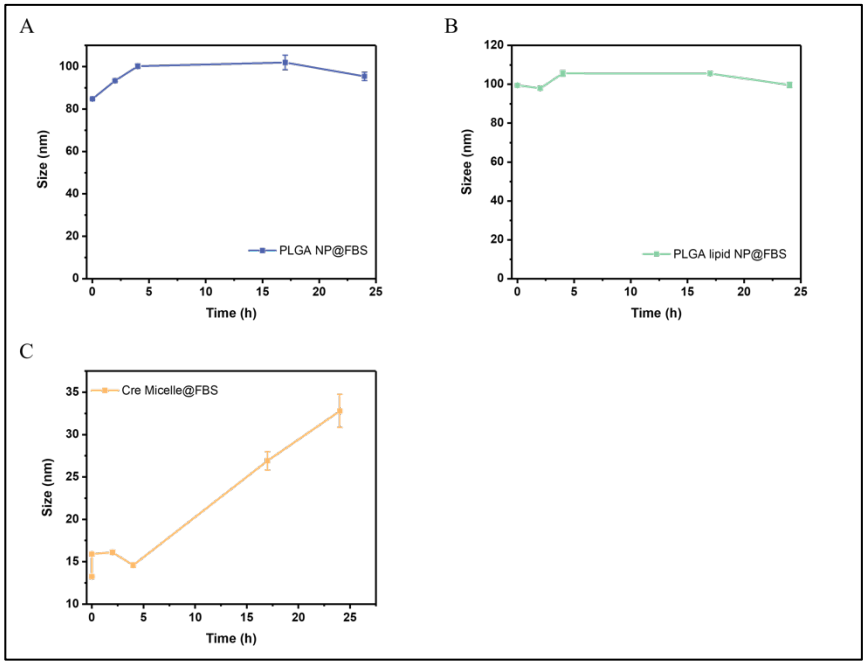

Figure 29. Stability study of PLGA NP, PLGA lipid NP and Cre Micelle in plasma

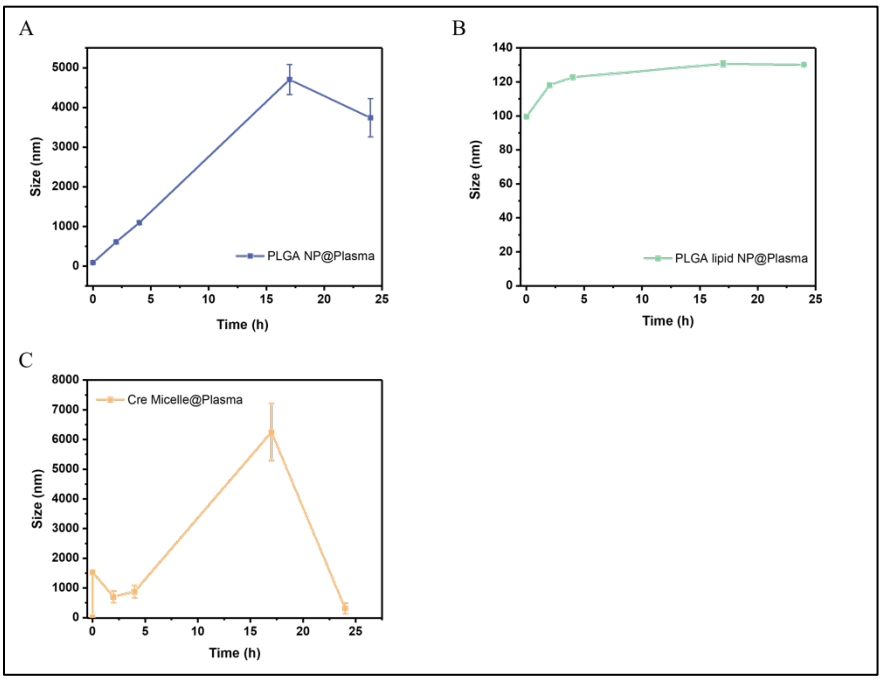

Figure 30. Stability study of PTX-PLGA lipid NP, and PTX-Cre Micelle in biological environment

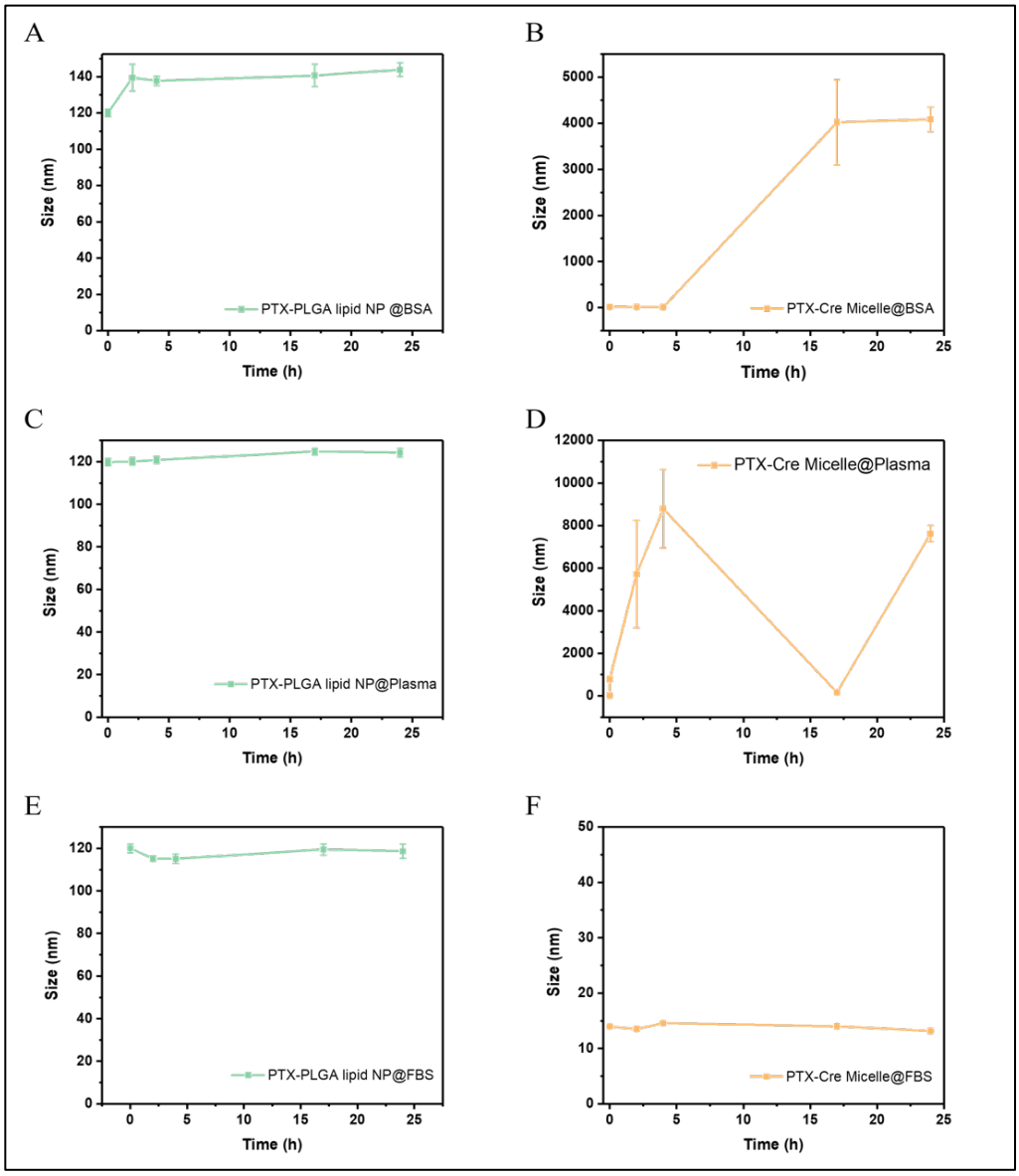

Figure 31. Stability study of PTX-Cre Micelle before/after interaction with plasma

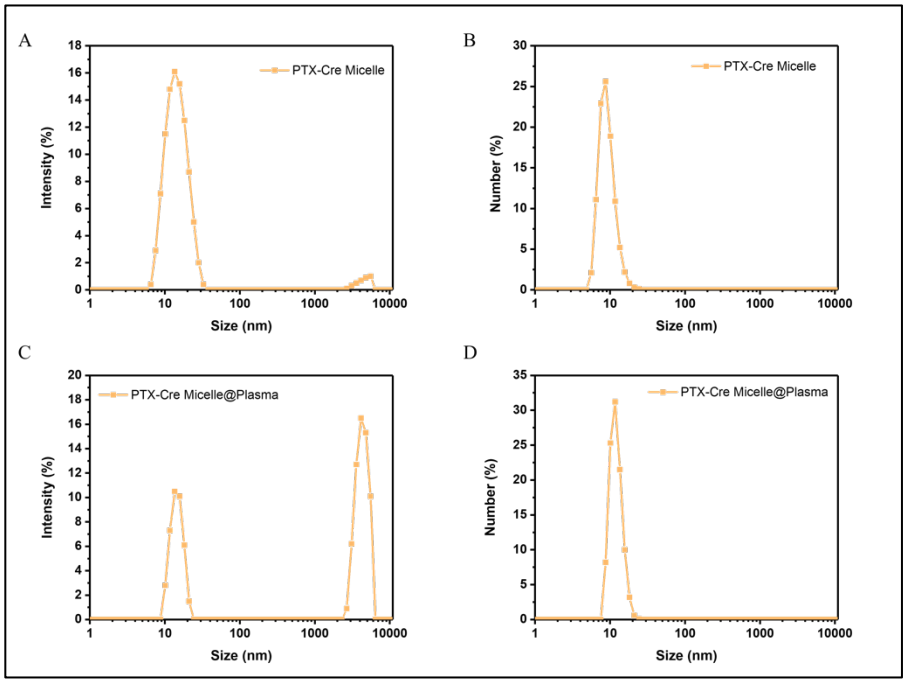

Figure 32. Stability study of PTX-PLGA lipid NP before/after interaction with plasma

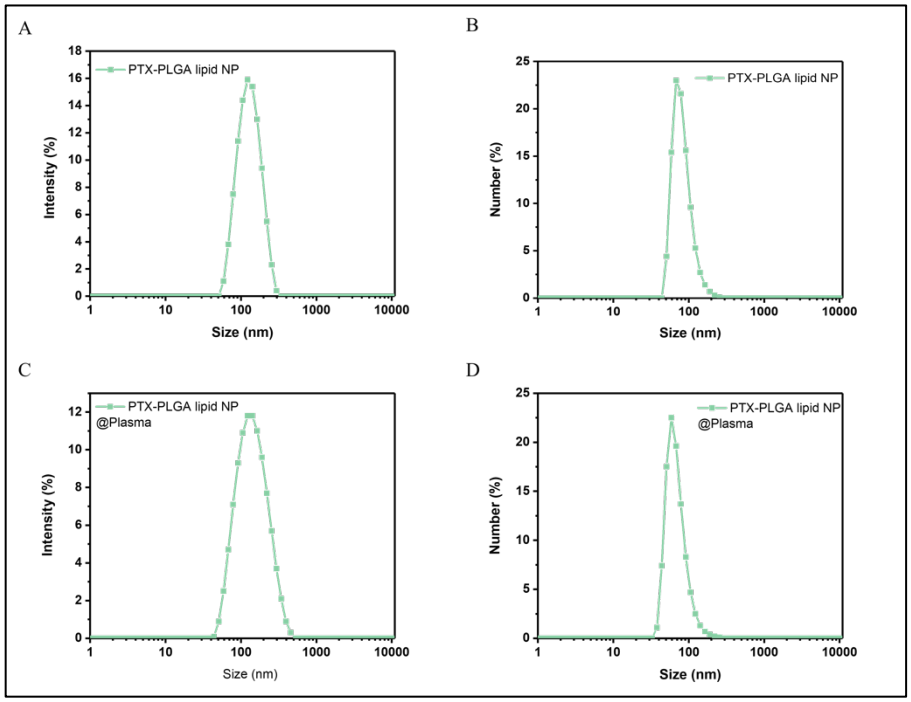

3.4 Conclusion

Due to the lipid layer design and the corresponding properties assumption, it is important to validate the surface modification of the PLGA core with lipid layers before proceeding with any subsequent *in vitro* or *in vivo* experiments. In Chapter 3, the surface modification with lipid layer was confirmed through size characterization and ζ potential measurements using DLS equipment. The results indicated a slightly larger size of PLGA lipid NPs compared to pure PLGA NPs because of the lipid layer. Moreover, the ζ potential of PLGA lipid NP became more negative with the incorporation of anionic lipids when comparing with pure PLGA NP. In TEM analysis, the distinctive core-shell structure was found in PLGA lipid NP, indicating the shell layer formation from lipid layer, comparing with naked pure PLGA NP. Even the dehydration during sample preparation may lead to the lipid precipitation and cause the low quality of imaging, the lipid layer surrounding the PLGA core is still evident.

The encapsulation efficiency was confirmed with LCMS to verify the drug delivery platform structure as one of the parameters for the following *in vitro* characterization. Then series of *in vitro* characterizations were conducted before final *in vivo* evaluation. *In vitro* drug release studies highlighted the superior sustained release profile without significant burst release at the beginning of PLGA lipid NP, compared to pure PLGA NP. By elucidating that the degradation/erosion and diffusion get involve the release mechanism, the incorporation of lipid layer impede the drug diffusion, slow the matrix degradation, and cause the suppression of the release rate in final delayed release profile.

MTT assay revealed that PTX-PLGA lipid NP and PTX-Cre Micelle exhibited similar cytotoxicity based on the estimated IC_{50} values. Internalization by target cells is the prerequisite

to the pharmacological effects of each drug formulation. In cellular uptake experiment, both PLGA lipid NP and Cre Micelle facilitated the endocytosis process of the anticancer drug, where the biocompatible lipid layer of PLGA lipid NP accelerated the cytosolic drug delivery, Cremophor surfactant and ethanol disrupt the cell membrane, compared to free PTX. However, as MTT assay spanned over 2 days, the difference between each formulation in PTX uptake by cells was diminished progressively during the assay duration, compensate the gap in cellular uptake rate, ultimately resulting in similar IC_{50} values, where PTX-PLGA lipid NP and PTX-Cre Micelle only show slightly higher cytotoxicity than free PTX.

Once the drug formulation is administered into the peritoneal cavity, the protein absorption in peritoneal cavity and systemic circulation can lead to phagocytosis and significantly impair the formulation efficacy during IP treatment, so it is crucial to assess and optimize the stability of drug delivery platforms in mimic biological environments before *in vivo* experiments. Starting from the biological fluid with low concentration of protein, PLGA lipid NPs and Cre micelles were stable in PBS environment, while PLGA NPs aggregated due to a charge screening effect. In 5wt% BSA solution, all carriers were relatively stable, which may be attributed to the weak interaction between carriers and BSA. In 5 vol% FBS solution, PLGA lipid NPs were still the most stable formulation among all candidates. In 5 vol% plasma environment, PLGA lipid NPs only showed slight size increase, while PLGA NPs and Cre micelles exhibited significant size fluctuation. The different stability properties further highlight the efficacy of PEG in preventing protein adsorption on particles. Upon close examination, PTX-Cre micelles showed significant size changes after interacting with plasma, possibly due to the PTX-protein interactions that disrupt the micelle stability and cause the aggregation of precipitated PTX or PTX-albumin

complexes. Conversely, PTX-PLGA lipid NPs were kept stable before and after the interaction with plasma.

Chapter 4. Exploring *In Vivo* Anti-Tumor Efficacy Across Diverse Formulations

4.1 Introduction

Through *in vitro* experiments, the mechanism of action and properties of drug formulation has been thoroughly evaluated with *in vitro* models including cells culture and simulated biological environment. Even the *in vitro* models provided starting point for us to gather important information into how the drug formulation interact with isolated biological environment, it is still difficult to extrapolate the final clinical effect due to the absence of living organism with more complex biological variables. *In vivo* experiments, typically include pharmacokinetics, biodistribution, anti-tumor efficacy studies, and toxicity evaluation, can be employed to advance therapeutic system development design.

Both pharmacokinetic and biodistribution studies evaluate the tissue-specific targeting and overall disposition of therapeutic system, including the fundamental information with its absorption, distribution, metabolism, and excretion (ADME). Specifically, pharmacokinetic studies measure the drug exposure in systemic circulation over time, demonstrating the shielding efficacy of the PLGA lipid NP to prevent drug from clearance during circulation compared to other two formulations. In biodistribution studies, the targeting efficiency of carriers in tumor tissues and important organs can be assessed. Given the goal of treating colorectal cancer peritoneal metastasis is to elevate drug concentration at the tumor site in the peritoneal cavity, biodistribution studies not only assess how effectively PLGA lipid NPs safeguard the drug's efficacy on tumor tissues, but also evaluate their potential toxicity or burden on major organs compared to other formulations.

Additionally, by directly comparing the tumor growth under each formulation treatment in anti-tumor efficacy experiment, we can investigate the capability of each drug delivery platform to suppress tumor growth or prompt tumor regression in animal cancer models. Following with the survival rate experiment and *in vivo* imaging monitoring, the influence of the drug delivery platform on the overall survival of tumor-bearing animals can be further evaluated.
Variations in the mice body weight were collected, analyzed, and interpreted for overall toxicity from each therapeutic formulation. Administration of different drug delivery platforms may cause the body weight changes, including decreased food intake, metabolic shifts, organ impairment, or fluid retention, due to the potential modifications in the pharmacokinetic and pharmacodynamic behavior of the drug by different platforms. By monitoring the alterations in body weight, the severity and advancement of toxicity induced by each formulation can be closely evaluated.

4.2 Experimental Details

4.2.1 Materials

All chemicals were used as received unless otherwise specified: PLGA (poly (D, L-lactide-co-glycolic acid), Resomer RG 505) with a 50:50 monomer ratio, ester-terminated, Mw 54,000-69,000 was purchased from Sigma-Aldrich. Soybean lecithin consisting of 90% phosphatidylcholine was obtained from Thermo Scientific Chemicals. DSPE-PEG_{2000}(1,2-diastearoyl-sn-glycero-3-phosphoethanolamine- N- [amino (polyethylene glycol)2000]) was purchased from Avanti Polar Lipids. Paclitaxel with 99.96% purity was obtained from

MedChemExpress. Acetone (ACS Grade) was obtained from Fisher Scientific. Absolute Ethanol (200 Proof, Molecular Biology Grade) was obtained from Fisher BioReagents. Cremophor EL (Assay:99.52%) was purchased from MedChemExpress. Milli Q water was obtained by Milli-Q EQ 7000 Ultrapure Water Purification System connected with 0.22μm Millipak Filter. PVDF 0.45μm/0.22 μm filters were purchased from Celltreat Scientific Products. Amicon Ultra-15 centrifugal filter with a molecular weight cutoff of 10,000 Da was purchased from Millipore. HCT116 cell line was obtained from ATCC (isolated from the colon of an adult male with colon cancer). CMV-Firefly luciferase (Puro) was obtained from Cellomics Tech. 6-8 weeks old female Nu/Nu mice (strain:002019-NU/J) were obtained from the Jackson Laboratory. A micro-sample tube coated with Lithium heparin was purchased from Sarstedt. 0.5M Ethylenediamine tetraacetic acid (EDTA, pH 8.0) was purchased from Invitrogen from Thermo Fisher Scientific. Acetonitrile (HPLC grade) was purchased from Fisher Scientific. D-luciferin, Potassium Salt was purchased from Gold Biotechnology. Isospire™ (isoflurane) Inhalation Anesthetic was purchased from Dechra.

4.2.2 Pharmacokinetic Study

Female Nu/Nu mice aged 6-8 weeks were housed in a pathogen-free environment at the University of Chicago's Animal Resources Center (ARC), following a 12-hour light-dark cycle. The housing facility maintained a temperature range of 70–73°F (with an average of 72°F) and humidity between 40–50% (averaging at 44%). Mice had ad libitum access to standard laboratory chow and water. All procedures involving animals were conducted by protocols approved by the Institutional Animal Care and Use Committee (IACUC) of the University of

Chicago's Animal Care Center, ensuring humane treatment throughout the experimental period. Animals were euthanized when tumor burden or ascites fluid reached protocol-defined guidelines.

To compare the pharmacokinetic profiles of three formulations, Nu/Nu mice weighing approximately 20g were randomly assigned to four groups: 1) PTX-PLGA lipid NP, 2) PTX-Cre Micelle, 3) Free PTX and 4) PBS. Mice were intraperitoneally (i.p.) injected with 2×10^6 HCT116-Luc cells in 300 µl PBS. Tumors were allowed to grow for 1 week before treatment initiation. Each group received single dose with equivalent amounts of PTX in PLGA lipid NP, Cre Micelle and free form (at a dose of 10mg/kg) via i.p. administration. Blood samples were collected in a micro-sample tube coated with lithium heparin from the tail vein at 5-minute intervals, as well as at 4, 8, 24, and 48 hours post-administration. Plasma was obtained through centrifugation at 6000 rpm for 10 minutes at 4°C. Plasma samples were stored at -80ºC until processed.

During the sampling process, plasma samples were mixed with acetonitrile by vortexing, and centrifuged at 9000G for 25 minutes at 4°C to precipitate the protein. The supernatant was then extracted, filtered through a 0.2 µm pore size PVDF syringe filter, and analyzed using LC-MS. The mobile phase consisted of 0.1% formic acid in a water-acetonitrile mixture (40:60, v/v), with a flow rate of 0.2ml/min and a runtime of 6 minutes.

4.2.3 Sample in Plasma standard curve

The PTX standard stock solution was made by dissolving it in DMSO at a concentration of 0.4 mg/ml. Through serial dilution with plasma obtained from nude mice, PTX standard samples in

plasma will be generated, with concentration ranging from 0.01, 0.005, 0.001, 0.0005, 0.0002, and 0.0001 mg/ml for the calibration curve.

4.2.4 Biodistribution Study

A biodistribution study of the three formulations was conducted using a mouse model with experimentally induced colorectal peritoneal metastasis. Concurrent with the pharmacokinetic investigation, mice were euthanized via cervical dislocation at the 24-hour and 48-hour time points. Various organs (including the heart, liver, spleen, lung, kidney, and tumor) were collected, washed with PBS, and stored at -80°C until analysis. Before LC-MS assessment, the organs and tumors underwent careful washing with DI water, were weighed, and were then placed in Eppendorf tubes submerged in PBS. Subsequently, they were sliced into small pieces and homogenized at 40% amplitude for 2 minutes of sonication time, with a cycle of 10 seconds on and 2 seconds off, in an ice water bath, repeated twice (Sonic dismembrator Model 500 was purchased from Fisher Scientific). The concentration of paclitaxel in the homogenized tissue was determined via LC-MS, following the analytical procedure described above.

4.2.5 Tumor Model and *In Vivo* Anti-tumor Efficacy Study

The efficacy of the developed PTX-PLGA lipid NP formulation, along with PTX-Cre Micelle and free PTX formulations, in combating tumors was assessed using an experimentally induced colorectal cancer peritoneal metastasis mice model. Nu/Nu mice weighing approximately 20g were randomly divided into four groups: 1) receiving treatment with PTX-PLGA lipid NP, 2) receiving treatment with PTX-Cre Micelle, 3) receiving treatment with free PTX, and 4) control

groups with PBS. Mice were intraperitoneally (i.p.) injected with 2×10^6 HCT116-Luc cells in 300 µl PBS. After one week of inoculation, treatments were administered i.p. with a dose of 10mg/kg of PTX twice a week for 2 weeks. Prior to injection, mice were safely restrained using the scruff technique and placed in dorsal recumbency with the head tilted downward to facilitate clear access to the abdomen. The injection site was disinfected with 70% alcohol, and the needle was inserted bevel up in line with the natural extension of the hip at approximately a 60^o angle, with the plunger withdrawn slightly to prevent puncture of the intestines or any organ. Mice were imaged using an *in vivo* imaging system (IVIS 200; Xenogen Corporation) twice a week by i.p. injecting 150 µl of 15mg/ml luciferin in PBS. The Living Image® software was utilized for the *in vivo* imaging system. Mice were anesthetized via continuous inhalation of 2% isoflurane, and bioluminescence images were then captured with a 1.00 s exposure time, F-Stop setting of 1, medium binning, and a subject height of 1.5 cm setup.

The body weights of the mice were measured twice a week. Animals were euthanized if their body weight loss exceeded 20% or if they exhibited other signs of illness, such as breathing problems, failure to eat and drink, lethargy, serious bowel obstruction, or abnormal posture. Animal survival was analyzed using Kaplan-Meier analysis. P value by one-way ANOVA with Tukey's multiple comparisons tests. A log-rank (Mantel−Cox) test was used for the statistical analysis of survival curves.

4.3 Result and Discussion

4.3.1 Calibration Curve of PTX standard sample in plasma

Plasma is a complex biological matrix containing various proteins, lipids, salts, and other endogenous compounds, which can interfere with the quantification analysis of the PTX in LC-MS experiment and generate inaccurate results.[222, 223] Biological matrix effects from plasma components can alter the ionization of PTX and reduce the LC-MS sensitivity or accuracy of PTX. For example, the high propensity for PTX to bind with plasma protein can potentially affect the distribution of PTX in sample. Another risky factor is that endogenous compounds can compete with PTX for ionization in the mass spectrometer, suppress the ionization process and reduce signal intensity of PTX at the end.[224-226] By preparing standard PTX in plasma, we can mimic the matrix environment of the actual samples and diminish the matrix effects during analysis, compared to PTX in standard organic solvent (Figure 33).

Figure 33. Calibration curve of PTX standard samples in plasma

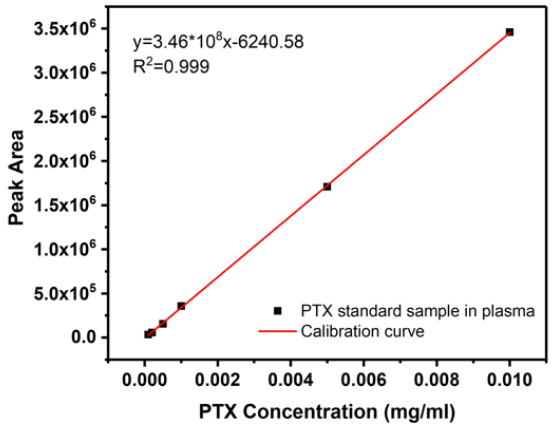

4.3.2 Pharmacokinetics Study

As illustrated in Figure 34, after intraperitoneal injection of three formulations, they have shown varying levels of PTX within a 48-hour timeframe. When administering the free PTX solution, PTX was promptly observed in plasma and reach its peak concentration shortly after injection (nearly right after i.p. injection, typically within 5 minutes), followed with a rapid clearance from the peritoneal cavity to systemic circulation through blood vessels under the thin peritoneal membrane, facilitated by diffusion or convection.[189] On the contrary, both PTX-Cre Micelle or PTX-PLGA lipid NP demonstrated a delayed peak concentration and followed with a decline. This pattern is a characteristic of absorption from an extravascular site. Because both Cre micelles and nanoparticles are sizable particles, they will be drained through the lymphatic ducts before entering the systemic circulation.[212, 227, 228] Notably, among all the three formulations, nanoparticles demonstrated significantly enhanced systemic pharmacokinetic profiles *in vivo*, with the highest peak concentration, prolonged retention time and total drug exposure that is still available in circulation, compared to the other two formulations. The information provided thus far strongly suggests that PTX-PLGA lipid NP exhibited significantly improved bioavailability and is stable during systemic circulation for a longer duration. This suggests that the effective shielding from the lipid layer and the controlled release properties of nanoparticles enable the retention of high concentrations of intact PTX without triggering clearance by the immune system during circulation. This is also proved by the stability experiment (Figure 30 and 32), where the PTX-PLGA lipid NP only shows a slight increase in size, comparing with dramatic size increment for micelle. Consequently, this allows the carrier to consistently deliver substantial amounts of intact PTX back to the tumor site by the EPR effect, even after being

taken up by the lymphatics during the absorption/clearance stage from the peritoneal cavity. The lipid layer stealthily coating the surface of PLGA serves to prevent rapid clearance by absorbed proteins from the blood (opsonins), which would otherwise initiate immune reactions, prompting phagocytosis through the mononuclear phagocyte system to eliminate the particles from the bloodstream.[128, 130, 229-231] Simultaneously, the controlled release property endows the particle with the ability to retain cargo within the nanoparticle reservoir upon reaching the tumor site. In contrast, free drugs and micelles lack such protection and are easily cleared and metabolized by the immune system. Following i.p. injection, a portion of the initial dose can reach the tumor site due to spatial proximity. However, once absorbed from the peritoneum, these agents are destined for metabolism during circulation and are unable to circulate back to the tumor site.

Figure 34. Plasma pharmacokinetics of paclitaxel

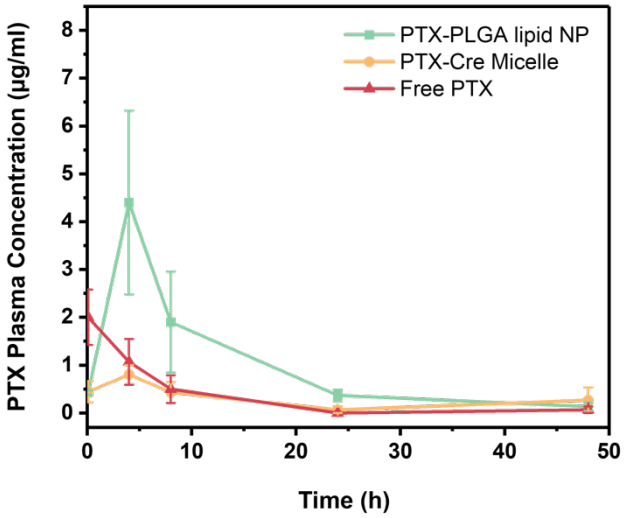

4.3.3 Biodistribution Study

The biodistribution study was conducted concurrently to establish the tissue distribution profile of PTX from three formulations after intraperitoneal injection at 24-hour and 48-hour intervals.

Figure 35 A and B illustrate the deposition of PTX in the peritoneal cavity tumor, liver, heart, spleen, lung, and kidney. At 24 hours post-injection, the PTX concentration within the tumors of mice for all three formulations is similar. In the early stages following IP injection of the three formulations, spatial proximity significantly influences the disposition of PTX within the tumor, which may compensate the impact from different platforms. Penetration becomes the dominant pathway for all three formulations to reach the tumor site. Because of the controlled release property, there might be a delay in PTX concentration within the tumor at 24 hours for PLGA lipid NP. Considering that all three formulations are at the nano level, they will be absorbed

Figure 35. Paclitaxel biodistribution profile after 24 hours and 48 hours IP treatment

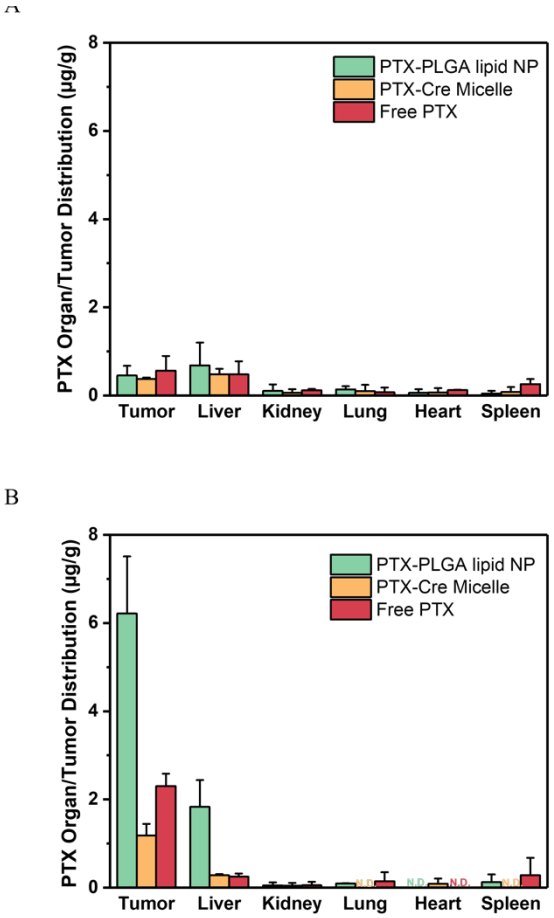

through different routes: free PTX via blood vessels, while PTX-PLGA lipid NP and PTX-Cre Micelle will be drained through lymphatic ducts. Once they enter the peritoneal cavity, all three formulations will be absorbed to varying extents and enter systemic circulation, as evident from the pharmacokinetic profile (Figure 34). These factors collectively contribute to comparable PTX concentrations within the solid tumor.

The spatial proximity may partially impair the cellular uptake promotion effect contributed by the lipid layer. Additionally, the promotion effect observed during cellular uptake was studied in a two-dimensional (2D) monolayer cell culture system, which oversimplifies the complex microenvironment of a solid tumor. Solid tumors are surrounded by a three-dimensional (3D) network of extracellular matrix (ECM), which plays a crucial role in drug metabolism and penetration[232-234] since the dense ECM may impede nanoparticle passage through tiny holes within the matrix.[235-237]

Among the major organs in mice, PTX accumulates most prominently in the liver, where it undergoes metabolism. As a result of absorption by the peritoneum, all three formulations undergo the first-pass effect within the liver. The protective lipid layer of PTX-PLGA lipid NP allows it to retain more PTX available for metabolism compared to the other two formulations, where PTX cargo is either absorbed with serum albumin, resulting in activity loss, or undergoes endocytosis by macrophages before reaching the liver. This phenomenon may explain the highest PTX concentration observed in PTX-PLGA lipid NP. Moreover, PTX concentration in other organs, such as the heart, kidney is notably low, indicating minimal toxicity to these organs.

After 48 hours, the effectiveness of lipid layer of PTX-PLGA lipid NP became significant. It can shield the drug and protect it from immune system clearance within peritoneal cavity and systemic circulation. This helps the drug avoid the plasma protein absorption and macrophages

attack, resulting in an increased accumulation of PTX at the tumor site compared to the other two formulations. Specifically, the PTX concentration significantly rises from 0.46 μg/g to 6.2 μg/g for PTX-PLGA lipid NP. Conversely, the administered PTX-Cre micelle might be unstable according to the stability study, causing PTX aggregates in microscale in peritoneal cavity and lower the available effective concentration of drug. As for free PTX, once the solvent is dissipated, due to the moderate solubility, the free PTX may also precipitate and lose the effective concentration as well. On the other hand, for those intact PTX-Cre Micelle or free PTX absorbed by the peritoneum, only limited amount of PTX can be transported back to the tumor via the circulation system due to immune system clearance, resulting in less PTX concentration at tumor site. According to the LC-MS data, PTX concentration of PTX-Cre Micelle increased from 0.37 μg/g to 1.1 μg/g, free PTX increased from 0.56 μg/g to 2.3 μg/g (Figure 35).

Since IP injection route is subject to the first-pass metabolism by liver, we also studied the drug accumulation in the liver. Due to the protection from the PLGA lipid NP carrier, a substantial amount of PTX remains intact and available for metabolism within the liver compared to PTX from the other two formulations, where the PTX-PLGA lipid NP had highest PTX concentration in liver. Furthermore, the PTX concentration in other organs remains low even after the 48-hour time interval, indicating insignificant systemic toxicity of all carriers (Figure 35).

4.3.4 *In Vivo* Antitumor Efficacy

The *in vivo* antitumor efficacy of PTX-PLGA lipid NP, PTX-Cre micelle, free PTX and PBS was assessed in i.p. injected HCT116 mouse tumor xenograft models of human colorectal cancer peritoneal metastasis. Mice received i.p. injections of PTX-PLGA lipid NP, PTX-Cre micelle, or free PTX at a dosage equivalent to 10mg/kg of PTX, while the control group received PBS injections. All the mice were treated once every three days. The antitumor efficacy was assessed by measuring the total photon emission resulting from the bioluminescent reaction of luciferin, which was intraperitoneally injected at each monitoring interval. This reaction was catalyzed by luciferase, an abundantly expressed enzymatically active protein in the tumor (HCT116 cells) when oxygen is present. Since the emitted light is typically imperceptible to the human eye, an ultra-sensitive charge-coupled device (CCD) camera was utilized for detection.

Figure 36. Tumor growth curve of human colon cancer HCT116 tumor-bearing athymic nude mice after indicated treatments

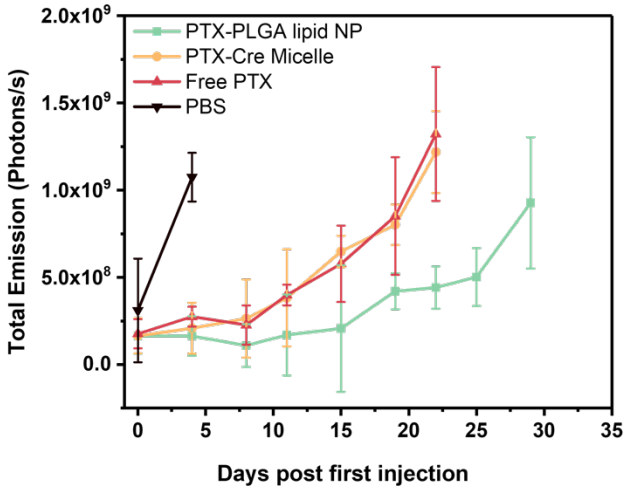

Following four injections of the different formulations, mice treated with PBS experienced rapid mortality starting on day 5, owing to the high oncogenic aggressiveness of the HCT116 cells.[238-

[240] Both PTX-Cre micelle and free PTX exhibited moderate inhibition of tumor growth, prolonging the survival of mice until day 22, with little discrepancy observed between the two formulations in terms of anticancer efficacy. In contrast, PTX-PLGA lipid NP demonstrated potent antitumor efficacy compared to both PTX-Cre micelle and free PTX, resulting in a 67% reduction in tumor growth and postponing mortality until day 30 (Figure 36). Throughout the four doses treatment, PTX-PLGA lipid NP did not initially exhibit a profound antitumor effect compared to PTX-Cre micelle and free PTX formulations. However, after the treatment regimen, the antitumor effect of PLGA lipid NP became more pronounced and surpassed other two formulations.

There are in general two factors contribute to this enhanced efficacy. Firstly, the protective lipid layer of PTX-PLGA lipid NP prevents PTX from clearance during peritoneal cavity and systemic circulation, enabling substantial PTX accumulation in the tumor. Secondly, the controlled release property of PTX-PLGA lipid NP facilitate sustained release of PTX at the tumor site and

Figure 37. Representative IVIS image of nude mice after indicated treatments

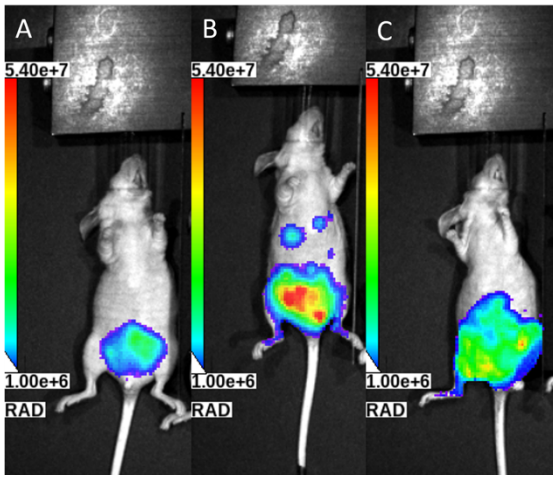

(A) Representative mouse treated with PTX-PLGA lipid NP (B) Representative mouse treated with PTX-Cre micelle (C) Representative mouse treated with free PTX.

maintain an effective therapeutic concentration for inhibiting tumor growth over time.

Representative IVIS images of nude mice from each treatment group are also presented in Figure 37, showing the tumor inhibition effect from PTX-PLGA lipid NP, as evidenced by reductions in both the size of the tumor area and its intensity.

We further examined mouse survival rates (refer to Figure 38). PTX-Cre Micelle and free PTX

Figure 38. Survival curves of colorectal tumor-bearing athymic nude mice after indicated treatments

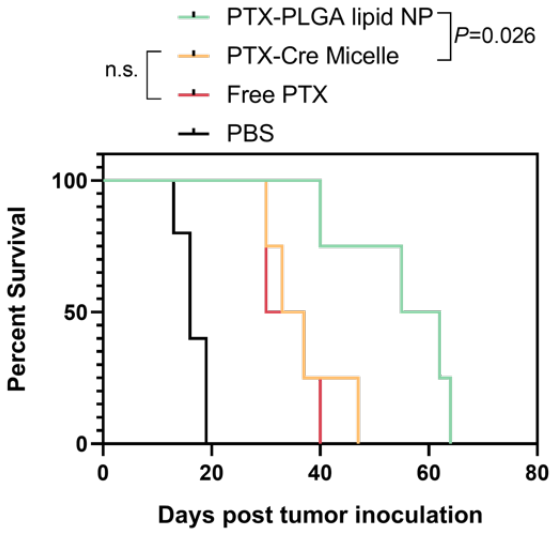

treatments extended the median survival time to 35 days and 33.5 days, respectively, compared to 16 days with PBS treatment. In contrast, PTX-PLGA lipid NP markedly prolonged the median survival to 58.5 days (Table 2). In conclusion, PTX-PLGA lipid NP exhibited enhanced antitumor effects and significantly prolonged survival rate compared to the other formulations.

Table 2. Summary of the median survival duration (in days post-tumor inoculation) among mice with peritoneal metastases of colorectal carcinoma following various treatments.

	PBS	PTX-PLGA lipid NP	PTX-Cre Micelle	Free PTX
Median Survival (Day)	16	58.5	35	33.5

Toxicity of each formulation was assessed by measuring the changes in mice weight (Figure 39). Mice receiving free PTX experienced a minor decrease in body weight throughout the treatment period, returning to their initial weight thereafter, whereas mice with PTX-PLGA lipid NP and

Figure 39. Body weight changes of colorectal tumor-bearing athymic nude mice after indicated treatments

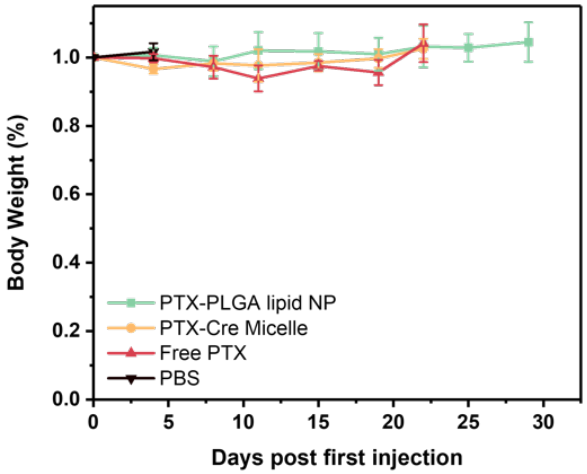

PTX-Cre Micelle treatments maintained consistent body weights. This outcome indicates the absence of overall toxicity following repeated administrations of each formulation.

4.4 Conclusion

The IP injection of three formulations, including PTX-PLGA lipid NP, PTX-Cre micelle and free PTX solution, resulted in distinct pharmacokinetic profiles over a 48-hour period. Free PTX exhibited rapid absorption into plasma via blood vessels due to its small molecule property, reaching peak concentrations shortly after injection, followed by swift clearance from systemic

circulation. For free PTX, the rapid absorption of water and ethanol may cause PTX to precipitate within the peritoneal cavity as a microscale particle, hindering its absorption by the peritoneum. Meanwhile the intact free PTX may also subject to opsonization, cleared by the immune system in both peritoneal cavity and systemic circulation.

In contrast, encapsulated PTX formulations exhibited an extravascular absorption behavior with delayed peak concentrations. Remarkably, PTX-PLGA lipid NPs displayed superior systemic pharmacokinetics profile, including highest peak concentration, retention time, total drug availability in circulation. Taken together, these enhanced properties attribute to the robust stability and sustained release property of PLGA lipid NP, which can not only penetrate directly into tumors in peritoneal cavity after administration, but also reaccumulate in tumors during systemic circulation without losing many drugs in the transportation process.

The pharmacokinetic profile of PTX-Cre micelle also indicated its extravascular absorption route via lymphatic vessels. However, based on the *in vitro* stability test, the PTX-Cre micelle formulation is unstable after interacting with plasma protein. Since the plasma protein adequately exist in both peritoneal fluid and plasma, the instability significantly weakens the treatment efficacy in both direct and indirect pathway. In the peritoneal cavity, the PTX leakage can easily lead to clearance by immune system and precipitation as microscale drug particle. On the other hand, disassembling the micelle platform also exposes the PTX to metabolization in the systemic circulation, which causes it to lose its effective dosage before reaching the tumor site.

After 24-hour post-administration, all three formulations showed comparable PTX accumulation within solid tumors in biodistribution study, which may be dominated by spatial proximity, since all the nanomedicines penetrate tumor site once they were introduced into peritoneal cavity. However, the longer they stay in peritoneal cavity, the stability factor became more significant in

determining the biodistribution profile of each formulation. PTX-PLGA lipid NP exhibited profound advantages in shielding PTX from immune system clearance in both peritoneal fluid and plasma, thereby facilitating its accumulation at the tumor site through sustained release, particularly at the 48-hour interval. In contrast, the other two formulations demonstrated lower drug accumulation due to immune system clearance from the peritoneal cavity and plasma. Without potent and stable protection of PTX, both PTX-Cre micelle and free PTX show low PTX accumulation in the liver since the leaked PTX may go through rapid metabolism in the body and precipitation in peritoneal cavity, lymphatic nodes, or circulation. For other important organ detection, the PTX levels was low, showing minimal systemic toxicity that each formulation may possess.

In an *in vivo* antitumor efficacy assessment using HCT116 mouse tumor xenograft models, PTX-PLGA lipid NP demonstrated potent antitumor effects compared to PTX-Cre micelle and free PTX. Starting from the first dosage, PTX-PLGA lipid NP demonstrated the most effective impact on tumor suppression, even it is not that profound. After the whole regimen, PTX-PLGA lipid NP exhibited superior efficacy on treating tumor growth, attributed to their protective lipid layer and controlled release properties. During the antitumor efficacy monitoring, where PTX-PLGA lipid NP prolonged median survival to 58.5 days, while PTX-Cre mice and free PTX extended median survival to 35 and 33.5 days, respectively. When comparing with representative IVIS images, the impressive tumor suppression from PTX-PLGA lipid NP were further demonstrated in terms of tumor growth area and tumor intensity. The similar antitumor efficacy from PTX-Cre micelle and free PTX may indicate that the major function from Cremophor EL in formulation setup is probably to increase the solubility of PTX that possess inferior stability. Moreover, PTX-PLGA lipid NPs showed minimal overall toxicity to mice with nearly no weight loss.

In summary, PLGA lipid NP offers a promising platform to treat colorectal cancer peritoneal metastasis by effectively delivering chemotherapeutic PTX drug. Our results demonstrated enhanced drug exposure during systemic circulation, greatly improved tumor accumulation and antitumor efficacy with minimal systemic toxicity. Our finding presented an effective approach for drug delivery in IP treatment and pave the way for potential collaboration with other therapy methods.

Chapter 5. Summary and Future Perspective

In this thesis, our objective was to improve the effectiveness of IP treatment for colorectal cancer peritoneal metastases (CRC-PM) and improve patient compliance. The current IP treatment is regarded as aggressive and complicated modality, involving long-term perfusion through indwelling catheters. This approach can lead to potential problems such as inflammation and reduced patient adherence with marked by fatigue, nausea, and diarrhea in challenging recovery period, due to the open abdominal surgery during CRS-HIPEC procedure.These factors continue to impede the widespread adoption of IP treatment for CRC-PM. Primarily, the rapid clearance of chemotherapy agents from the peritoneal cavity and their inefficient delivery during systemic circulation hinder the accumulation of effective doses, necessitating prolonged exposure to chemotherapy perfusion.

Currently, PLGA based micro/nanoparticles and liposomes are widely used for drug delivery research for IP treatment. However, some fatal drawbacks still limit their further development for IP treatment, including the elevated risk of peritoneal adhesion, susceptibility to clearance by the immune system via opsonization, and instability during IP treatment. The PLGA lipid hybrid nanoparticle (PLGA lipid NP) can be a promising candidate for addressing the obstacles encountered in IP treatment. Its superior stability in both peritoneal fluid and plasma enhances effective drug exposure and accumulation to tumors within the cavity. Upon administration into the peritoneal cavity, these nanoparticles can either directly diffuse into tumors or re-accumulate in tumors via the enhanced permeability and retention (EPR) effect after systemic circulation, owing to the integrity of the drug delivery system. Furthermore, the sustained release profile of these nanoparticles facilitates the administration of high doses of chemotherapeutic agents,

reducing administration times and preventing unnecessary drug leakage during systemic circulation before reaching the tumor site.

In Chapter 2, by optimization of fabrication processes, we developed an effective nanoparticle system for IP treatment, marking the first study to leverage PLGA lipid NP for CRC-PM treatment, which will be evaluated against the current Taxol formulation.

In Chapter 3, by various examinations of physicochemical attributes of different materials for the drug delivery platform, we confirmed the surface modification of the PLGA core with lipid layers through size characterization, ζ potential measurements using DLS and TEM. Later in Chapter 3 and Chapter 4, through a comprehensive examination of both *in vitro* and *in vivo* experiments, this thesis showcases the potential of PLGA lipid NP as a promising candidate for drug delivery in colorectal cancer peritoneal metastases, exhibiting superior stability, *in vitro* release profile and encouraging survival rates.

Although the PTX-PLGA lipid NP exhibited excellent anti-tumor efficacy while IP treatment for colorectal cancer peritoneal metastasis, it is important to highlight certain drawbacks and limitations identified in experiments. Here we try to put forward some promising future research directions, aiming to comprehensively understand and practically address these issues in a tangible way.

For producing hydrophobic drug-loaded polymeric nanoparticles, both emulsification-solvent evaporation and nanoprecipitation are commonly employed, while nanoprecipitation method usually show higher encapsulation efficiency.[241] For instance, Aws et al. observed that nanoprecipitation method is more efficient to encapsulate the hydrophobic cucurbitacin I than emulsification-solvent evaporation.[242] Due to the supersaturation condition, rapid precipitation of polymer nanoparticle will occur immediately once water-miscible acetone is added into water,

the hydrophobic drug can remain and precipitate within nanoparticle without emulsification step and solvent evaporation in the emulsification-solvent technique. The moderate encapsulation efficiency of PLGA lipid NP via nanoprecipitation is still a common challenge in many nanoparticle systems.[243-246] This limitation hinders the administration of sufficient drug dosages with nanoparticles, potentially leading to both toxicity risks from overdosing with drug delivery materials and inefficiencies in production due to increased material waste.

The disparate solubilities between the drug and polymer in a single organic solvent is the primary reason that causes the low encapsulation efficiency during the nanoprecipitation process. In the process of nanoprecipitation when introducing only one organic solvent into water, the drug may precipitate either significantly earlier or later than the polymer. Overall, the different precipitation time causes the drug aggregation and the limited drug encapsulation within the polymeric nanoparticles. Considering the different solubilities in different solvent conditions, the solubility of one substance can be determined by a specific solvent combination. By dissolving both drug and polymer in the same multiple organic solvent environment, the solubility of drug and polymer can be tailored to be similar. Following this approach, we can potentially narrow the precipitation gap between the drug and polymer, where the drug and polymer can have a closed precipitation time. Ideally, the drug may precipitate slightly before the polymer, which can potentially improve the encapsulation efficiency.[247]

In this thesis, the PLGA lipid NP has been shown to improve the effectiveness and safety of chemotherapeutic paclitaxel during IP treatment for colorectal cancer peritoneal metastasis as a novel drug delivery system. However, we are still seeking alternatives to improve its efficacy. Checkpoint inhibitor immunotherapy (CPI), exemplified by anti-cytotoxic-T-lymphocyte antigen-4 (CTLA-4) and anti-programmed death-1 (PD-1) antibodies, leverages the body's

immune system to combat cancer cells and has emerged as a promising avenue in cancer therapy. CPI provides an alternative approach to cancer treatment by tackling the complexities of tumor biology. Huang and colleagues developed a combined approach to employ a CD4+ T cell epitope-based heterologous immunization strategy with PD-1 immunotherapy for enhancing the effectiveness of cancer immunotherapy.[248]

The tumor microenvironment of solid colorectal tumors is often in an "immunologically cold" state with low immune activity. However, this immune activity is an essential precondition for CPI therapy to exert influence. Hubbell and colleagues developed a tumor-targeting cytokine known as collagen-binding domain fused Interleukin-12 (CBD-IL-12). This cytokine not only actively accumulates in the tumor, where collagen is exposed in the disordered tumor vasculature, but also stimulates the immune response within the tumor microenvironment. With the supplementary assistance of CBD-IL-12, the efficacy of traditional CPI treatments, such as anti-PD-1 antibodies, can be significantly enhanced.[249, 250] Antibody nanoparticle conjugates is an ideal platform to incorporate different cancer treatment strategy together. By conjugating the high-affinity neutralizing antibodies to photothermal nanoparticle that can generate heat by irradiation to inactivate virus, Huang and coworkers have shown its profound capability to inhibit and inactivate SARS-CoV-2.[251] Inspired by these novel hybrid particle platform with innovative targeting immunotherapy, it is promising to integrate CBD-IL-12 and anti-PD-1 antibody onto the surface of PTX-PLGA lipid NP to enhance overall cancer treatment outcomes through a combination of chemotherapy and immunotherapy.

Besides the *in vitro* release and stability test, it is essential to include pure PLGA NP as an additional control group with Cre Micelles in future *in vivo* experiments to further elaborate the specific impact of the lipid layer within living organisms. When the PLGA NP is exposed to a

more complex environment to interact with different biological components, we can conduct a more comprehensive study on its efficacy and safety profile. Simultaneously, it is fundamental to incorporate pharmacokinetic experiments of each formulation in peritoneal fluid and plasma without tumor. The tumor microenvironment is a complicated system; it is an easy but efficient approach to investigate the impact of tumors and how they interact with other parts of the body as the disease progresses by comparing the pharmacokinetic experiments with/without tumors. In the meantime, it can provide a more holistic picture of the biological fate of each formulation as they transport from the peritoneal cavity to systemic circulation.

Reference

1. Sung, H.; Ferlay, J.; Siegel, R. L.; Laversanne, M.; Soerjomataram, I.; Jemal, A.; F., B., Global Cancer Statistics 2020: GLOBOCAN Estimates of Incidence and Mortality Worldwide for 36 Cancers in 185 Countries. *CA Cancer J Clin* **2020,** *70* (4), 313.
2. Klimeck, L.; Heisser, T.; Hoffmeister, M.; Brenner, H., Colorectal cancer: A health and economic problem. *Best Pract Res Clin Gastroenterol* **2023,** *66*, 101839.
3. Sommariva, A.; Tonello, M.; Coccolini, F.; De Manzoni, G.; Delrio, P.; Pizzolato, E.; Gelmini, R.; Serra, F.; Rreka, E.; Pasqual, E. M.; Marano, L.; Biacchi, D.; Carboni, F.; Kusamura, S.; Sammartino, P., Colorectal Cancer with Peritoneal Metastases: The Impact of the Results of PROPHYLOCHIP, COLOPEC, and PRODIGE 7 Trials on Peritoneal Disease Management. *Cancers (Basel)* **2022,** *15* (1).
4. Kranenburg, O.; van der Speeten, K.; de Hingh, I., Peritoneal Metastases From Colorectal Cancer: Defining and Addressing the Challenges. *Front Oncol* **2021,** *11*, 650098.
5. Labianca, R.; Beretta, G. D.; Kildani, B.; Milesi, L.; Merlin, F.; Mosconi, S.; Pessi, M. A.; Prochilo, T.; Quadri, A.; Gatta, G.; de Braud, F.; Wils, J., Colon cancer. *Crit Rev Oncol Hematol* **2010,** *74* (2), 106-33.
6. Bharucha, A. E., Update of tests of colon and rectal structure and function. *Journal of clinical gastroenterology 40* (2), 96-103.
7. Compton, C. C.; Byrd, D. R.; Garcia-Aguilar, J.; Kurtzman, S. H.; Olawaiye, A.; Washington, M. K., Colon and rectum. In *AJCC Cancer Staging Atlas: A Companion to the Seventh Editions of the AJCC Cancer Staging Manual and Handbook*, Compton, C. C.; Byrd, D. R.; Garcia-Aguilar, J.; Kurtzman, S. H.; Olawaiye, A.; Washington, M. K., Eds. 2012; pp 185-201.
8. Washington, M. K.; Berlin, J.; Branton, P. A.; Burgart, L. J.; Carter, D. K.; Fitzgibbons, P. L.; Frankel, W. L.; Jessup, J. M.; Kakar, S.; Minsky, B.; Nakhleh, R. E., Protocol for the examination of specimens from patients with primary carcinomas of the colon and rectum. *Archives of pathology & laboratory medicine* **2008,** *132* (7), 1182-1193.
9. Shussman, N.; Wexner, S. D., Colorectal polyps and polyposis syndromes. *Gastroenterol Rep (Oxf)* **2014,** *2* (1), 1-15.
10. Imperiale, T. F.; Ransohoff, D. F., Risk for colorectal cancer in persons with a family history of adenomatous polyps: a systematic review. *Annals of internal medicine* **2012,** *156* (10), 703-709.
11. Kim, E. C.; Lance, P., Colorectal polyps and their relationship to cancer. *Gastroenterology Clinics* **1997,** *26* (1), 1-17.
12. Lenos, K. J.; Bach, S.; Ferreira Moreno, L.; Ten Hoorn, S.; Sluiter, N. R.; Bootsma, S.; Vieira Braga, F. A.; Nijman, L. E.; van den Bosch, T.; Miedema, D. M.; van Dijk, E.; Ylstra, B.; Kulicke, R.; Davis, F. P.; Stransky, N.; Smolen, G. A.; Coebergh van den Braak, R. R. J.; JNM, I. J.; Martens, J. W. M.; Hallam, S.; Beggs, A. D.; Kops, G.; Lansu, N.; Bastiaenen, V. P.; Klaver, C. E. L.; Lecca, M. C.; El Makrini, K.; Elbers, C. C.; Dings, M. P. G.; van Noesel, C. J. M.; Kranenburg, O.; Medema, J. P.; Koster, J.; Koens, L.; Punt, C. J. A.; Tanis, P. J.; de Hingh, I. H.; Bijlsma, M. F.; Tuynman, J. B.; Vermeulen, L., Molecular characterization of colorectal cancer related peritoneal metastatic disease. *Nat Commun* **2022,** *13* (1), 4443.

13. Koh, J. L.; Yan, T. D.; Glenn, D.; Morris, D. L., Evaluation of preoperative computed tomography in estimating peritoneal cancer index in colorectal peritoneal carcinomatosis. *Ann Surg Oncol* **2009,** *16* (2), 327-33.
14. Franko, J.; Shi, Q.; Meyers, J. P.; Maughan, T. S.; Adams, R. A.; Seymour, M. T.; Saltz, L.; Punt, C. J. A.; Koopman, M.; Tournigand, C.; Tebbutt, N. C.; Diaz-Rubio, E.; Souglakos, J.; Falcone, A.; Chibaudel, B.; Heinemann, V.; Moen, J.; De Gramont, A.; Sargent, D. J.; Grothey, A.; Analysis; Research in Cancers of the Digestive System, G., Prognosis of patients with peritoneal metastatic colorectal cancer given systemic therapy: an analysis of individual patient data from prospective randomised trials from the Analysis and Research in Cancers of the Digestive System (ARCAD) database. *Lancet Oncol* **2016,** *17* (12), 1709-1719.
15. Lemmens, V. E.; Klaver, Y. L.; Verwaal, V. J.; Rutten, H. J.; Coebergh, J. W.; de Hingh, I. H., Predictors and survival of synchronous peritoneal carcinomatosis of colorectal origin: a population-based study. *Int J Cancer* **2011,** *128* (11), 2717-25.
16. Ren, K.; Xie, X.; Min, T.; Sun, T.; Wang, H.; Zhang, Y.; Dang, C.; Zhang, H., Development of the Peritoneal Metastasis: A Review of Back-Grounds, Mechanisms, Treatments and Prospects. *J Clin Med* **2022,** *12* (1).
17. Heldin, C. H.; Rubin, K.; Pietras, K.; Ostman, A., High interstitial fluid pressure - an obstacle in cancer therapy. *Nat Rev Cancer* **2004,** *4* (10), 806-13.
18. Aoyagi, T.; Terracina, K. P.; Raza, A.; Takabe, K., Current treatment options for colon cancer peritoneal carcinomatosis. *World J Gastroenterol* **2014,** *20* (35), 12493-500.
19. Esquivel, J., Embryology and anatomy of the peritoneal cavity. In *Intraperitoneal Cancer Therapy: Principles and Practice*, Esquivel, J., Ed. 2015; pp 3-8.
20. Levy, A. D.; Shaw, J. C.; Sobin, L. H., Secondary tumors and tumorlike lesions of the peritoneal cavity: imaging features with pathologic correlation. *Radiographics* **2009,** *29* (2), 347-373.
21. Moreno, A.; Sarav, M., Physiology of Peritoneal Dialysis. In *Surgical aspects of peritoneal dialysis*, Haggerty, S., Ed. 2017; pp 7-15.
22. Hanbidge, A. E.; Lynch, D.; Wilson, S. R., US of the peritoneum. *Radiographics* **2003,** *23* (3), 663-685.
23. Hartveit, F.; Thunold, S., Peritoneal fluid volume and the oestrus cycle in mice. *Nature* **1966,** *210* (5041), 1123-1125.
24. Sarfarazi, A.; Lee, G.; Mirjalili, S. A.; Phillips, A. R. J.; Windsor, J. A.; Trevaskis, N. L., Therapeutic delivery to the peritoneal lymphatics: Current understanding, potential treatment benefits and future prospects. *Int J Pharm* **2019,** *567*, 118456.
25. Al Shoyaib, A.; Archie, S. R.; Karamyan, V. T., Intraperitoneal Route of Drug Administration: Should it Be Used in Experimental Animal Studies? *Pharm Res* **2019,** *37* (1), 12.
26. Aune, S., Transperitoneal exchange: IV. The effect of transperitoneal fluid transport on the transfer of solutes. *Scandinavian Journal of Gastroenterology* **1970,** *5* (4), 241-252.
27. Schwager, S.; Detmar, M., Inflammation and Lymphatic Function. *Front Immunol* **2019,** *10*, 308.
28. Kakroo, M. A.; Vaitkevicius, P. V.; Baliga, R. R., Edema. In *Practical Cardiology: Evaluation and Treatment of Common Cardiovascular Disorders,*, Eagle, K. A.; Baliga, R. R., Eds. 2020; pp 39-46.

29. Cho, S.; Atwood, J. E., Peripheral edema. *The American journal of medicine* **2002,** *113* (7), 580-586.
30. McMullen, J. R.; Selleck, M.; Wall, N. R.; Senthil, M., Peritoneal carcinomatosis: limits of diagnosis and the case for liquid biopsy. *Oncotarget* **2017,** *8* (26), 43481.
31. Xia, W.; Geng, Y.; Hu, W., Peritoneal Metastasis: A Dilemma and Challenge in the Treatment of Metastatic Colorectal Cancer. *Cancers (Basel)* **2023,** *15* (23).
32. De Gaetano, A. M.; Calcagni, M. L.; Rufini, V.; Valenza, V.; Giordano, A.; Bonomo, L., Imaging of peritoneal carcinomatosis with FDG PET-CT: diagnostic patterns, case examples and pitfalls. *Abdom Imaging* **2009,** *34* (3), 391-402.
33. Nindra, U.; Shahnam, A.; Mahon, K. L., Review of systemic chemotherapy in unresectable colorectal peritoneal carcinomatosis. *Asia Pac J Clin Oncol* **2022,** *18* (1), 7-12.
34. Hompes, D.; D'Hoore, A.; Van Cutsem, E.; Fieuws, S.; Ceelen, W.; Peeters, M.; Van der Speeten, K.; Bertrand, C.; Legendre, H.; Kerger, J., The treatment of peritoneal carcinomatosis of colorectal cancer with complete cytoreductive surgery and hyperthermic intraperitoneal peroperative chemotherapy (HIPEC) with oxaliplatin: a Belgian multicentre prospective phase II clinical study. *Ann Surg Oncol* **2012,** *19* (7), 2186-94.
35. van Oudheusden, T. R.; Razenberg, L. G.; van Gestel, Y. R.; Creemers, G. J.; Lemmens, V. E.; de Hingh, I. H., Systemic treatment of patients with metachronous peritoneal carcinomatosis of colorectal origin. *Sci Rep* **2015,** *5*, 18632.
36. Elias, D.; Lefevre, J. H.; Chevalier, J.; Brouquet, A.; Marchal, F.; Classe, J. M.; Ferron, G.; Guilloit, J. M.; Meeus, P.; Goere, D.; Bonastre, J., Complete cytoreductive surgery plus intraperitoneal chemohyperthermia with oxaliplatin for peritoneal carcinomatosis of colorectal origin. *J Clin Oncol* **2009,** *27* (5), 681-5.
37. Foster, J. M.; Sleightholm, R.; Patel, A.; Shostrom, V.; Hall, B.; Neilsen, B.; Bartlett, D.; Smith, L., Morbidity and Mortality Rates Following Cytoreductive Surgery Combined With Hyperthermic Intraperitoneal Chemotherapy Compared With Other High-Risk Surgical Oncology Procedures. *JAMA Netw Open* **2019,** *2* (1), e186847.
38. Dedrick, R. L.; Myers, C. E.; Bungay, P. M.; DeVita, V. T., Pharmacokinetic rationale for peritoneal drug administration. *Cancer Treat Rep* **1978,** *62*, 1-13.
39. Wolinsky, J. B.; Colson, Y. L.; Grinstaff, M. W., Local drug delivery strategies for cancer treatment: gels, nanoparticles, polymeric films, rods, and wafers. *J Control Release* **2012,** *159* (1), 14-26.
40. Tydings, C.; Sharma, K. V.; Kim, A.; Yarmolenko, P. S., Emerging hyperthermia applications for pediatric oncology. *Adv Drug Deliv Rev* **2020,** *163-164*, 157-167.
41. Sugarbaker, P. H., Surgical management of peritoneal carcinosis: diagnosis, prevention and treatment. *Langenbecks Archiv für Chirurgie* **1988,** *373*, 189-196.
42. Nowacki, M.; Zegarski, W., The scientific report from the first pressurized intraperitoneal aerosol chemotherapy (PIPAC) procedures performed in the eastern part of Central Europe. *J Int Med Res* **2018,** *46* (9), 3748-3758.
43. Solass, W.; Giger-Pabst, U.; Zieren, J.; Reymond, M. A., Pressurized intraperitoneal aerosol chemotherapy (PIPAC): occupational health and safety aspects. *Ann Surg Oncol* **2013,** *20* (11), 3504-11.
44. Nadiradze, G.; Horvath, P.; Sautkin, Y.; Archid, R.; Weinreich, F. J.; Konigsrainer, A.; Reymond, M. A., Overcoming Drug Resistance by Taking Advantage of Physical Principles: Pressurized Intraperitoneal Aerosol Chemotherapy (PIPAC). *Cancers (Basel)* **2019,** *12* (1).

45. Solass, W.; Kerb, R.; Murdter, T.; Giger-Pabst, U.; Strumberg, D.; Tempfer, C.; Zieren, J.; Schwab, M.; Reymond, M. A., Intraperitoneal chemotherapy of peritoneal carcinomatosis using pressurized aerosol as an alternative to liquid solution: first evidence for efficacy. *Ann Surg Oncol* **2014,** *21* (2), 553-9.
46. Yakati, V.; Vangala, S.; Madamsetty, V. S.; Banerjee, R.; Moku, G., Enhancing the anticancer effect of paclitaxel by using polymeric nanoparticles decorated with colorectal cancer targeting CPKSNNGVC-peptide. *Journal of Drug Delivery Science and Technology* **2022,** *68*.
47. Pham, D. T.; Saelim, N.; Tiyaboonchai, W., Paclitaxel loaded EDC-crosslinked fibroin nanoparticles: a potential approach for colon cancer treatment. *Drug Deliv Transl Res* **2020,** *10* (2), 413-424.
48. Barbuti, A. M.; Chen, Z. S., Paclitaxel Through the Ages of Anticancer Therapy: Exploring Its Role in Chemoresistance and Radiation Therapy. *Cancers (Basel)* **2015,** *7* (4), 2360-71.
49. Delhorme, J. B.; Sauvinet, G.; Severac, F.; Diab, S.; Liu, D.; Rohr, S.; Romain, B.; Brigand, C., Peritoneal Metastases of Colorectal Origin Treated with Complete Cytoreduction and Hyperthermic Intraperitoneal Chemotherapy: The Efficiency of Mitomycin C. *Ann Surg Oncol* **2022,** *29* (12), 7568-7576.
50. Shen, P.; Levine, E. A.; Hall, J.; Case, D.; Russell, G.; Fleming, R.; McQuellon, R.; Geisinger, K. R.; Loggie, B. W., Factors predicting survival after intraperitoneal hyperthermic chemotherapy with mitomycin C after cytoreductive surgery for patients with peritoneal carcinomatosis. *Archives of surgery* **2003,** *138* (1), 26-33.
51. Murono, K.; Kawai, K.; Hata, K.; Emoto, S.; Kaneko, M.; Sasaki, K.; Nishikawa, T.; Otani, K.; Tanaka, T.; Nozawa, H., Regimens of Intraperitoneal Chemotherapy for Peritoneal Carcinomatosis from Colorectal Cancer. *Anticancer Res* **2018,** *38* (1), 15-22.
52. Laoukili, J.; Constantinides, A.; Wassenaar, E. C. E.; Elias, S. G.; Raats, D. A. E.; van Schelven, S. J.; van Wettum, J.; Volckmann, R.; Koster, J.; Huitema, A. D. R.; Nienhuijs, S. W.; de Hingh, I.; Wiezer, R. J.; van Grevenstein, H. M. U.; Rinkes, I.; Boerma, D.; Kranenburg, O., Peritoneal metastases from colorectal cancer belong to Consensus Molecular Subtype 4 and are sensitised to oxaliplatin by inhibiting reducing capacity. *Br J Cancer* **2022,** *126* (12), 1824-1833.
53. Glockzin, G.; Gerken, M.; Lang, S. A.; Klinkhammer-Schalke, M.; Piso, P.; Schlitt, H. J., Oxaliplatin-based versus irinotecan-based hyperthermic intraperitoneal chemotherapy (HIPEC) in patients with peritoneal metastasis from appendiceal and colorectal cancer: a retrospective analysis. *BMC Cancer* **2014,** *14*, 1-9.
54. Ducreux, M.; Bennouna, J.; Adenis, A.; Conroy, T.; Lievre, A.; Portales, F.; Jeanes, J.; Li, L.; Romano, A., Efficacy and safety of nab-paclitaxel in patients with previously treated metastatic colorectal cancer: a phase II COLO-001 trial. *Cancer Chemother Pharmacol* **2017,** *79* (1), 9-16.
55. Van Tellingen, O.; Huizing, M. T.; Panday, V. R.; Schellens, J. H. M.; Nooijen, W. J.; Beijnen, J. H., Cremophor EL causes (pseudo-) non-linear pharmacokinetics of paclitaxel in patients. *British journal of cancer* **1999,** *81* (2), 330-335.
56. Irizarry, L. D.; Luu, T. H.; McKoy, J. M.; Samaras, A. T.; Fisher, M. J.; Carias, E. E.; Raisch, D. W.; Calhoun, E. A.; Bennett, C. L., Cremophor EL-containing paclitaxel-induced anaphylaxis: a call to action. *Community oncology* **2009,** *6* (3), 132.

57. Gelderblom, H.; Verweij, J.; Nooter, K.; Sparreboom, A., Cremophor EL: the drawbacks and advantages of vehicle selection for drug formulation. *European journal of cancer* **2001,** *37* (13), 1590-1598.
58. Jacquet, P.; Averbach, A.; Stuart, O. A.; Chang, D.; Sugarbaker, P. H., Hyperthermic intraperitoneal doxorubicin: pharmacokinetics, metabolism, and tissue distribution in a rat model. *Cancer chemotherapy and pharmacology* **1997,** *41*, 147-154.
59. Harada, S.; Ping, L.; Obara, T.; Oikawa, H.; Miyata, M.; Matsuo, M.; Takahashi, T.; Yanagisawa, T., The antitumor effect of hyperthermia combined with fluorouracil and its analogues. *Radiation research* **1995,** *142* (2), 232-241.
60. Kuh, H. J.; Jang, S. H.; Wientjes, M. G.; Weaver, J. R.; Au, J. L. S., Determinants of paclitaxel penetration and accumulation in human solid tumor. *Journal of Pharmacology and Experimental Therapeutics* **1999,** *290* (2), 871-880.
61. Van de Vaart, P. J. M.; Vange., N. V. d.; Zoetmulder., F. A. N.; Goethem., A. R. V.; Tellingen., O. V.; Huinink., W. W. t. B.; Beijnen., J. H.; Bartelink., H.; Begg., A. C., Intraperitoneal cisplatin with regional hyperthermia in advanced ovarian cancer: pharmacokinetics and cisplatin–DNA adduct formation in patients and ovarian cancer cell lines. *European journal of cancer* **1998,** *34* (1), 148-154.
62. Gentile, P.; Chiono, V.; Carmagnola, I.; Hatton, P. V., An overview of poly(lactic-co-glycolic) acid (PLGA)-based biomaterials for bone tissue engineering. *Int J Mol Sci* **2014,** *15* (3), 3640-59.
63. Chen, W.; Yang, H.; Wang, R.; Cheng, R.; Meng, F.; Wei, W.; Zhong, Z., Versatile Synthesis of Functional Biodegradable Polymers by Combining Ring-Opening Polymerization and Postpolymerization Modification via Michael-Type Addition Reaction. *Macromolecules* **2009,** *43* (1), 201-207.
64. Rudolph, A.; Teske, M.; Illner, S.; Kiefel, V.; Sternberg, K.; Grabow, N.; Wree, A.; Hovakimyan, M., Surface Modification of Biodegradable Polymers towards Better Biocompatibility and Lower Thrombogenicity. *PLoS One* **2015,** *10* (12), e0142075.
65. Akbari Javar, R.; Bin Noordin, M. I.; Khoobi, M.; Ghaedi, A., Fatty Acid Based Polyamide for Application in Drug Delivery System: Synthesis, Characterization, Drug Loading and In Vitro Drug Release Study. *Journal of Inorganic and Organometallic Polymers and Materials* **2020,** *30* (7), 2520-2532.
66. Menezes, P. D.; Frank, L. A.; Lima, B. D.; de Carvalho, Y. M.; Serafini, M. R.; Quintans-Junior, L. J.; Pohlmann, A. R.; Guterres, S. S.; Araujo, A. A., Hesperetin-loaded lipid-core nanocapsules in polyamide: a new textile formulation for topical drug delivery. *Int J Nanomedicine* **2017,** *12*, 2069-2079.
67. Boddu, S. H. S.; Bhagav, P.; Karla, P. K.; Jacob, S.; Adatiya, M. D.; Dhameliya, T. M.; Ranch, K. M.; Tiwari, A. K., Polyamide/Poly(Amino Acid) Polymers for Drug Delivery. *J Funct Biomater* **2021,** *12* (4).
68. Liu, N.; Li, B.; Gong, C.; Liu, Y.; Wang, Y.; Wu, G., A pH- and thermo-responsive poly(amino acid)-based drug delivery system. *Colloids Surf B Biointerfaces* **2015,** *136*, 562-9.
69. Washington, K. E.; Kularatne, R. N.; Karmegam, V.; Biewer, M. C.; Stefan, M. C., Recent advances in aliphatic polyesters for drug delivery applications. *Wiley Interdiscip Rev Nanomed Nanobiotechnol* **2017,** *9* (4).

70. Gupta, P. K.; Gahtori, R.; Govarthanan, K.; Sharma, V.; Pappuru, S.; Pandit, S.; Mathuriya, A. S.; Dholpuria, S.; Bishi, D. K., Recent trends in biodegradable polyester nanomaterials for cancer therapy. *Mater Sci Eng C Mater Biol Appl* **2021,** *127*, 112198.
71. Molavi, F.; Barzegar-Jalali, M.; Hamishehkar, H., Polyester based polymeric nano and microparticles for pharmaceutical purposes: A review on formulation approaches. *J Control Release* **2020,** *320*, 265-282.
72. Tan, R. Y. H.; Lee, C. S.; Pichika, M. R.; Cheng, S. F.; Lam, K. Y., PH Responsive Polyurethane for the Advancement of Biomedical and Drug Delivery. *Polymers (Basel)* **2022,** *14* (9).
73. Bil, M.; Kijenska-Gawronska, E.; Glodkowska-Mrowka, E.; Manda-Handzlik, A.; Mrowka, P., Design and in vitro evaluation of electrospun shape memory polyurethanes for self-fitting tissue engineering grafts and drug delivery systems. *Mater Sci Eng C Mater Biol Appl* **2020,** *110*, 110675.
74. Abbasnezhad, N.; Zirak, N.; Shirinbayan, M.; Kouidri, S.; Salahinejad, E.; Tcharkhtchi, A.; Bakir, F., Controlled release from polyurethane films: Drug release mechanisms. *Journal of Applied Polymer Science* **2020,** *138* (12).
75. Park, K.; Skidmore, S.; Hadar, J.; Garner, J.; Park, H.; Otte, A.; Soh, B. K.; Yoon, G.; Yu, D.; Yun, Y.; Lee, B. K.; Jiang, X.; Wang, Y., Injectable, long-acting PLGA formulations: Analyzing PLGA and understanding microparticle formation. *J Control Release* **2019,** *304*, 125-134.
76. Lim, Y. W.; Tan, W. S.; Ho, K. L.; Mariatulqabtiah, A. R.; Abu Kasim, N. H.; Abd Rahman, N.; Wong, T. W.; Chee, C. F., Challenges and Complications of Poly(lactic-co-glycolic acid)-Based Long-Acting Drug Product Development. *Pharmaceutics* **2022,** *14* (3).
77. Alsaab, H. O.; Alharbi, F. D.; Alhibs, A. S.; Alanazi, N. B.; Alshehri, B. Y.; Saleh, M. A.; Alshehri, F. S.; Algarni, M. A.; Almugaiteeb, T.; Uddin, M. N.; Alzhrani, R. M., PLGA-Based Nanomedicine: History of Advancement and Development in Clinical Applications of Multiple Diseases. *Pharmaceutics* **2022,** *14* (12).
78. Wang, Y.; Qu, W.; Choi, S. H., FDA's regulatory science program for generic PLA/PLGA-based drug products. *American Pharmaceutical Review* **2016**.
79. Chereddy, K. K.; Payen, V. L.; Preat, V., PLGA: From a classic drug carrier to a novel therapeutic activity contributor. *J Control Release* **2018,** *289*, 10-13.
80. Lagreca, E.; Onesto, V.; Di Natale, C.; La Manna, S.; Netti, P. A.; Vecchione, R., Recent advances in the formulation of PLGA microparticles for controlled drug delivery. *Prog Biomater* **2020,** *9* (4), 153-174.
81. Sarkar, C.; Kommineni, N.; Butreddy, A.; Kumar, R.; Bunekar, N.; Gugulothu, K., *Nanoengineering of Biomaterials*. 2022.
82. Han, F. Y.; Thurecht, K. J.; Whittaker, A. K.; Smith, M. T., Bioerodable PLGA-Based Microparticles for Producing Sustained-Release Drug Formulations and Strategies for Improving Drug Loading. *Front Pharmacol* **2016,** *7*, 185.
83. Yoo, J.; Won, Y. Y., Phenomenology of the Initial Burst Release of Drugs from PLGA Microparticles. *ACS Biomater Sci Eng* **2020,** *6* (11), 6053-6062.
84. Park, H.; Ha, E. S.; Kim, J. S.; Kim, M. S., Injectable sustained-release poly(lactic-co-glycolic acid) (PLGA) microspheres of exenatide prepared by supercritical fluid extraction of emulsion process based on a design of experiment approach. *Bioeng Transl Med* **2023,** *8* (3), e10485.

85. Pan, Z.; Ding, J., Poly(lactide-co-glycolide) porous scaffolds for tissue engineering and regenerative medicine. *Interface Focus* **2012,** *2* (3), 366-77.
86. Yan, B.; Hua, Y.; Wang, J.; Shao, T.; Wang, S.; Gao, X.; Gao, J., Surface Modification Progress for PLGA-Based Cell Scaffolds. *Polymers (Basel)* **2024,** *16* (1).
87. Eviana Putri, N. R.; Wang, X.; Chen, Y.; Li, X.; Kawazoe, N.; Chen, G., Preparation of PLGA-collagen hybrid scaffolds with controlled pore structures for cartilage tissue engineering. *Progress in Natural Science: Materials International* **2020,** *30* (5), 642-650.
88. Lü, J. M.; Wang, X.; Marin-Muller, C.; Wang, H.; Lin, P. H.; Yao, Q.; Chen, C., Current advances in research and clinical applications of PLGA-based nanotechnology. *Expert review of molecular diagnostics* **2009,** *9* (4), 325-341.
89. Athanasiou, K. A.; Niederauer, G. G.; Agrawal, C. M., Sterilization, toxicity, biocompatibility and clinical applications of polylactic acid/polyglycolic acid copolymers. *Biomaterials* **1996,** *17* (2), 93-102.
90. Castro, V. O.; Livi, S.; Sperling, L. E.; Dos Santos, M. G.; Merlini, C., Biodegradable Electrospun Conduit with Aligned Fibers Based on Poly(lactic-co-glycolic Acid) (PLGA)/Carbon Nanotubes and Choline Bitartrate Ionic Liquid. *ACS Appl Bio Mater* **2024**.
91. Liu, G.; McEnnis, K., Glass Transition Temperature of PLGA Particles and the Influence on Drug Delivery Applications. *Polymers (Basel)* **2022,** *14* (5).
92. Wise, D. L., *Encyclopedic handbook of biomaterials and bioengineering: v. 1-2.* CRC Press: 1995; Vol. 1.
93. Langer, R.; Chasin, M., *Biodegradable polymers as drug delivery systems*. Informa Health Care: 1990.
94. Makadia, H. K.; Siegel, S. J., Poly Lactic-co-Glycolic Acid (PLGA) as Biodegradable Controlled Drug Delivery Carrier. *Polymers (Basel)* **2011,** *3* (3), 1377-1397.
95. Castagna, A.; Zander, A. J.; Sautkin, I.; Schneider, M.; Shegokar, R.; Königsrainer, A.; Reymond, M. A., Enhanced intraperitoneal delivery of charged, aerosolized curcumin nanoparticles by electrostatic precipitation. *Nanomedicine* **2020,** *16* (2), 109-120.
96. Fraguas-Sanchez, A. I.; Torres-Suarez, A. I.; Cohen, M.; Delie, F.; Bastida-Ruiz, D.; Yart, L.; Martin-Sabroso, C.; Fernandez-Carballido, A., PLGA Nanoparticles for the Intraperitoneal Administration of CBD in the Treatment of Ovarian Cancer: In Vitro and In Ovo Assessment. *Pharmaceutics* **2020,** *12* (5).
97. Colson, Y. L.; Liu, R.; Southard, E. B.; Schulz, M. D.; Wade, J. E.; Griset, A. P.; Zubris, K. A.; Padera, R. F.; Grinstaff, M. W., The performance of expansile nanoparticles in a murine model of peritoneal carcinomatosis. *Biomaterials* **2011,** *32* (3), 832-40.
98. Tsai, M.; Lu, Z.; Wientjes, M. G.; Au, J. L., Paclitaxel-loaded polymeric microparticles: quantitative relationships between in vitro drug release rate and in vivo pharmacodynamics. *J Control Release* **2013,** *172* (3), 737-44.
99. Yeo, Y.; Kohane, D. S., Polymers in the prevention of peritoneal adhesions. *Eur J Pharm Biopharm* **2008,** *68* (1), 57-66.
100. Samad, A.; Sultana, Y.; Aqil, M., Liposomal drug delivery systems: an update review. *Current drug delivery* **2007,** *4* (4), 297-305.
101. Allen, T. M.; Cullis, P. R., Liposomal drug delivery systems: from concept to clinical applications. *Adv Drug Deliv Rev* **2013,** *65* (1), 36-48.
102. Sercombe, L.; Veerati, T.; Moheimani, F.; Wu, S. Y.; Sood, A. K.; Hua, S., Advances and Challenges of Liposome Assisted Drug Delivery. *Front Pharmacol* **2015,** *6*, 286.

103. Torchilin, V. P., Recent advances with liposomes as pharmaceutical carriers. *Nat Rev Drug Discov* **2005,** *4* (2), 145-60.
104. Pauli, G.; Chao, P. H.; Qin, Z.; Bottger, R.; Lee, S. E.; Li, S. D., Liposomal Resiquimod for Enhanced Immunotherapy of Peritoneal Metastases of Colorectal Cancer. *Pharmaceutics* **2021,** *13* (10).
105. Mirahmadi, N.; Babaei, M. H.; Vali, A. M.; Dadashzadeh, S., Effect of liposome size on peritoneal retention and organ distribution after intraperitoneal injection in mice. *Int J Pharm* **2010,** *383* (1-2), 7-13.
106. Pasarin, D.; Ghizdareanu, A. I.; Enascuta, C. E.; Matei, C. B.; Bilbie, C.; Paraschiv-Palada, L.; Veres, P. A., Coating Materials to Increase the Stability of Liposomes. *Polymers (Basel)* **2023,** *15* (3).
107. Bajaj, G.; Yeo, Y., Drug delivery systems for intraperitoneal therapy. *Pharm Res* **2010,** *27* (5), 735-8.
108. Statler, P. A.; McPherson, R. J.; Bauer, L. A.; Kellert, B. A.; Juul, S. E., Pharmacokinetics of high-dose recombinant erythropoietin in plasma and brain of neonatal rats. *Pediatr Res* **2007,** *61* (6), 671-5.
109. Colby, A. H.; Kirsch, J.; Patwa, A. N.; Liu, R.; Hollister, B.; McCulloch, W.; Burdette, J. E.; Pearce, C. J.; Oberliels, N. H.; Colson, Y. L.; Liu, K.; Grinstaff, M. W., Radiolabeled Biodistribution of Expansile Nanoparticles: Intraperitoneal Administration Results in Tumor Specific Accumulation. *ACS Nano* **2023,** *17* (3), 2212-2221.
110. Long, R. T.; Edwards, R. H., Implantation metastasis as a cause of local recurrence of colorectal carcinoma. *The American journal of surgery* **1989,** *157* (2), 194-201.
111. Braam, H. J.; Van Oudheusden, T. R.; De Hingh, I. H.; Nienhuijs, S. W.; Boerma, D.; Wiezer, M. J.; Van Ramshorst, B., Patterns of recurrence following complete cytoreductive surgery and hyperthermic intraperitoneal chemotherapy in patients with peritoneal carcinomatosis of colorectal cancer. *Journal of surgical oncology* **2014,** *109* (8), 841-847.
112. Tomlinson, J. S.; Jarnagin, W. R.; DeMatteo, R. P.; Fong, Y.; Kornprat, P.; Gonen, M.; Kemeny, N.; Brennan, M. F.; Blumgart, L. H.; D'Angelica, M., Actual 10-year survival after resection of colorectal liver metastases defines cure. *J Clin Oncol* **2007,** *25* (29), 4575-80.
113. Lu, Z.; Wang, J.; Wientjes, M. G.; Au, J. L., Intraperitoneal therapy for peritoneal cancer. *Future oncology* **2010,** *6* (10), 1625-1641.
114. Ceelen, W.; Braet, H.; van Ramshorst, G.; Willaert, W.; Remaut, K., Intraperitoneal chemotherapy for peritoneal metastases: an expert opinion. *Expert Opin Drug Deliv* **2020,** *17* (4), 511-522.
115. Ernsting, M. J.; Murakami, M.; Roy, A.; Li, S. D., Factors controlling the pharmacokinetics, biodistribution and intratumoral penetration of nanoparticles. *J Control Release* **2013,** *172* (3), 782-94.
116. Huo, S.; Ma, H.; Huang, K.; Liu, J.; Wei, T.; Jin, S.; Zhang, J.; He, S.; Liang, X. J., Superior penetration and retention behavior of 50 nm gold nanoparticles in tumors. *Cancer Res* **2013,** *73* (1), 319-30.
117. Kohane, D. S.; Tse, J. Y.; Yeo, Y.; Padera, R.; Shubina, M.; Langer, R., Biodegradable polymeric microspheres and nanospheres for drug delivery in the peritoneum. *J Biomed Mater Res A* **2006,** *77* (2), 351-61.
118. Kohane, D. S.; Langer, R., Biocompatibility and drug delivery systems. *Chem. Sci.* **2010,** *1* (4), 441-446.

119. Wani, T. U.; Raza, S. N.; Khan, N. A., Nanoparticle opsonization: forces involved and protection by long chain polymers. *Polymer Bulletin* **2019,** *77* (7), 3865-3889.
120. Zheng, C.; Liang, W., A one-step modified method to reduce the burst initial release from PLGA microspheres. *Drug Deliv* **2010,** *17* (2), 77-82.
121. Rodrigues de Azevedo, C.; von Stosch, M.; Costa, M. S.; Ramos, A. M.; Cardoso, M. M.; Danhier, F.; Preat, V.; Oliveira, R., Modeling of the burst release from PLGA micro- and nanoparticles as function of physicochemical parameters and formulation characteristics. *Int J Pharm* **2017,** *532* (1), 229-240.
122. Nsairat, H.; Khater, D.; Sayed, U.; Odeh, F.; Al Bawab, A.; Alshaer, W., Liposomes: structure, composition, types, and clinical applications. *Heliyon* **2022,** *8* (5), e09394.
123. Gajbhiye, K. R.; Salve, R.; Narwade, M.; Sheikh, A.; Kesharwani, P.; Gajbhiye, V., Lipid polymer hybrid nanoparticles: a custom-tailored next-generation approach for cancer therapeutics. *Mol Cancer* **2023,** *22* (1), 160.
124. Sharma, A.; Sharma, U. S., Liposomes in drug delivery: progress and limitations. *International journal of pharmaceutics* **1997,** *154* (2), 123-140.
125. Gleue, L.; Schupp, J.; Zimmer, N.; Becker, E.; Frey, H.; Tuettenberg, A.; Helm, M., Stability of Alkyl Chain-Mediated Lipid Anchoring in Liposomal Membranes. *Cells* **2020,** *9* (10).
126. Maurer, N.; Fenske, D. B.; Cullis, P. R., Developments in liposomal drug delivery systems. *Expert opinion on biological therapy* **2001,** *1* (6), 923-947.
127. Jeon, S. I.; Lee, J. H.; Andrade, J. D.; De Gennes, P., Protein—surface interactions in the presence of polyethylene oxide: I. Simplified theory. *Journal of colloid and interface science* **1991,** *142* (1), 149-158.
128. Danhier, F.; Ansorena, E.; Silva, J. M.; Coco, R.; Le Breton, A.; Preat, V., PLGA-based nanoparticles: an overview of biomedical applications. *J Control Release* **2012,** *161* (2), 505-22.
129. Sadeghi, A.; PourEskandar, S.; Askari, E.; Akbari, M., Polymeric Nanoparticles and Nanogels: How Do They Interact with Proteins? *Gels* **2023,** *9* (8).
130. El-Hammadi, M. M.; Arias, J. L., Recent Advances in the Surface Functionalization of PLGA-Based Nanomedicines. *Nanomaterials (Basel)* **2022,** *12* (3).
131. Zeng, W.; Li, Y.; Wang, Y.; Cao, Y., Tissue Engineering of Blood Vessels. In *Encyclopedia of Tissue Engineering and Regenerative Medicine*, Reis, R. L.; Gomes, M. E., Eds. Academic Press: 2019; pp 413-424.
132. Chan, J. M.; Zhang, L.; Yuet, K. P.; Liao, G.; Rhee, J. W.; Langer, R.; Farokhzad, O. C., PLGA-lecithin-PEG core-shell nanoparticles for controlled drug delivery. *Biomaterials* **2009,** *30* (8), 1627-34.
133. Chan, J. M.; Zhang, L.; Tong, R.; Ghosh, D.; Gao, W.; Liao, G.; Yuet, K. P.; Gray, D.; Rhee, J. W.; Cheng, J.; Golomb, G.; Libby, P.; Langer, R.; Farokhzad, O. C., Spatiotemporal controlled delivery of nanoparticles to injured vasculature. *Proc Natl Acad Sci U S A* **2010,** *107* (5), 2213-8.
134. Zhang, L.; Chan, J. M.; Gu, F. X.; Rhee, J. W.; Wang, A. Z.; Radovic-Moreno, A. F.; Alexis, F.; Langer, R.; Farokhzad, O. C., Self-assembled lipid−polymer hybrid nanoparticles: a robust drug delivery platform. *ACS nano* **2008,** *2* (8), 1696-1702.
135. Reed, A. M.; Gilding, D. K., Biodegradable polymers for use in surgery—poly (glycolic)/poly (Iactic acid) homo and copolymers: 2. In vitro degradation. *Polymer* **1981,** *22* (4), 494-498.

136. Jain, R. A., The manufacturing techniques of various drug loaded biodegradable poly (lactide-co-glycolide)(PLGA) devices. *Biomaterials* **2000,** *21* (23), 2475-2490.
137. Kim, G.; Gavande, V.; Shaikh, V.; Lee, W. K., Degradation Behavior of Poly(Lactide-Co-Glycolide) Monolayers Investigated by Langmuir Technique: Accelerating Effect. *Molecules* **2023,** *28* (12).
138. Anderson, J. M.; Shive, M. S., Biodegradation and biocompatibility of PLA and PLGA microspheres. *Advanced drug delivery reviews* **1997,** *28* (1), 5-24.
139. Felix Lanao, R. P.; Jonker, A. M.; Wolke, J. G.; Jansen, J. A.; van Hest, J. C.; Leeuwenburgh, S. C., Physicochemical properties and applications of poly(lactic-co-glycolic acid) for use in bone regeneration. *Tissue Eng Part B Rev* **2013,** *19* (4), 380-90.
140. Cruz, L. J.; Tacken, P. J.; Fokkink, R.; Figdor, C. G., The influence of PEG chain length and targeting moiety on antibody-mediated delivery of nanoparticle vaccines to human dendritic cells. *Biomaterials* **2011,** *32* (28), 6791-803.
141. Marques, A. C.; Costa, P. J.; Velho, S.; Amaral, M. H., Functionalizing nanoparticles with cancer-targeting antibodies: A comparison of strategies. *J Control Release* **2020,** *320*, 180-200.
142. Suberi, A.; Grun, M. K.; Mao, T.; Israelow, B.; Reschke, M.; Grundler, J.; Akhtar, L.; Lee, T.; Shin, K.; Piotrowski-Daspit, A. S.; Homer, R. J., Polymer nanoparticles deliver mRNA to the lung for mucosal vaccination. *Science Translational Medicine* **2023,** *15* (709), eabq0603.
143. Xu, Y.; Fourniols, T.; Labrak, Y.; Preat, V.; Beloqui, A.; des Rieux, A., Surface Modification of Lipid-Based Nanoparticles. *ACS Nano* **2022,** *16* (5), 7168-7196.
144. Kost, B.; Basko, M.; Bednarek, M.; Socka, M.; Kopka, B.; Łapienis, G.; Biela, T.; Kubisa, P.; Brzeziński, M., The influence of the functional end groups on the properties of polylactide-based materials. *Progress in Polymer Science* **2022,** *130*.
145. Roussel, S.; Grenier, P.; Chenard, V.; Bertrand, N., Dual-Labelled Nanoparticles Inform on the Stability of Fluorescent Labels In Vivo. *Pharmaceutics* **2023,** *15* (3).
146. Kar, M.; Mandal, T. K., End-/side-chain fluorescent polymer conjugates: Stimuli-responsiveness and biological applications. *Journal of Polymer Science* **2023**.
147. Robin, M. P.; O'Reilly, R. K., Strategies for preparing fluorescently labelled polymer nanoparticles. *Polymer International* **2014,** *64* (2), 174-182.
148. D'Souza, S.; Dorati, R.; DeLuca, P. P., Effect of Hydration on Physicochemical Properties of End-Capped PLGA. *Advances in Biomaterials* **2014,** *2014*, 1-9.
149. Wang, J.; Helder, L.; Shao, J.; Jansen, J. A.; Yang, M.; Yang, F., Encapsulation and release of doxycycline from electrospray-generated PLGA microspheres: Effect of polymer end groups. *Int J Pharm* **2019,** *564*, 1-9.
150. Felix Lanao, R. P.; Leeuwenburgh, S. C.; Wolke, J. G.; Jansen, J. A., In vitro degradation rate of apatitic calcium phosphate cement with incorporated PLGA microspheres. *Acta Biomater* **2011,** *7* (9), 3459-68.
151. Saraf, I.; Kushwah, V.; Alva, C.; Koutsamanis, I.; Rattenberger, J.; Schroettner, H.; Mayrhofer, C.; Modhave, D.; Braun, M.; Werner, B.; Zangger, K.; Paudel, A., Influence of PLGA End Groups on the Release Profile of Dexamethasone from Ocular Implants. *Mol Pharm* **2023,** *20* (2), 1307-1322.
152. Yadav, S.; Sharma, A. K.; Kumar, P., Nanoscale Self-Assembly for Therapeutic Delivery. *Front Bioeng Biotechnol* **2020,** *8*, 127.

153. Wang, H.; Zhao, P.; Su, W.; Wang, S.; Liao, Z.; Niu, R.; Chang, J., PLGA/polymeric liposome for targeted drug and gene co-delivery. *Biomaterials* **2010,** *31* (33), 8741-8.
154. Zhao, P.; Wang, H.; Yu, M.; Liao, Z.; Wang, X.; Zhang, F.; Ji, W.; Wu, B.; Han, J.; Zhang, H.; Wang, H.; Chang, J.; Niu, R., Paclitaxel loaded folic acid targeted nanoparticles of mixed lipid-shell and polymer-core: in vitro and in vivo evaluation. *Eur J Pharm Biopharm* **2012,** *81* (2), 248-56.
155. Hu, C.-M. J.; Zhang, L.; Aryal, S.; Cheung, C.; Fang, R. H.; Zhang, L., Erythrocyte membrane-camouflaged polymeric nanoparticles as a biomimetic delivery platform. *Proceedings of the National Academy of Sciences* **2011,** *108* (27), 10980-10985.
156. Sengupta, S.; Eavarone, D.; Capila, I.; Zhao, G.; Watson, N.; Kiziltepe, T.; Sasisekharan, R., Temporal targeting of tumour cells and neovasculature with a nanoscale delivery system. *Nature* **2005,** *436* (7050), 568-72.
157. Tao, J.; Chow, S. F.; Zheng, Y., Application of flash nanoprecipitation to fabricate poorly water-soluble drug nanoparticles. *Acta Pharm Sin B* **2019,** *9* (1), 4-18.
158. Zielinska, A.; Carreiro, F.; Oliveira, A. M.; Neves, A.; Pires, B.; Venkatesh, D. N.; Durazzo, A.; Lucarini, M.; Eder, P.; Silva, A. M.; Santini, A.; Souto, E. B., Polymeric Nanoparticles: Production, Characterization, Toxicology and Ecotoxicology. *Molecules* **2020,** *25* (16).
159. Sánchez-Iglesias, A.; Grzelczak, M.; Altantzis, T.; Goris, B.; Perez-Juste, J.; Bals, S.; Van Tendeloo, G.; Donaldson Jr, S. H.; Chmelka, B. F.; Israelachvili, J. N.; Liz-Marzán, L. M., Hydrophobic interactions modulate self-assembly of nanoparticles. *ACS NANO* **2012,** *6* (12), 11059-11065.
160. Meyer, E. E.; Rosenberg, K. J.; Israelachvili, J., Recent progress in understanding hydrophobic interactions. *Proc Natl Acad Sci U S A* **2006,** *103* (43), 15739-46.
161. Ben-Naim, A. Y., *Hydrophobic interactions*. Springer Science & Business Media: 2012.
162. Vembanur, S.; Patel, A. J.; Sarupria, S.; Garde, S., On the thermodynamics and kinetics of hydrophobic interactions at interfaces. *J Phys Chem B* **2013,** *117* (35), 10261-70.
163. Lomize, A. L.; Pogozheva, I. D.; Lomize, M. A.; Mosberg, H. I., The role of hydrophobic interactions in positioning of peripheral proteins in membranes. *BMC Struct Biol* **2007,** *7*, 44.
164. Baldwin, R. L., Temperature dependence of the hydrophobic interaction in protein folding. *Proceedings of the National Academy of Sciences* **1986,** *83* (21), 8069-8072.
165. White, S. H.; Wimley, W. C., Hydrophobic interactions of peptides with membrane interfaces. *Biochimica et Biophysica Acta (BBA)-Reviews on Biomembranes* **1998,** *1376* (3), 339-352.
166. Strobl, G. R.; Strobl, G. R., The physics of polymers. **1997,** *2*, 17.
167. Moghimi, S. M.; Hunter, A. C.; Murray, J. C., Long-circulating and target-specific nanoparticles: theory to practice. *Pharmacological reviews* **2001,** *53* (2), 283-318.
168. Zheng, M.; Gong, P.; Jia, D.; Zheng, C.; Ma, Y.; Cai, L., Plga–Lecithin–Peg Core-Shell Nanoparticles for Cancer Targeted Therapy. *Nano LIFE* **2012,** *02* (01).
169. Hadinoto, K.; Sundaresan, A.; Cheow, W. S., Lipid-polymer hybrid nanoparticles as a new generation therapeutic delivery platform: a review. *Eur J Pharm Biopharm* **2013,** *85* (3 Pt A), 427-43.
170. Li, L.; Xiang, D.; Shigdar, S.; Yang, W.; Li, Q.; Lin, J.; Liu, K.; Duan, W., Epithelial cell adhesion molecule aptamer functionalized PLGA-lecithin-curcumin-PEG nanoparticles for

targeted drug delivery to human colorectal adenocarcinoma cells. *Int J Nanomedicine* **2014,** *9*, 1083-96.
171. Savage, D. T.; Hilt, J. Z.; Dziubla, T. D., *Nanotoxicity: Methods and Protocols*. 2019.
172. Garg, N. K.; Singh, B.; Jain, A.; Nirbhavane, P.; Sharma, R.; Tyagi, R. K.; Kushwah, V.; Jain, S.; Katare, O. P., Fucose decorated solid-lipid nanocarriers mediate efficient delivery of methotrexate in breast cancer therapeutics. *Colloids Surf B Biointerfaces* **2016,** *146*, 114-26.
173. Pistone, S.; Qoragllu, D.; Smistad, G.; Hiorth, M., Multivariate analysis for the optimization of polysaccharide-based nanoparticles prepared by self-assembly. *Colloids Surf B Biointerfaces* **2016,** *146*, 136-43.
174. Martinez, N. Y.; Andrade, P. F.; Duran, N.; Cavalitto, S., Development of double emulsion nanoparticles for the encapsulation of bovine serum albumin. *Colloids Surf B Biointerfaces* **2017,** *158*, 190-196.
175. Farkas, N.; Kramar, J. A., Dynamic light scattering distributions by any means. *Journal of Nanoparticle Research* **2021,** *23* (5).
176. Golan-Paz, S.; Frizzell, H.; Woodrow, K. A., Cross-Platform Comparison of Therapeutic Delivery from Multilamellar Lipid-Coated Polymer Nanoparticles. *Macromol Biosci* **2019,** *19* (4), e1800362.
177. Mura, S.; Hillaireau, H.; Nicolas, J.; Le Droumaguet, B.; Gueutin, C.; Zanna, S.; Tsapis, N.; Fattal, E., Influence of surface charge on the potential toxicity of PLGA nanoparticles towards Calu-3 cells. *Int J Nanomedicine* **2011,** *6*, 2591-605.
178. Cao, J.; Choi, J. S.; Oshi, M. A.; Lee, J.; Hasan, N.; Kim, J.; Yoo, J. W., Development of PLGA micro- and nanorods with high capacity of surface ligand conjugation for enhanced targeted delivery. *Asian J Pharm Sci* **2019,** *14* (1), 86-94.
179. Govender, T.; Stolnik, S.; Garnett, M. C.; Illum, L.; Davis, S. S., PLGA nanoparticles prepared by nanoprecipitation: drug loading and release studies of a water soluble drug. *Journal of controlled release* **1999,** *57* (2), 171-185.
180. Kowalska, M.; Broniatowski, M.; Mach, M.; Płachta, Ł.; Wydro, P., The effect of the polyethylene glycol chain length of a lipopolymer (DSPE-PEGn) on the properties of DPPC monolayers and bilayers. *Journal of Molecular Liquids* **2021,** *335*.
181. Woodle, M. C.; Collins, L. R.; Sponsler, E.; Kossovsky, N.; Papahadjopoulos, D.; Martin, F. J., Sterically stabilized liposomes. Reduction in electrophoretic mobility but not electrostatic surface potential. *Biophysical journal* **1992,** *61* (4), 902-910.
182. Massover, W. H., On the experimental use of light metal salts for negative staining. *Microsc Microanal* **2008,** *14* (2), 126-37.
183. Liu, L.; Yu, W.; Seitsonen, J.; Xu, W.; Lehto, V. P., Correct Identification of the Core-Shell Structure of Cell Membrane-Coated Polymeric Nanoparticles. *Chemistry* **2022,** *28* (68), e202200947.
184. A. Monnier, C.; C. Thévenaz, D.; Balog, S.; L. Fiore, G.; Vanhecke, D.; Rothen-Rutishauser, B.; Petri-Fink, A., A guide to investigating colloidal nanoparticles by cryogenic transmission electron microscopy: pitfalls and benefits. *AIMS Biophysics* **2015,** *2* (3), 245-258.
185. Helvig, S.; D. M. Azmi, I.; M. Moghimi, S.; Yaghmur, A., Recent Advances in Cryo-TEM Imaging of Soft Lipid Nanoparticles. *AIMS Biophysics* **2015,** *2* (2), 116-130.
186. Fatouros, D. G.; Bergenstahl, B.; Mullertz, A., Morphological observations on a lipid-based drug delivery system during in vitro digestion. *Eur J Pharm Sci* **2007,** *31* (2), 85-94.

187. Liu, C.; Zhang, W.; Li, Y.; Chang, J.; Tian, F.; Zhao, F.; Ma, Y.; Sun, J., Microfluidic Sonication To Assemble Exosome Membrane-Coated Nanoparticles for Immune Evasion-Mediated Targeting. *Nano Lett* **2019,** *19* (11), 7836-7844.
188. Lu, B.; Lv, X.; Le, Y., Chitosan-Modified PLGA Nanoparticles for Control-Released Drug Delivery. *Polymers (Basel)* **2019,** *11* (2).
189. Tsai, M.; Lu, Z.; Wang, J.; Yeh, T. K.; Wientjes, M. G.; Au, J. L., Effects of carrier on disposition and antitumor activity of intraperitoneal Paclitaxel. *Pharm Res* **2007,** *24* (9), 1691-701.
190. Fredenberg, S.; Wahlgren, M.; Reslow, M.; Axelsson, A., The mechanisms of drug release in poly(lactic-co-glycolic acid)-based drug delivery systems--a review. *Int J Pharm* **2011,** *415* (1-2), 34-52.
191. Göpferich, A., Polymer bulk erosion. *Macromolecules* **1997,** *30* (9), 2598-2604.
192. Faisant, N.; Siepmann, J.; Benoit, J. P., PLGA-based microparticles: elucidation of mechanisms and a new, simple mathematical model quantifying drug release. *European Journal of Pharmaceutical Sciences* **2002,** *15* (4), 355-366.
193. Burkersroda, F. V.; Goepferich, A. M., An approach to classify degradable polymers. *MRS Online Proceedings Library* **1998,** *550* (1998), 17.
194. Hines, D. J.; Kaplan, D. L., Poly (lactic-co-glycolic) acid− controlled-release systems: experimental and modeling insights. *Critical Reviews™ in Therapeutic Drug Carrier Systems* **2013,** *30* (3).
195. Abuzar, S. M.; Ahn, J. H.; Park, K. S.; Park, E. J.; Baik, S. H.; Hwang, S. J., Pharmacokinetic Profile and Anti-Adhesive Effect of Oxaliplatin-PLGA Microparticle-Loaded Hydrogels in Rats for Colorectal Cancer Treatment. *Pharmaceutics* **2019,** *11* (8).
196. Armstrong, D. K.; Fleming, G. F.; Markman, M.; Bailey, H. H., A phase I trial of intraperitoneal sustained-release paclitaxel microspheres (Paclimer) in recurrent ovarian cancer: a Gynecologic Oncology Group study. *Gynecol Oncol* **2006,** *103* (2), 391-6.
197. An, W. F.; Tolliday, N., Cell-based assays for high-throughput screening. *Mol Biotechnol* **2010,** *45* (2), 180-6.
198. Michelini, E.; Cevenini, L.; Mezzanotte, L.; Coppa, A.; Roda, A., Cell-based assays: fuelling drug discovery. *Anal Bioanal Chem* **2010,** *398* (1), 227-38.
199. Kumar, P., Nagarajan, A.; Uchil, P. D., Analysis of cell viability by the MTT assay. *Cold spring harbor protocols* **2018,** *2018* (6), pdb-prot095505.
200. Van Meerloo, J.; Kaspers, G. J.; Cloos, J., Cell sensitivity assays: the MTT assay. *Cancer cell culture: methods and protocols* **2011**, 237-245.
201. Tolosa, L.; Donato, M. T.; Gómez-Lechón, M. J., *Protocols in in vitro hepatocyte research*. 2015.
202. Berridge, M. V.; Herst, P. M.; Tan, A. S., Tetrazolium dyes as tools in cell biology: new insights into their cellular reduction. *Biotechnology annual review* **2005,** *11*, 127-152.
203. Stockert, J. C.; Horobin, R. W.; Colombo, L. L.; Blázquez-Castro, A., Tetrazolium salts and formazan products in Cell Biology: Viability assessment, fluorescence imaging, and labeling perspectives. *Acta histochemica* **2018,** *120* (3), 159-167.
204. Ghasemi, M.; Turnbull, T.; Sebastian, S.; Kempson, I., The MTT Assay: Utility, Limitations, Pitfalls, and Interpretation in Bulk and Single-Cell Analysis. *Int J Mol Sci* **2021,** *22* (23).

205. Sigward, E.; Mignet, N.; Rat, P.; Dutot, M.; Muhamed, S.; Guigner, J. M.; Scherman, D.; Brossard, D.; Crauste-Manciet, S., Formulation and cytotoxicity evaluation of new self-emulsifying multiple W/O/W nanoemulsions. *Int J Nanomedicine* **2013,** *8*, 611-25.
206. Koley, D.; Bard, A. J., Triton X-100 concentration effects on membrane permeability of a single HeLa cell by scanning electrochemical microscopy (SECM). *Proc Natl Acad Sci U S A* **2010,** *107* (39), 16783-7.
207. Cornett, J. B.; Shockman, G. D., Cellular lysis of Streptococcus faecalis induced with Triton X-100. *Journal of bacteriology* **1978,** *135* (1), 153-160
.
208. Truong, K. D.; Nguyen, H. T.-L.; Nguyen, S. T., Comparative cytotoxic effects of methanol, ethanol and DMSO on human cancer cell lines. *Biomedical Research and Therapy* **2020,** *7* (7), 3855-3859.
209. Goldstein, D. B., Effect of alcohol on cellular membranes. *Annals of emergency medicine* **1986,** *15* (9), 1013-1018.
210. Toth, M. E.; Vigh, L.; Santha, M., Alcohol stress, membranes, and chaperones. *Cell Stress Chaperones* **2014,** *19* (3), 299-309.
211. Utreja, P.; Jain, S.; Tiwary, A. K., Evaluation of biosafety and intracellular uptake of Cremophor EL free paclitaxel elastic liposomal formulation. *Drug Deliv* **2012,** *19* (1), 11-20.
212. Tanase, M. A.; Raducan, A.; Oancea, P.; Ditu, L. M.; Stan, M.; Petcu, C.; Scomoroscenco, C.; Ninciuleanu, C. M.; Nistor, C. L.; Cinteza, L. O., Mixed Pluronic-Cremophor Polymeric Micelles as Nanocarriers for Poorly Soluble Antibiotics-The Influence on the Antibacterial Activity. *Pharmaceutics* **2021,** *13* (4).
213. Jadon, R. S.; Sharma, M., Docetaxel-loaded lipid-polymer hybrid nanoparticles for breast cancer therapeutics. *Journal of Drug Delivery Science and Technology* **2019,** *51*, 475-484.
214. Xiao, B.; Han, M. K.; Viennois, E.; Wang, L.; Zhang, M.; Si, X.; Merlin, D., Hyaluronic acid-functionalized polymeric nanoparticles for colon cancer-targeted combination chemotherapy. *Nanoscale* **2015,** *7* (42), 17745-55.
215. Yalcin, T. E.; Ilbasmis-Tamer, S.; Takka, S., Antitumor activity of gemcitabine hydrochloride loaded lipid polymer hybrid nanoparticles (LPHNs): In vitro and in vivo. *Int J Pharm* **2020,** *580*, 119246.
216. Lu, J.; Owen, S. C.; Shoichet, M. S., Stability of Self-Assembled Polymeric Micelles in Serum. *Macromolecules* **2011,** *44* (15), 6002-6008.
217. Liu, J.; Zeng, F.; Allen, C., Influence of serum protein on polycarbonate-based copolymer micelles as a delivery system for a hydrophobic anti-cancer agent. *J Control Release* **2005,** *103* (2), 481-97.
218. Dulbecco, R.; Vogt, M., Plaque formation and isolation of pure lines with poliomyelitis viruses. *The Journal of experimental medicine* **1954,** *99* (2), 167-182.
219. Karthikeyan, S.; Bharanidharan, G.; Ragavan, S.; Kandasamy, S.; Chinnathambi, S.; Udayakumar, K.; Mangaiyarkarasi, R.; Suganya, R.; Aruna, P.; Ganesan, S., Exploring the Binding Interaction Mechanism of Taxol in beta-Tubulin and Bovine Serum Albumin: A Biophysical Approach. *Mol Pharm* **2019,** *16* (2), 669-681.
220. Qi, H.; Wang, Y.; Wang, X.; Su, L.; Wang, Y.; Wang, S., The different interactions of two anticancer drugs with bovine serum albumin based on multi-spectrum method combined with molecular dynamics simulations. *Spectrochim Acta A Mol Biomol Spectrosc* **2021,** *259*, 119809.

221. Yordanova, D.; Ritter, E.; Gerlach, T.; Jensen, J. H.; Smirnova, I.; Jakobtorweihen, S., Solute Partitioning in Micelles: Combining Molecular Dynamics Simulations, COSMOmic, and Experiments. *J Phys Chem B* **2017,** *121* (23), 5794-5809.
222. Posocco, B.; Buzzo, M.; Follegot, A.; Giodini, L.; Sorio, R.; Marangon, E.; Toffoli, G., A new high-performance liquid chromatography-tandem mass spectrometry method for the determination of paclitaxel and 6alpha-hydroxy-paclitaxel in human plasma: Development, validation and application in a clinical pharmacokinetic study. *PLoS One* **2018,** *13* (2), e0193500.
223. Vasantha, J.; Kannan, G.; Goud, T.; Palani, T.; Vanitha, R.; Anitha, R.; Priya, J., Pharmacokinetic evaluation of Paclitaxel in South Indian cancer patients: a prospective study. *J Young Pharm* **2011,** *3* (4), 322-8.
224. Panuwet, P.; Hunter, R. E., Jr.; D'Souza, P. E.; Chen, X.; Radford, S. A.; Cohen, J. R.; Marder, M. E.; Kartavenka, K.; Ryan, P. B.; Barr, D. B., Biological Matrix Effects in Quantitative Tandem Mass Spectrometry-Based Analytical Methods: Advancing Biomonitoring. *Crit Rev Anal Chem* **2016,** *46* (2), 93-105.
225. Mallet, C. R.; Lu, Z.; Mazzeo, J. R., A study of ion suppression effects in electrospray ionization from mobile phase additives and solid-phase extracts. *Rapid Commun Mass Spectrom* **2004,** *18* (1), 49-58.
226. Schuhmacher, J.; Zimmer, D.; Tesche, F.; Pickard, V., Matrix effects during analysis of plasma samples by electrospray and atmospheric pressure chemical ionization mass spectrometry: practical approaches to their elimination. *Rapid Commun Mass Spectrom* **2003,** *17* (17), 1950-7.
227. Jo, M. J.; Jo, Y. H.; Lee, Y. J.; Park, C. W.; Kim, J. S.; Hong, J. T.; Chung, Y. B.; Lee, M. K.; Shin, D. H., Physicochemical, Pharmacokinetic, and Toxicity Evaluation of Methoxy Poly(ethylene glycol)-b-Poly(d,l-Lactide) Polymeric Micelles Encapsulating Alpinumisoflavone Extracted from Unripe Cudrania tricuspidata Fruit. *Pharmaceutics* **2019,** *11* (8).
228. Han, L. M.; Guo, J.; Zhang, L. J.; Wang, Q. S.; Fang, X. L., Pharmacokinetics and biodistribution of polymeric micelles of paclitaxel with Pluronic P123. *Acta Pharmacol Sin* **2006,** *27* (6), 747-53.
229. Alexis, F.; Pridgen, E.; Molnar, L. K.; Farokhzad, O. C., Factors affecting the clearance and biodistribution of polymeric nanoparticles. *Molecular pharmaceutics* **2008,** *5* (4), 505-515.
230. Godara, S.; Lather, V.; Kirthanashri, S. V.; Awasthi, R.; Pandita, D., Lipid-PLGA hybrid nanoparticles of paclitaxel: Preparation, characterization, in vitro and in vivo evaluation. *Mater Sci Eng C Mater Biol Appl* **2020,** *109*, 110576.
231. Yang, C.; Merlin, D., Lipid-Based Drug Delivery Nanoplatforms for Colorectal Cancer Therapy. *Nanomaterials (Basel)* **2020,** *10* (7), 1424.
232. Van Zundert, I.; Fortuni, B.; Rocha, S., From 2D to 3D Cancer Cell Models-The Enigmas of Drug Delivery Research. *Nanomaterials (Basel)* **2020,** *10* (11).
233. Kapalczynska, M.; Kolenda, T.; Przybyla, W.; Zajaczkowska, M.; Teresiak, A.; Filas, V.; Ibbs, M.; Blizniak, R.; Luczewski, L.; Lamperska, K., 2D and 3D cell cultures - a comparison of different types of cancer cell cultures. *Arch Med Sci* **2018,** *14* (4), 910-919.
234. Munir, M. U., Nanomedicine Penetration to Tumor: Challenges, and Advanced Strategies to Tackle This Issue. *Cancers (Basel)* **2022,** *14* (12).
235. Lu, P.; Weaver, V. M.; Werb, Z., The extracellular matrix: a dynamic niche in cancer progression. *J Cell Biol* **2012,** *196* (4), 395-406.

236. Khawar, I. A.; Kim, J. H.; Kuh, H. J., Improving drug delivery to solid tumors: priming the tumor microenvironment. *J Control Release* **2015,** *201*, 78-89.
237. Pluen, A.; Boucher, Y.; Ramanujan, S.; McKee, T. D.; Gohongi, T.; di Tomaso, E.; Brown, E. B.; Izumi, Y.; Campbell, R. B.; Berk, D. A.; Jain, R. K., Role of tumor-host interactions in interstitial diffusion of macromolecules: cranial vs. subcutaneous tumors. *Proc Natl Acad Sci U S A* **2001,** *98* (8), 4628-33.
238. Yeung, T. M.; Gandhi, S. C.; Wilding, J. L.; Muschel, R.; Bodmer, W. F., Cancer stem cells from colorectal cancer-derived cell lines. *Proc Natl Acad Sci U S A* **2010,** *107* (8), 3722-7.
239. Li, W.; Du, B.; Wang, T.; Wang, S.; Zhang, J., Kaempferol induces apoptosis in human HCT116 colon cancer cells via the Ataxia-Telangiectasia Mutated-p53 pathway with the involvement of p53 Upregulated Modulator of Apoptosis. *Chem Biol Interact* **2009,** *177* (2), 121-7.
240. Awwad, R. A.; Sergina, N.; Yang, H.; Ziober, B.; Willson, J. K.; Zborowska, E.; Humphrey, L. E.; Fan, R.; Ko, T. C.; Brattain, M. G.; Howell, G. M., The role of transforming growth factor α in determining growth factor independence. *Cancer research* **2003,** *63* (15), 4731-4738.
241. Thakur, R.; Sharma, A.; Arora, V., Nanoparticles Methods for Hydrophobic Drugs — A Novel Approach: Graphical Abstract. *Materials Open* **2023,** *01*.
242. Alshamsan, A., Nanoprecipitation is more efficient than emulsion solvent evaporation method to encapsulate cucurbitacin I in PLGA nanoparticles. *Saudi Pharm J* **2014,** *22* (3), 219-22.
243. Couvreur, P., Nanoparticles in drug delivery: past, present and future. *Adv Drug Deliv Rev* **2013,** *65* (1), 21-3.
244. Chan, J. M.; Rhee, J. W.; Drum, C. L.; Bronson, R. T.; Golomb, G.; Langer, R.; Farokhzad, O. C., In vivo prevention of arterial restenosis with paclitaxel-encapsulated targeted lipid-polymeric nanoparticles. *Proc Natl Acad Sci U S A* **2011,** *108* (48), 19347-52.
245. Hernandez-Giottonini, K. Y.; Rodriguez-Cordova, R. J.; Gutierrez-Valenzuela, C. A.; Penunuri-Miranda, O.; Zavala-Rivera, P.; Guerrero-German, P.; Lucero-Acuna, A., PLGA nanoparticle preparations by emulsification and nanoprecipitation techniques: effects of formulation parameters. *RSC Adv* **2020,** *10* (8), 4218-4231.
246. Liu, Z.; Jiao, Y.; Wang, Y.; Zhou, C.; Zhang, Z., Polysaccharides-based nanoparticles as drug delivery systems. *Adv Drug Deliv Rev* **2008,** *60* (15), 1650-62.
247. Liu, Y.; Yang, G.; Baby, T.; Tengjisi; Chen, D.; Weitz, D. A.; Zhao, C. X., Stable Polymer Nanoparticles with Exceptionally High Drug Loading by Sequential Nanoprecipitation. *Angewandte Chemie* **2020,** *132* (12), 4750-4758.
248. Xiao, M.; Xie, L.; Cao, G.; Lei, S.; Wang, P.; Wei, Z.; Luo, Y.; Fang, J.; Yang, X.; Huang, Q.; Xu, L.; Guo, J.; Wen, S.; Wang, Z.; Wu, Q.; Tang, J.; Wang, L.; Chen, X.; Chen, C.; Zhang, Y.; Yao, W.; Ye, J.; He, R.; Huang, J.; Ye, L., CD4(+) T-cell epitope-based heterologous prime-boost vaccination potentiates anti-tumor immunity and PD-1/PD-L1 immunotherapy. *J Immunother Cancer* **2022,** *10* (5).
249. Mansurov, A.; Ishihara, J.; Hosseinchi, P.; Potin, L.; Marchell, T. M.; Ishihara, A.; Williford, J. M.; Alpar, A. T.; Raczy, M. M.; Gray, L. T.; Swartz, M. A.; Hubbell, J. A., Collagen-binding IL-12 enhances tumour inflammation and drives the complete remission of established immunologically cold mouse tumours. *Nat Biomed Eng* **2020,** *4* (5), 531-543.

250. Kang, S.; Mansurov, A.; Kurtanich, T.; Chun, H. R.; Slezak, A. J.; Volpatti, L. R.; Chang, K.; Wang, T.; Alpar, A. T.; Refvik, K. C.; Hansen, O. I.; Borjas, G. J.; Shim, H.; Hultgren, K. T.; Gomes, S.; Solanki, A.; Ishihara, J.; Swartz, M. A.; Hubbell, J. A., Engineered IL-7 synergizes with IL-12 immunotherapy to prevent T cell exhaustion and promote memory without exacerbating toxicity. *Science Advances* **2023,** *9* (48), eadh9879.
251. Cai, X.; Chen, M.; Prominski, A.; Lin, Y.; Ankenbruck, N.; Rosenberg, J.; Nguyen, M.; Shi, J.; Tomatsidou, A.; Randall, G.; Missiakas, D.; Fung, J.; Chang, E. B.; Penaloza-MacMaster, P.; Tian, B.; Huang, J., A Multifunctional Neutralizing Antibody-Conjugated Nanoparticle Inhibits and Inactivates SARS-CoV-2. *Adv Sci (Weinh)* **2022,** *9* (2), e2103240.